Title
Strategies Toward the Homogeneous Synthesis and Functionalization of Covalent Organic Frameworks

Author
Guo, Lei

Publication Date
2019

Peer reviewed|Thesis/dissertation

Strategies Toward the Homogeneous Synthesis and Functionalization of Covalent Organic Frameworks

By

Lei Guo

A dissertation submitted in partial satisfaction of the

requirements for the degree of

Doctor of Philosophy

in

Chemistry

in the

Graduate Division

of the

University of California, Berkeley

Committee in charge:

Professor Omar M. Yaghi, Chair
Professor Peter C. Vollhardt
Professor Mark Asta

Spring 2019

Abstract

Strategies Toward the Homogeneous Synthesis and Functionalization of Covalent Organic Frameworks

by

Lei Guo

Doctor of Philosophy in Chemistry

University of California, Berkeley

Professor Omar M. Yaghi, Chair

This dissertation focuses on a range of methods for expanding the complexity of covalent organic frameworks (COFs). COFs are a class of highly porous crystalline materials constructed by stitching organic building blocks together into extended frameworks. Since the first COF was reported in 2005, extensive efforts have been devoted to expanding the scope of this field. In this dissertation, the development of a novel synthetic route and three post-synthetic modifications are covered. The applicability of these strategies is demonstrated by the successful synthesis of monodisperse COF nanoparticles, highly oriented COF thin films, woven COF crystals, and a functionalizable COF platform.

Chapter I encompasses a general introduction of COFs. Unlike amorphous polymers, which are typically formed under kinetic control, COFs represent a thermodynamic product. As such, they possess high structural periodicity that results from reversible bond formation and cleavage, eventually yielding the linkage between the organic building units as the result of dynamic error correction. With directional linkages and rigid molecular building units, COFs can be precisely designed on the atomic level. Efforts have been devoted to developing new synthetic strategies and accessing functionalized imine-linked COFs. The resultant tunability and well-defined morphology of COFs have allowed for application of the materials to numerous fields.

In Chapter II, a newly developed homogeneous synthetic route for imine COFs is presented. Conventional imine-linked COF synthesis is carried out in heterogeneous suspensions, where polyimine formation occurs too rapidly to effectively control crystal nucleation. In order to address this shortcoming, Boc-protected (Boc = *tert*-butyloxycarbonyl) amine linkers are used as starting materials, which are slowly deprotected *in situ* and grow into extended structures when reacted with aldehyde

counterparts. Under the synthetic conditions reported here, the initial nucleation rate is slowed down such that it is comparable to that of the dynamic error correction for the structure. Additionally, the reaction intermediates are readily soluble in the solution. These phenomena allow for the synthesis of imine COFs to be carried out under homogeneous conditions and enable the growth of imine COFs to be tuned using modulators. The work herein brings COFs into nanometer size regime and paves the way for the integration of COFs into mesoscopic constructs.

Chapter III further discusses how the newly developed homogeneous synthetic route leads to the successful synthesis of high quality COF thin films. By employing the Boc-protected amine building blocks and initiating the reaction under highly acidic conditions, selective secondary nucleation of COF nanoparticles will occur on the polar oxides in the reaction system (*e.g.*, a silicon wafer substrate). The nucleation barrier in the homogeneous COF synthesis enables film growth without precipitation from the solution and eventually yields highly oriented thin films.

Reticular chemistry, the chemistry of linking rigid molecular building units together by strong chemical bonds into extended structures with long-range periodicity, has led to a plethora of COF structures. Chapter IV presents the design and synthesis of a new class of materials, woven COFs with one-dimensional covalently linked molecular chains designed to intersect at regular intervals by means of metal templates. COF-112 is constructed from cobalt bis(diiminopyridine) complexes with a near-perfect tetrahedral geometry and pyridinedicarboxaldehyde, and is an ideal example of molecular weaving. It represents one of the simplest three-dimensional woven structures, as it involves only two sets of threads that are straight and parallel with only one point of registry.

Chapter V continues to focus on expanding the scope of COF chemistry by developing strategies to design and synthesize functionalized COFs in a rapid and efficient manner. In this chapter, three new post-synthetic modification reactions, namely amidation, esterification, and thioesterification, are demonstrated on a novel, highly crystalline, two-dimensional COF, COF-616, bearing pre-installed carboxylic acid groups. The strategy can be used to introduce a large variety of functional groups into COFs and the modifications can be carried out under mild reaction conditions with high yields and an easy work-up protocol. Therefore, COF-616 can serve as a functionalizable platform that can be readily tailored for various applications. As a proof of concept, various chelating functional groups were successfully incorporated into COF-616 to yield a family of adsorbents for efficient removal of heavy metal ions from water.

Strategies Toward the Homogeneous Synthesis and Functionalization of Covalent Organic Frameworks

Table of Contents

Acknowledgements

First of all, I would like to thank Prof. Omar M. Yaghi for his support and guidance throughout the course of my doctoral studies. He has provided me with ample resources and freedom to explore my ideas. His impact on my scientific development is long-lasting and will keep encouraging me to pursue innovative and creative research in my future endeavors. I am also deeply grateful to him for recruiting me to UC Berkeley in the first place. Not only did I get the chance to meet and work with amazing people in the Yaghi laboratory and in the department, which is a wonderful career experience one can only dream of, but it is right here, at UC Berkeley, where I met my husband Shang, which is the most important event in my life.

I would also like to thank my qualifying exam and thesis committee members, Prof. Peter C. Vollhardt, Prof. Richard A. Andersen, and Prof. Mask Asta for providing support throughout my graduate studies. Their challenging questions and inspiring discussions during my qualifying exam helped me a lot in the later portion of my doctorate research.

Furthermore, I want to thank my undergraduate research advisor Prof. Wei Wang for my first opportunity to engage in scientific research. It was in Prof. Wang's group where I developed my interest in materials science and basic experimental skills. He taught me to be creative, cautious, and innovative. I am grateful for his continued support throughout my entire academic career.

Additionally, I want to acknowledge Dr. Yingbo Zhao, Dr. Juncong Jiang, Dr. Jingjing Yang, and Prof. Yuebiao Zhang, who provided me a lot of guidance and mentorship through my early stage of my graduate research. I am also grateful to Prof. Yanhang Ma, Dr. Chenhui Zhu, Dr. Christopher Trickett, Dr. Eugene Kapustin, Dr. Christian Diercks, Prof. Xuejing Yang, Hao Lyu and Wentao Xu for their collaboration. I am also thankful for Peter, Robinson, Mathieu, Roc, Cornelius, Steven, Ha, and all the other Yaghi group members, for being so supportive and providing helpful discussions. It was my great honor to have worked with you all and I have learned so much from each of you. I will cherish this experience throughout my life.

Finally, I recognize the support of my parents during my graduate study. They are always there for me and give me their biggest support. I appreciate the education they gave me and the freedom to pursue the career that I love. I am so proud to have them as my parents. And Shang, meeting you is the greatest fortune and blessing to me. Since I met you, I've found everything I have been looking for my whole life. You are my best friend, my soul mate, and the love of my life. I enjoy every day I have spent with you, and I would love to spend the rest of my life with you.

To my beloved parents and my loving husband Shang

Chapter I. Introduction to Covalent Organic Frameworks

1.1 Covalent Organic Frameworks

Covalent organic frameworks (COFs) are a class of porous crystalline materials made by stitching together molecular building units through covalent bonds.[1,2] Due to reversible linkage formation in COFs, rigid organic building units are covalently linked into extended frameworks with long-range structural periodicity. During the reticular synthesis, the organic building units maintain their geometries and the resultant covalent bonds are endowed with directionality, resulting in porous, crystalline structures with predesigned metrics.[3,4] The high porosities and large surface areas of these frameworks have motivated researchers to investigate their application to areas such as gas storage and separation,[5–8] heterogeneous catalysis,[9–14] ion conductivity,[15–20] and sensing.[21–23]

In this chapter, each organic reaction applicable to COF synthesis is presented. Additionally, an overview of the design principles of COFs is detailed. The synthetic strategy for imine-linked COF formation is also discussed, as COFs with this linkage have been extensively studied due to their high chemical and thermal stability, and the ease with which they can be synthesized. To conclude, various approaches to synthesize functionalized COFs to expand their applications are summarized.

1.2 Linkages Used to Crystallize COFs

Linking organic building units by strong covalent bonds into extended structures generally leads to kinetically-favored amorphous products. In order to form crystalline materials, dynamic covalent chemistry (DCC) has been applied to COF synthesis.[24] In this context, linkage formation between the organic building units is highly reversible, which provides for error correction during the synthesis to yield highly crystalline material as the thermodynamically-favored product. The formation of boronate esters is among the first reactions used to synthesize COFs.[1] In this condensation reaction, the high reversibility is accomplished by regulating the amount of water, the byproduct of the reaction, in the reaction system. The reaction is conducted in a closed vessel in order to allow generated water vapor to equilibrate with the synthetic solution. Additionally, solvents in which water has limited solubility are used to further tweak this equilibrium. Since the first COF was reported in 2005, numerous new reactions have been developed to crystallize COFs (Scheme 1.1):

(1). B-O bond formation: boronate ester,[1] boroxine,[1] spiroborate,[20] and borosilicate;[25]

(2). B=N bond formation: borazine;[26]

(3). C=C bond formation: alkene;[27]

(4). C=N bond formation: imine,[28] hydrazone,[29] azine,[30] and squaraine;[31]

(5). C=$N_{(aromatic)}$ bond formation: triazine,[32] phenazine,[33] and oxazole;[34]

(6). C–N bond formation: β-ketoenamine,[35] imide,[36] and amide;[37]

(7). C-O bond formation: dioxin;[38]

(8). N=N bond formation: azodioxy;[39]

(9). Si-O bond formation: silicate.[40]

The diversity of these linkages has vastly expanded the scope of COF chemistry in terms of utilizing molecular building blocks with various functionalities and accessing COFs with different degrees of chemical reactivity.

Scheme 1.1. Linkages that have been reported for the COF synthesis, as summarized by the type of bond formation.

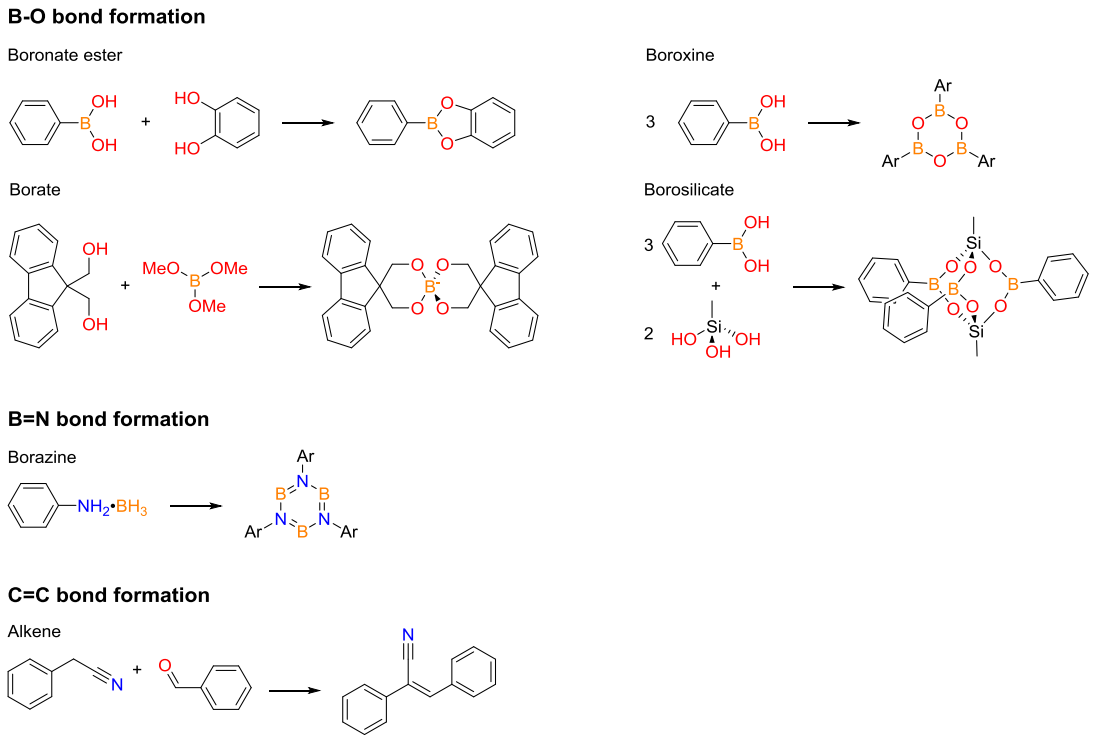

C=N bond formation

Imine

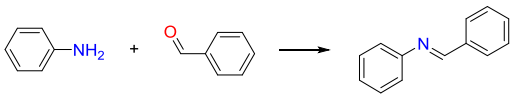

Hydrazone

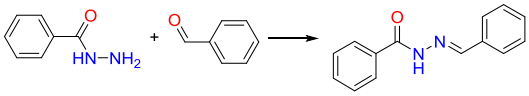

Azine

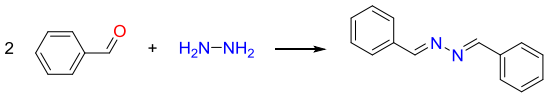

Squaraine

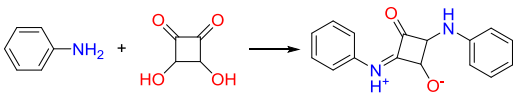

C=N_{Ar} bond formation

Triazine

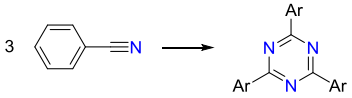

Phenazine

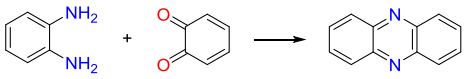

Oxazole

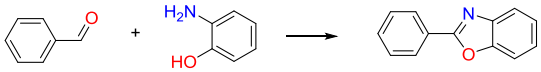

C-N bond formation

Imide

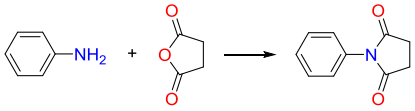

β-Ketoenamine

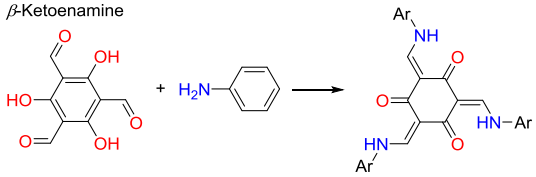

Amide

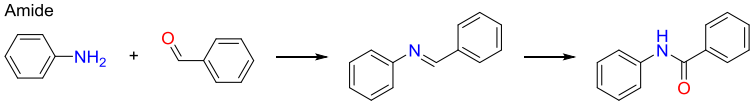

C-O bond formation

Dioxine

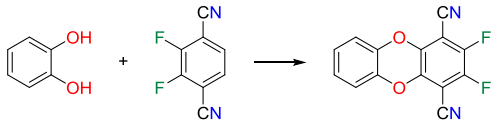

N=N bond formation

Azodioxide

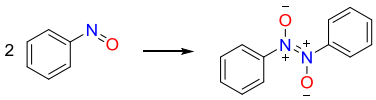

Si-O bond formation

Silicate

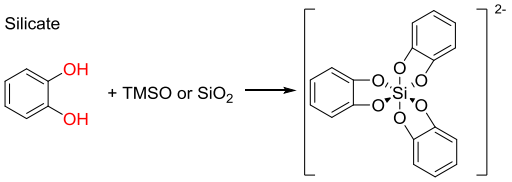

1.3 Reticular Design of COFs

Reticular chemistry, the chemistry of linking molecular building blocks by strong bonds to construct extended crystalline frameworks, has vastly expanded the scope of porous materials, including metal-organic frameworks (MOFs) and COFs.[41] Unlike MOFs, the geometry of the covalent linkages and organic building units used to synthesize COFs remain unaltered throughout the construction process. This enables precise control over the atomic arrangement of the structures that can be characterized by X-ray and electron diffraction.[42,43]

To design a COF with a targeted structure, organic building blocks which possess fixed points of extension, highly symmetrical geometry, and rigid backbones are first selected. These organic building blocks are then connected by directional linkages to form two-dimensional or three-dimensional COFs held together with strong covalent bonds. Reported two-dimensional nets (**hcb**,[1] **sql**,[44] **kgm**,[45] **hxl**,[46] **fxt**,[47] **bex**,[48] and **kgd**[49]) and three-dimensional frameworks (**dia**,[28] **lon**,[43] **srs**,[40] **ctn**,[50] **bor**,[50] **pts**,[51,52] **ffc**,[53] and **rra**[19]) have been summarized in Scheme 1.2.

Scheme 1.2. Summary of reported topology of COFs, as organized by the degree of symmetry of the building blocks.

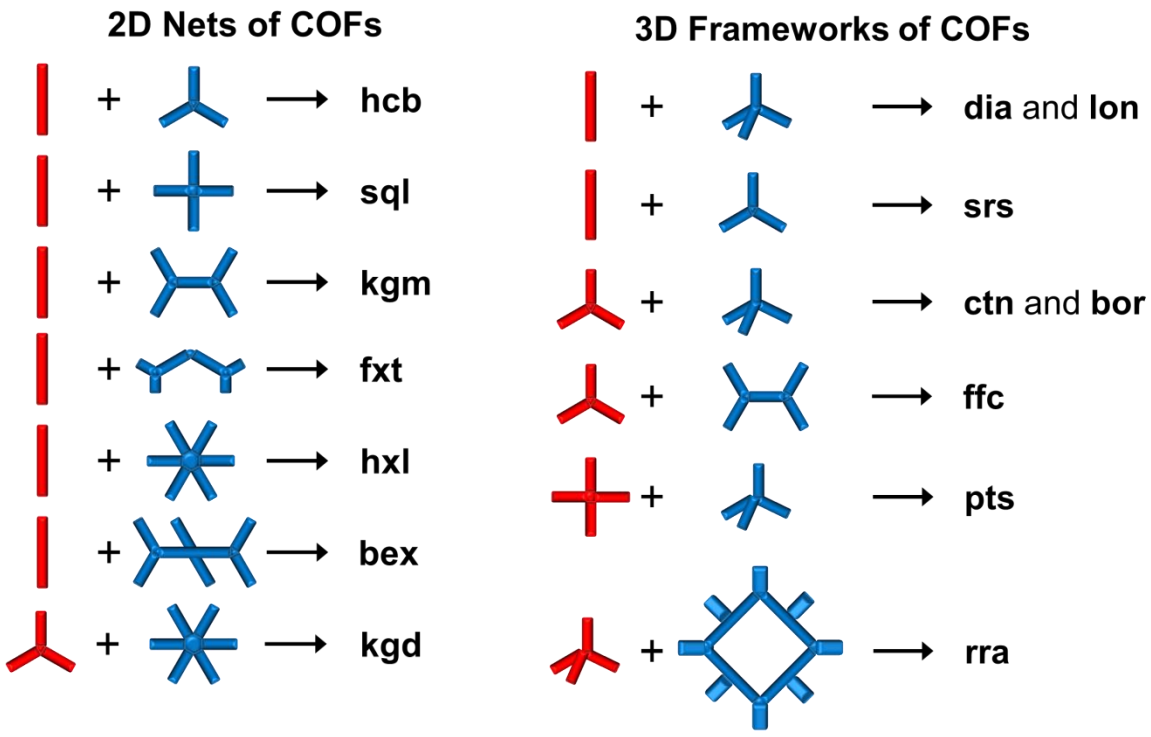

Recently, a new class of COFs, woven COFs, have been successfully synthesized based on the design principles discussed above.[54–57] These COFs are constructed by

linking organic building blocks with metal complexes *via* imine bonds, with metal coordination serving as the template to direct the propagation of the one-dimensional polyimine chains in the framework. This class of new materials can be further demetallated to introduce large degrees of freedom and spatial flexibility within the whole framework, which can lead to exceptional mechanical properties.

1.4 Synthetic Strategies for Structuring Imine-Linked COFs

Due to accessibility of the constituent starting materials, high thermal and chemical stability, and ease of synthesis, imine-linked COFs are mostly studied and synthesized for applied research, and the mechanism of their crystallization process has been carefully investigated.[58] Conventional imine COF synthesis is carried out heterogeneously, and the formation of a crystalline imine COF occurs in two steps:

(1). Upon the addition of the catalyst for imine formation (Lewis or Brønsted acid), a polyimine precipitate forms immediately. This precipitate is the kinetic product and is amorphous.

(2). Due to the reversibility of the linkage and the associated error correction mechanisms in the reaction system, the amorphous intermediates will subsequently transform into crystalline products at elevated temperature in the presence of acid over time.

For imine COF synthesis, an acid is generally preferred, because it can significantly increase the reversibility of the reaction and therefore shorten the reaction time needed for obtaining the crystalline phase. However, fast imine condensation upon acid addition also creates a challenge: there is little to no control over COF nucleation. Precipitation and crystallization of imine-linked COFs occur separately, which is divergent from the phenomena observed in the synthesis of MOFs, wherein crystals grow directly from clear solutions. Immediate formation of the amorphous polyimine at the beginning of the reaction determines the morphology of the resultant COF microcrystalline powders, which are generally highly aggregated and are of irregular sizes and shapes. These intermediates will then crystallize over time with their morphology remaining mostly unaltered. This shortcoming of conventional imine COF synthesis hinders the successful preparation of COF single crystals and limits the control over the interactions between COFs and specific substrates. To address this, new strategies to synthesize COF in a homogeneous solution need to be developed where the nucleation process of COF crystals can be well controlled.

1.5 Synthesis of Functional COFs

The high permanent porosities and tunable interior pore environments of COFs have been used successfully to tailor COFs for promising candidates in the areas of gas storage and separation,[5–8] heterogeneous catalysis,[9–14] ion conductivity,[15–20] and sensing.[21–23] Generally, to design a COF for a particular application, a specific chemical functionality needs to be introduced into the framework's pores to optimize its interactions with guest species. The functionality can be introduced by means of pre-synthetic and post-synthetic modification. For pre-synthetic modification, organic molecules decorated with the targeted moiety are used as the building blocks in the synthesis. This approach is sometimes limited since the incorporated functional groups need to be compatible with the COF forming reaction. For example, aldehydes and amines cannot be attached to the starting materials, since they will interfere with the formation of the framework. Against this backdrop, post-synthetic modification serves as a more generalized approach to synthesize functional COFs. In this case, the modification reaction is conducted on pre-installed functional groups throughout the entire COF framework to introduce the targeted functionality. To date, a number of post-synthetic modification reactions, including copper (I)-catalyzed alkyne-azide cycloaddition (CuAAC) click reaction,[10,59–63] thiol-ene reaction,[64–66] cyclic anhydride opening,[67,68] nitro reduction and acetylation,[69] Williamson ether synthesis,[70] bromination and quaternization,[71] Riemschneider reaction,[72] amidoxime formation,[38,73] Staudinger reduction,[74] nitrile hydrolysis,[38,75] and nitrile reduction[75] have been reported (Scheme 1.3).[76]

An effective post-synthetic modification reaction should be able to be carried out under mild reaction conditions, so that the underlying COF structure remains intact, with high yield and minimal side reactions, since it is difficult to separate by-products in the solid-state. With these criteria in mind, although a variety of post-synthetic modification reactions have been developed as listed above, the CuAAC click reaction is among the most common because of the ease of installation of alkyne functional groups and nearly quantitative conversion. However, conducting such reactions on COFs generally requires anaerobic handling, involves heterogeneous Cu(I) catalysts that is different to remove from the pores after the completion of the reaction, and is incompatible with molecules featuring chelating functionalities. All of these features greatly limit the generality of this approach and a more general strategy for post-synthetic modification of COFs is highly desirable.

Scheme 1.3. Post-synthetic modification reactions in COFs as summarized in the order of their discovery.

CuAAC click reaction (2011)

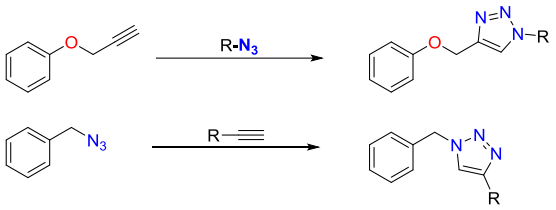

Thiol-ene reaction (2013)

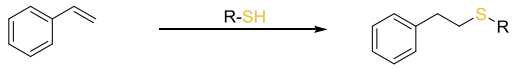

Cyclic anhydride opening (2015)

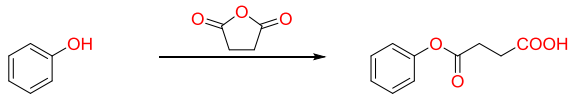

Nitro reduction and acetylation (2016)

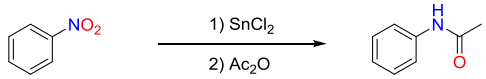

Williamson ether synthesis (2017)

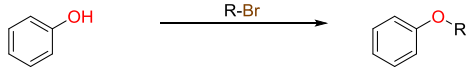

Bromination and quaternization (2018)

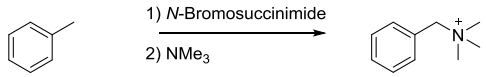

Riemschneider reaction (2018)

Amidoxime formation (2018)

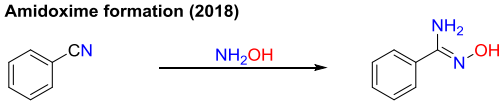

Staudinger reduction (2018)

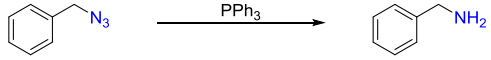

Nitrile hydrolysis (2018)

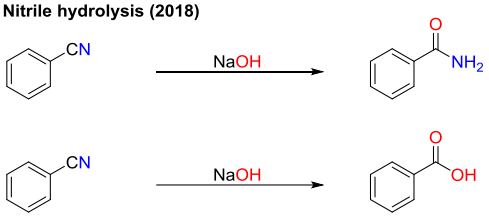

Nitrile reduction (2019)

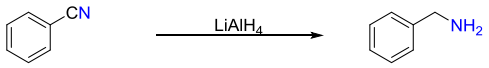

1.6 References

(1) Cote, A. P.; Benin, A. I.; Ockwig, N. W.; O'Keeffe, M.; Matzger, A. J.; Yaghi, O. M. Porous, Crystalline, Covalent Organic Frameworks. *Science* **2005**, *310* (6), 1166-1170.

(2) Yaghi, O. M.; Kalmutzki, M. J.; Diercks, C. S. *Introduction to Reticular Chemistry: Metal-Organic Frameworks and Covalent Organic Frameworks*; John Wiley & Sons, 2019.

(3) Yaghi, O. M.; O'Keeffe, M.; Ockwig, N. W.; Chae, H. K.; Eddaoudi, M.; Kim, J. Reticular Synthesis and the Design of New Materials. *Nature* **2003**, *423* (6941), 705–714.

(4) Côté, A. P.; El-Kaderi, H. M.; Furukawa, H.; Hunt, J. R.; Yaghi, O. M. Reticular Synthesis of Microporous and Mesoporous 2D Covalent Organic Frameworks. *J. Am. Chem. Soc.* **2007**, *129* (43), 12914–12915.

(5) Doonan, C. J.; Tranchemontagne, D. J.; Glover, T. G.; Hunt, J. R.; Yaghi, O. M. Exceptional Ammonia Uptake by a Covalent Organic Framework. *Nat. Chem.* **2010**, *2* (3), 235–238.

(6) Furukawa, H.; Yaghi, O. M. Storage of Hydrogen, Methane, and Carbon Dioxide in Highly Porous Covalent Organic Frameworks for Clean Energy Applications. *J. Am. Chem. Soc.* **2009**, *131* (25), 8875–8883.

(7) Stegbauer, L.; Hahn, M. W.; Jentys, A.; Savasci, G.; Ochsenfeld, C.; Lercher, J. A.; Lotsch, B. V. Tunable Water and CO2 Sorption Properties in Isostructural Azine-Based Covalent Organic Frameworks through Polarity Engineering. *Chem. Mater.* **2015**, *27* (23), 7874–7881.

(8) Baldwin, L. A.; Crowe, J. W.; Pyles, D. A.; McGrier, P. L. Metalation of a Mesoporous Three-Dimensional Covalent Organic Framework. *J. Am. Chem. Soc.* **2016**, *138* (46), 15134–15137.

(9) Ding, S.-Y.; Gao, J.; Wang, Q.; Zhang, Y.; Song, W.-G.; Su, C.-Y.; Wang, W. Construction of Covalent Organic Framework for Catalysis: Pd/COF-LZU1 in Suzuki–Miyaura Coupling Reaction. *J. Am. Chem. Soc.* **2011**, *133* (49), 19816–19822.

(10) Xu, H.; Gao, J.; Jiang, D. Stable, Crystalline, Porous, Covalent Organic Frameworks as a Platform for Chiral Organocatalysts. *Nat. Chem.* **2015**, *7* (11), 905–912.

(11) Vyas, V. S.; Haase, F.; Stegbauer, L.; Savasci, G.; Podjaski, F.; Ochsenfeld, C.; Lotsch, B. V. A Tunable Azine Covalent Organic Framework Platform for Visible Light-Induced Hydrogen Generation. *Nat. Commun.* **2015**, *6*, 8508.

(12) Lin, S.; Diercks, C. S.; Zhang, Y.-B.; Kornienko, N.; Nichols, E. M.; Zhao, Y.; Paris, A. R.; Kim, D.; Yang, P.; Yaghi, O. M.; Chang, C. J. Covalent Organic Frameworks

Comprising Cobalt Porphyrins for Catalytic CO_2 Reduction in Water. *Science* **2015**, *349* (6253), 1208–1213.

(13) Wang, X.; Han, X.; Zhang, J.; Wu, X.; Liu, Y.; Cui, Y. Homochiral 2D Porous Covalent Organic Frameworks for Heterogeneous Asymmetric Catalysis. *J. Am. Chem. Soc.* **2016**, *138* (38), 12332–12335.

(14) Sun, Q.; Aguila, B.; Perman, J.; Nguyen, N.; Ma, S. Flexibility Matters: Cooperative Active Sites in Covalent Organic Framework and Threaded Ionic Polymer. *J. Am. Chem. Soc.* **2016**, *138* (48), 15790–15796.

(15) Ma, H.; Liu, B.; Li, B.; Zhang, L.; Li, Y.-G.; Tan, H.-Q.; Zang, H.-Y.; Zhu, G. Cationic Covalent Organic Frameworks: A Simple Platform of Anionic Exchange for Porosity Tuning and Proton Conduction. *J. Am. Chem. Soc.* **2016**, *138* (18), 5897–5903.

(16) Chandra, S.; Kundu, T.; Kandambeth, S.; BabaRao, R.; Marathe, Y.; Kunjir, S. M.; Banerjee, R. Phosphoric Acid Loaded Azo (−N═N−) Based Covalent Organic Framework for Proton Conduction. *J. Am. Chem. Soc.* **2014**, *136* (18), 6570–6573.

(17) Montoro, C.; Rodríguez-San-Miguel, D.; Polo, E.; Escudero-Cid, R.; Ruiz-González, M. L.; Navarro, J. A. R.; Ocón, P.; Zamora, F. Ionic Conductivity and Potential Application for Fuel Cell of a Modified Imine-Based Covalent Organic Framework. *J. Am. Chem. Soc.* **2017**, *139* (29), 10079–10086.

(18) Vazquez-Molina, D. A.; Mohammad-Pour, G. S.; Lee, C.; Logan, M. W.; Duan, X.; Harper, J. K.; Uribe-Romo, F. J. Mechanically Shaped Two-Dimensional Covalent Organic Frameworks Reveal Crystallographic Alignment and Fast Li-Ion Conductivity. *J. Am. Chem. Soc.* **2016**, *138* (31), 9767–9770.

(19) Zhang, Y.; Duan, J.; Ma, D.; Li, P.; Li, S.; Li, H.; Zhou, J.; Ma, X.; Feng, X.; Wang, B. Three-Dimensional Anionic Cyclodextrin-Based Covalent Organic Frameworks. *Angew. Chem. Int. Ed.* **2017**, *56* (51), 16313–16317.

(20) Du, Y.; Yang, H.; Whiteley, J. M.; Wan, S.; Jin, Y.; Lee, S.-H.; Zhang, W. Ionic Covalent Organic Frameworks with Spiroborate Linkage. *Angew. Chem. Int. Ed.* **2016**, *55* (5), 1737–1741.

(21) Das, G.; Biswal, B. P.; Kandambeth, S.; Venkatesh, V.; Kaur, G.; Addicoat, M.; Heine, T.; Verma, S.; Banerjee, R. Chemical Sensing in Two Dimensional Porous Covalent Organic Nanosheets. *Chem. Sci.* **2015**, *6* (7), 3931–3939.

(22) Li, Z.; Huang, N.; Lee, K. H.; Feng, Y.; Tao, S.; Jiang, Q.; Nagao, Y.; Irle, S.; Jiang, D. Light-Emitting Covalent Organic Frameworks: Fluorescence Improving via Pinpoint Surgery and Selective Switch-On Sensing of Anions. *J. Am. Chem. Soc.* **2018**, *140* (39), 12374–12377.

(23) Ding, S.-Y.; Dong, M.; Wang, Y.-W.; Chen, Y.-T.; Wang, H.-Z.; Su, C.-Y.; Wang, W. Thioether-Based Fluorescent Covalent Organic Framework for Selective Detection and Facile Removal of Mercury(II). *J. Am. Chem. Soc.* **2016**, *138* (9), 3031–3037.

(24) Rowan, S. J.; Cantrill, S. J.; Cousins, G. R. L.; Sanders, J. K. M.; Stoddart, J. F. Dynamic Covalent Chemistry. *Angew. Chem. Int. Ed.* **2002**, *41* (6), 898–952.

(25) Hunt, J. R.; Doonan, C. J.; LeVangie, J. D.; Côté, A. P.; Yaghi, O. M. Reticular Synthesis of Covalent Organic Borosilicate Frameworks. *J. Am. Chem. Soc.* **2008**, *130* (36), 11872–11873.

(26) Jackson, K. T.; Reich, T. E.; El-Kaderi, H. M. Targeted Synthesis of a Porous Borazine-Linked Covalent Organic Framework. *Chem. Commun.* **2012**, *48* (70), 8823.

(27) Zhuang, X.; Zhao, W.; Zhang, F.; Cao, Y.; Liu, F.; Bi, S.; Feng, X. A Two-Dimensional Conjugated Polymer Framework with Fully Sp^2-Bonded Carbon Skeleton. *Polym. Chem.* **2016**, *7* (25), 4176–4181.

(28) Uribe-Romo, F. J.; Hunt, J. R.; Furukawa, H.; Klöck, C.; O'Keeffe, M.; Yaghi, O. M. A Crystalline Imine-Linked 3-D Porous Covalent Organic Framework. *J. Am. Chem. Soc.* **2009**, *131* (13), 4570–4571.

(29) Uribe-Romo, F. J.; Doonan, C. J.; Furukawa, H.; Oisaki, K.; Yaghi, O. M. Crystalline Covalent Organic Frameworks with Hydrazone Linkages. *J. Am. Chem. Soc.* **2011**, *133* (30), 11478–11481.

(30) Dalapati, S.; Jin, S.; Gao, J.; Xu, Y.; Nagai, A.; Jiang, D. An Azine-Linked Covalent Organic Framework. *J. Am. Chem. Soc.* **2013**, *135* (46), 17310–17313.

(31) Nagai, A.; Chen, X.; Feng, X.; Ding, X.; Guo, Z.; Jiang, D. A Squaraine-Linked Mesoporous Covalent Organic Framework. *Angew. Chem. Int. Ed.* **2013**, *52* (13), 3770–3774.

(32) Kuhn, P.; Antonietti, M.; Thomas, A. Porous, Covalent Triazine-Based Frameworks Prepared by Ionothermal Synthesis. *Angew. Chem. Int. Ed.* **2008**, *47* (18), 3450–3453.

(33) Guo, J.; Xu, Y.; Jin, S.; Chen, L.; Kaji, T.; Honsho, Y.; Addicoat, M. A.; Kim, J.; Saeki, A.; Ihee, H.; et al. Conjugated Organic Framework with Three-Dimensionally Ordered Stable Structure and Delocalized π Clouds. *Nat. Commun.* **2013**, *4* (1).

(34) Pyles, D. A.; Crowe, J. W.; Baldwin, L. A.; McGrier, P. L. Synthesis of Benzobisoxazole-Linked Two-Dimensional Covalent Organic Frameworks and Their Carbon Dioxide Capture Properties. *ACS Macro Lett.* **2016**, *5* (9), 1055–1058.

(35) DeBlase, C. R.; Silberstein, K. E.; Truong, T.-T.; Abruña, H. D.; Dichtel, W. R. β-Ketoenamine-Linked Covalent Organic Frameworks Capable of Pseudocapacitive Energy Storage. *J. Am. Chem. Soc.* **2013**, *135* (45), 16821–16824.

(36) Fang, Q.; Zhuang, Z.; Gu, S.; Kaspar, R. B.; Zheng, J.; Wang, J.; Qiu, S.; Yan, Y. Designed Synthesis of Large-Pore Crystalline Polyimide Covalent Organic Frameworks. *Nat. Commun.* **2014**, *5* (1).

(37) Waller, P. J.; Lyle, S. J.; Osborn Popp, T. M.; Diercks, C. S.; Reimer, J. A.; Yaghi, O. M. Chemical Conversion of Linkages in Covalent Organic Frameworks. *J. Am. Chem. Soc.* **2016**, *138* (48), 15519–15522.

(38) Zhang, B.; Wei, M.; Mao, H.; Pei, X.; Alshmimri, S. A.; Reimer, J. A.; Yaghi, O. M. Crystalline Dioxin-Linked Covalent Organic Frameworks from Irreversible Reactions. *J. Am. Chem. Soc.* **2018**, *140* (40), 12715–12719.

(39) Beaudoin, D.; Maris, T.; Wuest, J. D. Constructing Monocrystalline Covalent Organic Networks by Polymerization. *Nat. Chem.* **2013**, *5* (10), 830–834.

(40) Roeser, J.; Prill, D.; Bojdys, M. J.; Fayon, P.; Trewin, A.; Fitch, A. N.; Schmidt, M. U.; Thomas, A. Anionic Silicate Organic Frameworks Constructed from Hexacoordinate Silicon Centres. *Nat. Chem.* **2017**, *9* (10), 977–982.

(41) Yaghi, O. M. Reticular Chemistry—Construction, Properties, and Precision Reactions of Frameworks. *J. Am. Chem. Soc.* **2016**, *138* (48), 15507–15509.

(42) Zhang, Y.-B.; Su, J.; Furukawa, H.; Yun, Y.; Gándara, F.; Duong, A.; Zou, X.; Yaghi, O. M. Single-Crystal Structure of a Covalent Organic Framework. *J. Am. Chem. Soc.* **2013**, *135* (44), 16336–16339.

(43) Ma, T.; Kapustin, E. A.; Yin, S. X.; Liang, L.; Zhou, Z.; Niu, J.; Li, L.-H.; Wang, Y.; Su, J.; Li, J; Wang, X; Wang, D. W.; Wang, W.; Sun, J.; Yaghi, O. M. Single-Crystal x-Ray Diffraction Structures of Covalent Organic Frameworks. *Science* **2018**, *361* (6397), 48–52.

(44) Ding, X.; Guo, J.; Feng, X.; Honsho, Y.; Guo, J.; Seki, S.; Maitarad, P.; Saeki, A.; Nagase, S.; Jiang, D. Synthesis of Metallophthalocyanine Covalent Organic Frameworks That Exhibit High Carrier Mobility and Photoconductivity. *Angew. Chem. Int. Ed.* **2011**, *50* (6), 1289–1293.

(45) Zhou, T.-Y.; Xu, S.-Q.; Wen, Q.; Pang, Z.-F.; Zhao, X. One-Step Construction of Two Different Kinds of Pores in a 2D Covalent Organic Framework. *J. Am. Chem. Soc.* **2014**, *136* (45), 15885–15888.

(46) Qian, C.; Qi, Q.-Y.; Jiang, G.-F.; Cui, F.-Z.; Tian, Y.; Zhao, X. Toward Covalent Organic Frameworks Bearing Three Different Kinds of Pores: The Strategy for

Construction and COF-to-COF Transformation via Heterogeneous Linker Exchange. *J. Am. Chem. Soc.* **2017**, *139* (19), 6736–6743.

(47) Dalapati, S.; Addicoat, M.; Jin, S.; Sakurai, T.; Gao, J.; Xu, H.; Irle, S.; Seki, S.; Jiang, D. Rational Design of Crystalline Supermicroporous Covalent Organic Frameworks with Triangular Topologies. *Nat. Commun.* **2015**, *6*, 7786.

(48) Yin, Z.-J.; Xu, S.-Q.; Zhan, T.-G.; Qi, Q.-Y.; Wu, Z.-Q.; Zhao, X. Ultrahigh Volatile Iodine Uptake by Hollow Microspheres Formed from a Heteropore Covalent Organic Framework. *Chem. Commun.* **2017**, *53* (53), 7266–7269.

(49) Xu, S.-Q.; Liang, R.-R.; Zhan, T.-G.; Qi, Q.-Y.; Zhao, X. Construction of 2D Covalent Organic Frameworks by Taking Advantage of the Variable Orientation of Imine Bonds. *Chem. Commun.* **2017**, *53* (16), 2431–2434.

(50) El-Kaderi, H. M.; Hunt, J. R.; Mendoza-Cortés, J. L.; Côté, A. P.; Taylor, R. E.; O'Keeffe, M.; Yaghi, O. M. Designed Synthesis of 3D Covalent Organic Frameworks. *Science* **2007**, *316* (5822), 268–272.

(51) Lin, G.; Ding, H.; Yuan, D.; Wang, B.; Wang, C. A Pyrene-Based, Fluorescent Three-Dimensional Covalent Organic Framework. *J. Am. Chem. Soc.* **2016**, *138* (10), 3302–3305.

(52) Lin, G.; Ding, H.; Chen, R.; Peng, Z.; Wang, B.; Wang, C. 3D Porphyrin-Based Covalent Organic Frameworks. *J. Am. Chem. Soc.* **2017**, *139* (25), 8705–8709.

(53) Lan, Y.; Han, X.; Tong, M.; Huang, H.; Yang, Q.; Liu, D.; Zhao, X.; Zhong, C. Materials Genomics Methods for High-Throughput Construction of COFs and Targeted Synthesis. *Nat. Commun.* **2018**, *9* (1), 5274.

(54) Liu, Y.; Ma, Y.; Zhao, Y.; Sun, X.; Gándara, F.; Furukawa, H.; Liu, Z.; Zhu, H.; Zhu, C.; Suenaga, K.; Oleynikov, P.; Alshammari, A. S.; Zhang, X.; Terasaki, O.; Yaghi, O. M. Weaving of Organic Threads into a Crystalline Covalent Organic Framework. *Science* **2016**, *351* (6271), 365–369.

(55) Zhao, Y.; Guo, L.; Gándara, F.; Ma, Y.; Liu, Z.; Zhu, C.; Lyu, H.; Trickett, C. A.; Kapustin, E. A.; Terasaki, O.; et al. A Synthetic Route for Crystals of Woven Structures, Uniform Nanocrystals, and Thin Films of Imine Covalent Organic Frameworks. *J. Am. Chem. Soc.* **2017**, *139* (37), 13166–13172.

(56) Liu, Y.; Ma, Y.; Yang, J.; Diercks, C. S.; Tamura, N.; Jin, F.; Yaghi, O. M. Molecular Weaving of Covalent Organic Frameworks for Adaptive Guest Inclusion. *J. Am. Chem. Soc.* **2018**, *140* (47), 16015–16019.

(57) Liu, Y.; Diercks, C. S.; Ma, Y.; Lyu, H.; Zhu, C.; Alshmimri, S. A.; Alshihri, S.; Yaghi, O. M. 3D Covalent Organic Frameworks of Interlocking 1D Square Ribbons. *J. Am. Chem. Soc.* **2019**, *141* (1), 677–683.

(58) Smith, B. J.; Overholts, A. C.; Hwang, N.; Dichtel, W. R. Insight into the Crystallization of Amorphous Imine-Linked Polymer Networks to 2D Covalent Organic Frameworks. *Chem. Commun.* **2016**, *52* (18), 3690–3693.

(59) Xu, F.; Xu, H.; Chen, X.; Wu, D.; Wu, Y.; Liu, H.; Gu, C.; Fu, R.; Jiang, D. Radical Covalent Organic Frameworks: A General Strategy to Immobilize Open-Accessible Polyradicals for High-Performance Capacitive Energy Storage. *Angew. Chem. Int. Ed.* **2015**, *54* (23), 6814–6818.

(60) Huang, N.; Krishna, R.; Jiang, D. Tailor-Made Pore Surface Engineering in Covalent Organic Frameworks: Systematic Functionalization for Performance Screening. *J. Am. Chem. Soc.* **2015**, *137* (22), 7079–7082.

(61) Xu, H.; Chen, X.; Gao, J.; Lin, J.; Addicoat, M.; Irle, S.; Jiang, D. Catalytic Covalent Organic Frameworks via Pore Surface Engineering. *Chem. Commun.* **2014**, *50* (11), 1292–1294.

(62) Nagai, A.; Guo, Z.; Feng, X.; Jin, S.; Chen, X.; Ding, X.; Jiang, D. Pore Surface Engineering in Covalent Organic Frameworks. *Nat. Commun.* **2011**, *2*, 536.

(63) Mer íBof í L.; Royuela, S.; Zamora, F.; Ruiz-Gonz ález, M. L.; Segura, J. L.; Mu ñoz-Olivas, R.; Manche ño, M. J. Thiol Grafted Imine-Based Covalent Organic Frameworks for Water Remediation through Selective Removal of Hg(II). *J. Mater. Chem. A* **2017**, *5* (34), 17973–17981.

(64) Bunck, D. N.; Dichtel, W. R. Postsynthetic Functionalization of 3D Covalent Organic Frameworks. *Chem. Commun.* **2013**, *49* (24), 2457–2459.

(65) Sun, Q.; Aguila, B.; Perman, J. A.; Butts, T.; Xiao, F.-S.; Ma, S. Integrating Superwettability within Covalent Organic Frameworks for Functional Coating. *Chem* **2018**, *4* (7), 1726–1739.

(66) Sun, Q.; Aguila, B.; Perman, J.; Earl, L. D.; Abney, C. W.; Cheng, Y.; Wei, H.; Nguyen, N.; Wojtas, L.; Ma, S. Postsynthetically Modified Covalent Organic Frameworks for Efficient and Effective Mercury Removal. *J. Am. Chem. Soc.* **2017**, *139* (7), 2786–2793..

(67) Huang, N.; Chen, X.; Krishna, R.; Jiang, D. Two-Dimensional Covalent Organic Frameworks for Carbon Dioxide Capture through Channel-Wall Functionalization. *Angew. Chem. Int. Ed.* **2015**, *54* (10), 2986–2990.

(68) Lu, Q.; Ma, Y.; Li, H.; Guan, X.; Yusran, Y.; Xue, M.; Fang, Q.; Yan, Y.; Qiu, S.; Valtchev, V. Postsynthetic Functionalization of Three-Dimensional Covalent Organic Frameworks for Selective Extraction of Lanthanide Ions. *Angew. Chem. Int. Ed.* **2018**, *57* (21), 6042–6048.

(69) Lohse, M. S.; Stassin, T.; Naudin, G.; Wuttke, S.; Ameloot, R.; De Vos, D.; Medina, D. D.; Bein, T. Sequential Pore Wall Modification in a Covalent Organic Framework for Application in Lactic Acid Adsorption. *Chem. Mater.* **2016**, *28* (2), 626–631.

(71) Guo, H.; Wang, J.; Fang, Q.; Zhao, Y.; Gu, S.; Zheng, J.; Yan, Y. A Quaternary-Ammonium-Functionalized Covalent Organic Framework for Anion Conduction. *CrystEngComm* **2017**, *19* (33), 4905–4910.

(72) Rager, S.; Dogru, M.; Werner, V.; Gavryushin, A.; Götz, M.; Engelke, H.; Medina, D. D.; Knochel, P.; Bein, T. Pore Wall Fluorescence Labeling of Covalent Organic Frameworks. *CrystEngComm* **2017**, *19* (33), 4886–4891.

(73) Sun, Q.; Aguila, B.; Earl, L. D.; Abney, C. W.; Wojtas, L.; Thallapally, P. K.; Ma, S. Covalent Organic Frameworks as a Decorating Platform for Utilization and Affinity Enhancement of Chelating Sites for Radionuclide Sequestration. *Adv. Mater.* **2018**, *30* (20), 1705479.

(74) Ji, W.; Xiao, L.; Ling, Y.; Ching, C.; Matsumoto, M.; Bisbey, R. P.; Helbling, D. E.; Dichtel, W. R. Removal of GenX and Perfluorinated Alkyl Substances from Water by Amine-Functionalized Covalent Organic Frameworks. *J. Am. Chem. Soc.* **2018**, *140* (40), 12677–12681

(75) Guan, X.; Li, H.; Ma, Y.; Xue, M.; Fang, Q.; Yan, Y.; Valtchev, V.; Qiu, S. Chemically Stable Polyarylether-Based Covalent Organic Frameworks. *Nat. Chem.* **2019**, *1*.

(76) Lyle, S. J.; Waller, P. J.; Yaghi, O. M. Covalent Organic Frameworks: Organic Chemistry Extended into Two and Three Dimensions. *Trends in Chemistry* **2019**, *1* (2), 172–184.

Chapter II. Synthesis and Characterization of COF Nanoparticles

2.1 Introduction

The development of reticular chemistry has hinged upon our ability to crystallize the products of linking molecular building blocks by strong bonds into extended porous structures. In the original synthesis of metal-organic frameworks (MOFs), the key discovery for obtaining them as crystals is the controlled deprotonation of the organic acid linkers, which in turn controls the rate of reaction with the metal ions.[1] The fact that the starting points of these reactions are homogeneous solution mixtures allows for the control over nucleation and crystal growth using various synthetic methods,[2–6] and this has led to the vast expansion of MOF chemistry.[7,8] In contrast, synthesis of imine-linked COFs is generally conducted under heterogeneous conditions, where amorphous polyimine precipitates form as a result of linking organic building blocks in a kinetically-favored manner.[9] These solids are then annealed by heating to potentially obtain microcrystalline materials; an aspect that leads to lack of control in making COFs and severely limits the possibilities for controlling their nucleation and crystal growth.

In conventional imine COF synthesis, amine and aldehyde building blocks usually form amorphous polyimine precipitates upon their reaction in solvent mixtures containing aqueous acetic acid catalyst. Upon heating in sealed Pyrex tubes for days, the resulting heterogeneous mixture gradually turns into aggregates of microscopic COF crystallites.[10,11] Typically, the obtained imine COFs have morphologies resembling the initial polyimine precipitates, as the COF nucleation and growth are intrinsically heterogeneous and insensitive to the addition of modulators. In this process, crystallization relies on the reversible imine condensation reaction to correct defects in the polyimine precipitate. This process would not be successful if substantial structural differences are present between the desired COF and the polyimine precipitate. Such limitations have in turn restricted access to crystalline COFs and the scope of their synthesis.

In this study, this challenge is addressed by utilizing a *tert*-butyloxycarbonyl (Boc) protected amine functionality in the starting material to synthesize COFs homogeneously rather heterogeneously. The amine can be gradually deprotected *in situ* with trifluoroacetic acid to slow down the imine condensation reaction and to facilitate COF crystallization.

• Portions of this chapter have been previously published in:
Zhao, Y.*; Guo, L.*; Gándara, F.; Ma, Y.; Liu, Z.; Zhu, C.; Lyu, H.; Trickett, C. A.; Kapustin, E. A.; Terasaki, O.; Yaghi, O. M. A Synthetic Route for Crystals of Woven Structures, Uniform Nanocrystals, and Thin Films of Imine Covalent Organic Frameworks. *J. Am. Chem. Soc.* **2017**, *139* (37), 13166–13172.
*These authors contributed equally to this work.

This synthetic route thus enables imine COFs to be synthesized homogeneously without the usual complications of having amorphous insoluble intermediates. The power of this synthetic approach is demonstrated by synthesizing imine COFs as monodisperse nanocrystals.

2.2 Experimental Section

2.2.1 Methods and Materials

Chemicals. Polyvinylpyrrolidinone (PVP, M_w. = 10,000, and M_w. = 360,000), ethanol (anhydrous, purity ≥ 99.5 %), and triethylamine (TEA, purity ≥ 99.5 %) were obtained from Sigma-Aldrich. 1,3,5-Triformylbenzene (TFB, purity ≥ 98 %) and 4-(*tert*-butoxycarbonylamino)-aniline (NBPDA, purity ≥ 97 %) were purchased from Acros Organics. Toluene (anhydrous purity ≥ 99.8%) and trifluoroacetic acid (TFA, purity ≥ 99.7 %) were acquired from EMD Millipore Chemicals.

All reactions were performed under ambient laboratory conditions, and no precautions taken to exclude atmospheric moisture, unless otherwise specified.

Analytical techniques and instrument. Gas adsorption experiments (up to 760 torr) were carried out on a Quantachrome AUTOSORB-1 automatic volumetric instrument. Ultrahigh-purity-grade N_2 was used in all adsorption measurements. The N_2 (77 K) isotherms were measured using a liquid nitrogen bath (77 K). Powder X-ray diffraction (PXRD) patterns were recorded using a Rigaku Miniflex 600 (Bragg-Brentano geometry, Cu K_α radiation λ = 1.54 Å) instrument. Attenuated total reflectance (ATR) FTIR spectra of neat samples were performed on a Bruker ALPHA Platinum ATR-FTIR Spectrometer equipped with a single reflection diamond ATR module. Scanning electron microscope (SEM) images were recorded on a Zeiss Gemini Ultra-55 analytical scanning electron microscope with accelerating voltage of 5 kV. Transmission electron microscopy (TEM) was performed on a cold field emission JEM-2100F instrument equipped with a DELTA C_s corrector. Optical refractive index was measured using ellipsometer (Gaertner Scientific Corporation).

2.2.2 Synthesis

Synthesis of LZU-1 nanocrystals with size of 245 nm. TFB (5 mg, 0.03 mmol), NBPDA (10 mg, 0.05 mmol), and PVP (Mw. = 360,000, 20 mg) were dissolved in 2 mL ethanol and 0.24 mL TFA. The solution was transferred to a 10 mL glass microwave vessel and heated to 120 ℃ for 30 minutes. The reddish dispersion obtained was diluted with ethanol to 8 mL and centrifuged at 8000 rpm for 5 minutes. The red solid was collected and dispersed in 8 mL ethanol and 0.5 mL TEA to give a yellow suspension. The suspension

was further centrifuged at 8000 rpm to collect the nanocrystals, and the supernatant was decanted.

Synthesis of LZU-1 nanocrystals with size of 112 nm. TFB (5 mg, 0.03 mmol), NBPDA (10 mg, 0.05 mmol), and 40 mg PVP (M_w. = 10,000) were dissolved in 1 mL ethanol and 0.12 mL TFA. The solution was transferred to a 10 mL glass microwave vessel and heated to 120 ℃ for 30 minutes. The reaction was quenched by diluting the dispersion with ethanol and then centrifuging at 8000 rpm for 5 minutes. The red solid was collected and dispersed in 8 mL ethanol and 0.5 mL TEA to give a yellow suspension. The suspension was further centrifuged at 8000 rpm for 5 minutes to collect the nanocrystals.

Synthesis of LZU-1 nanocrystals with size of 500 nm. TFB (5 mg, 0.03 mmol), NBPDA (10 mg, 0.05 mmol), and 10 mg PVP (M_w. = 360,000) were dissolved in 1 mL ethanol and 0.12 mL TFA. The solution was transferred to a 10 mL glass microwave vessel and heated to 120 ℃ for 30 minutes. The reaction was quenched by diluting the dispersion with ethanol and then centrifuging at 8000 rpm for 5 minutes. The red solid was collected and dispersed in 8 mL ethanol and 0.5 mL TEA to give a yellow suspension. The suspesion was further centrifuged at 8000 rpm for 5 minutes to collect the nanocrystals.

Synthesis of LZU-1 nanocrystals with hexagonal shape. To obtain hexagonal shaped LZU-1 nanocrystals, the synthesis was conducted with a growth solution of TFB (5 mg, 0.03 mmol), NBPDA (10 mg, 0.05 mmol), and PVP (Mw. = 360,000, 20 mg) in a toluene/ethanol = 1:9 solvent mixture, instead of pure ethanol as the solvent. The reddish dispersion obtained was diluted with ethanol and then centrifuged at 8000 rpm for 5 minutes. The red solid was collected and dispersed in ethanol, treated with 0.5 mL TEA, and centrifuged again at 8000 rpm for 5 minutes to collect the nanocrystals.

Synthesis of Por-COF nanocrystals. 4,4',4",4'"-(porphyrin-5,10,15,20-tetrayl) tetrabenzaldehyde (5 mg), NBPDA (5 mg), and PVP (15 mg, M_w. = 360,000) were dissolved in 0.3 mL toluene, 0.7 mL ethanol, 60 μL TFA, and 10 μL water and heated under microwave irradiation at 120 °C for 30 minutes The reddish dispersion obtained was diluted with ethanol and then centrifuged at 8000 rpm for 5 minutes. The red solid was collected and dispersed in ethanol, treated with 0.5 mL TEA and then centrifuged again at 8000 rpm for 5 minutes to collect the nanocrystals.

Synthesis of TFPB-PDA COF nanocrystals. TFPB (5 mg), NBPDA (5 mg), and PVP (15 mg, M_w. = 360,000) were dissolved in 0.3 mL toluene, 0.7 mL ethanol, 60 μL TFA, and 10 μL water and heated under microwave irradiation at 120 °C for 30 minutes. The red solid was collected and dispersed in ethanol, treated with 0.5 mL TEA and then centrifuged again at 8000 rpm for 5 minutes to collect the nanocrystals.

Synthesis of COF-LZU-1 mixed-matrix membrane. The mixed-matrix membrane was synthesized by dispersing LZU-1 nanocrystals (100 mg) and PVDF (50 mg, M_w. =

27500) in 4 mL DMF to form a uniform solution. The solvent was removed by vacuum at 100 ℃ to afford free standing membranes.

2.3 Results and Discussion

2.3.1 Synthesis and Characterization of COF-LZU-1 Nanoparticles

Under homogenous imine-linked COF synthesis, nuclei form from a clear solution and grow into crystalline frameworks, thus enabling the control over COF nucleation and growth. Specifically, a 'burst of nucleation' induced by rapid heating combined with modulator regulated growth would give monodisperse nanocrystals, while under mild heating the nucleation barrier would facilitate the growth of COFs on substrates. This nucleation and growth control is first demonstrated on a prototype imine COF, LZU-1, before generalization to other ones (Scheme 2.1).

Scheme 2.1 Synthesis of COF-LZU-1 nanocrystal.

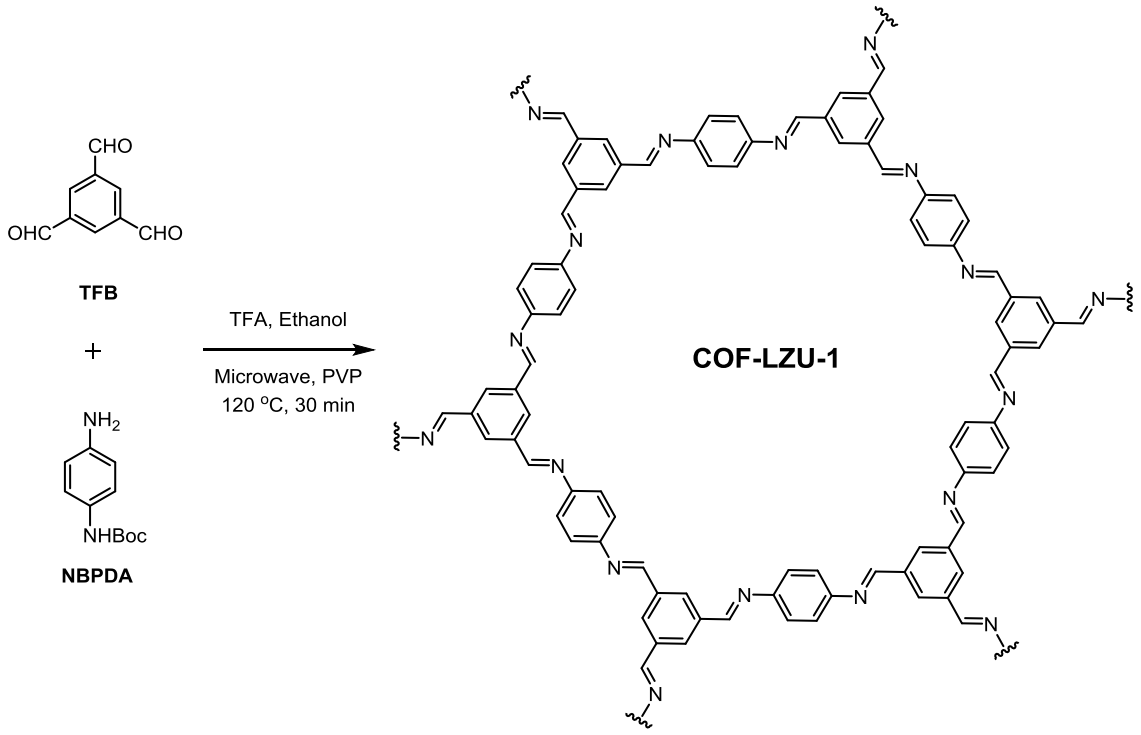

Monodisperse LZU-1 nanocrystals were synthesized by reacting NBPDA and TFB under microwave irradiation with PVP as the capping agent. The as-synthesized COF-LZU-1 nanocrystals were red instead of yellow, which was the result of protonation of the particles through the high concentration of TFA.[12] This was evidenced by a comparison of UV-Vis spectra of the as-synthesized COF-LZU-1 and deprotonated products (washed by triethylamine) (Figure 2.1). Protonation was also supported by FT-IR

spectra showing N-H and $C=NH^+$ stretching band in the as-synthesized sample (Figure 2.2). The suspension rapidly changed color from red to yellow upon washing with an ethanol/triethylamine mixture (Figure 2.3). The protonation of the imine COF rendered the COF nanocrystals polar during crystal growth and allowed PVP to bind and passivate their surface and regulate growth in alcoholic solution.

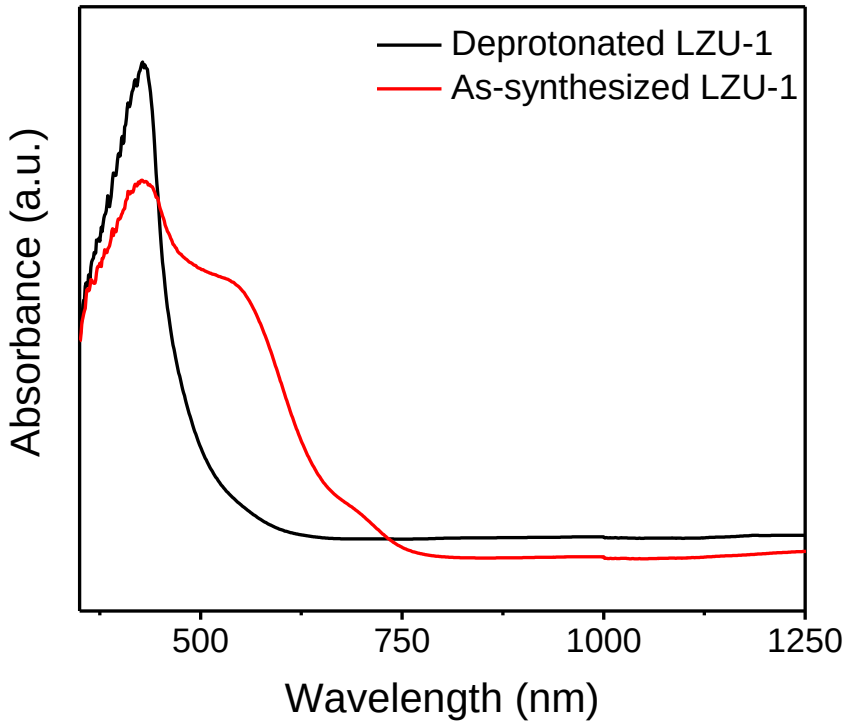

Figure 2.1. UV-Vis spectra of as-synthesized (protonated) and washed (deprotonated) LZU-1 nanocrystals.

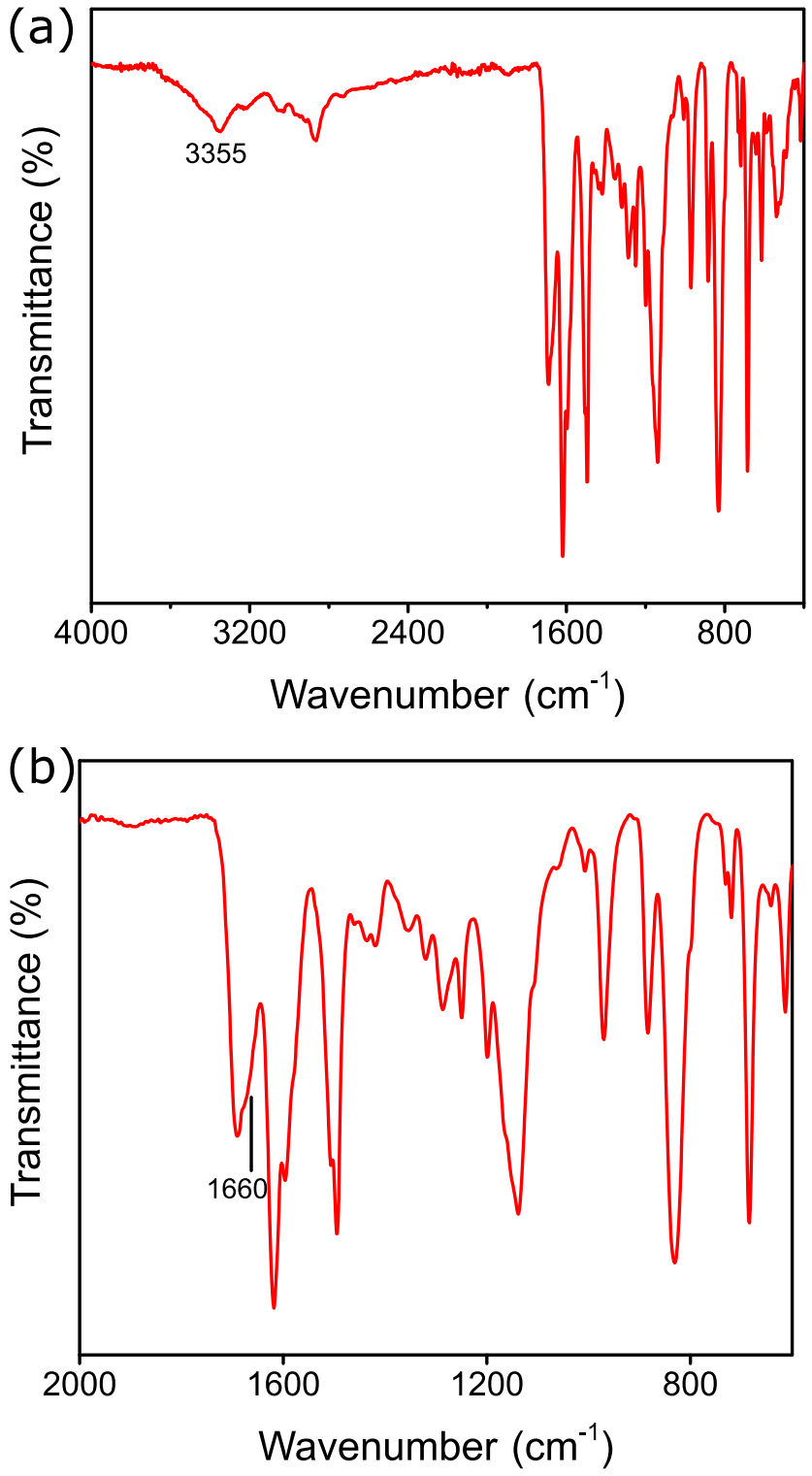

Figure 2.2. FT-IR spectra of as-synthesized COF-LZU-1 nanoparticle. The absorption band at 3355 cm^{-1} is attributed to N-H stretching and absorption at 1660 cm^{-} is attributed to $C=NH^{+}$ stretching. The stretching vibration at 1685 cm^{-1} is attributed to C=O in PVP.

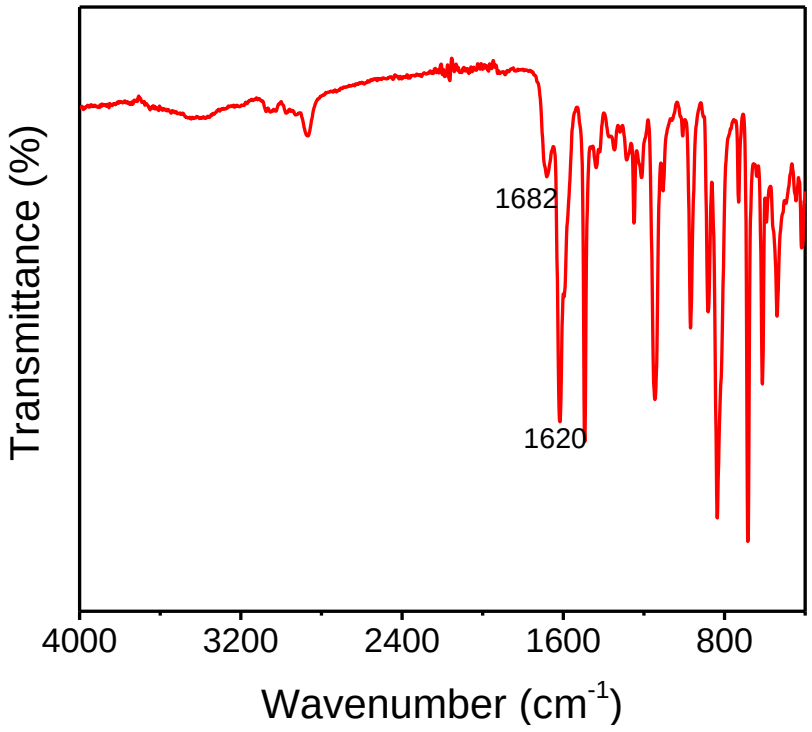

Figure 2.3. FT-IR spectrum of deprotonated COF-LZU-1 nanoparticles. The vibrational modes observed are consistent with the original report. Absorption at 1620 cm^{-1} results from the typical C=N stretching and that of 1682 cm^{-1} is attributed to C=O groups in PVP.

The concentration and molecular weight of PVP has a strong impact on the resulted COF nanoparticles. The optimal nanocrystal morphology can be obtained by 'matching' the PVP molecular weight with the desired particle size (essentially determined by the PVP concentration). The size of these nanocrystals can be tuned through the concentration of PVP: While 5 mg/mL PVP (M_w. = 360,000) gave 500 ± 52 nm COF particles (Figure 2.4a and b), 10 mg/mL PVP (M_w. = 360,000) afforded nanocrystals with size of 245 ± 25 nm (Figure 2.4c and d), and 40 mg/mL PVP (M_w. = 10,000) gave crystals of 112 ± 11 nm (Figure 2.4e and f). The size and morphology of the LZU-1 nanocrystals were characterized by SEM.

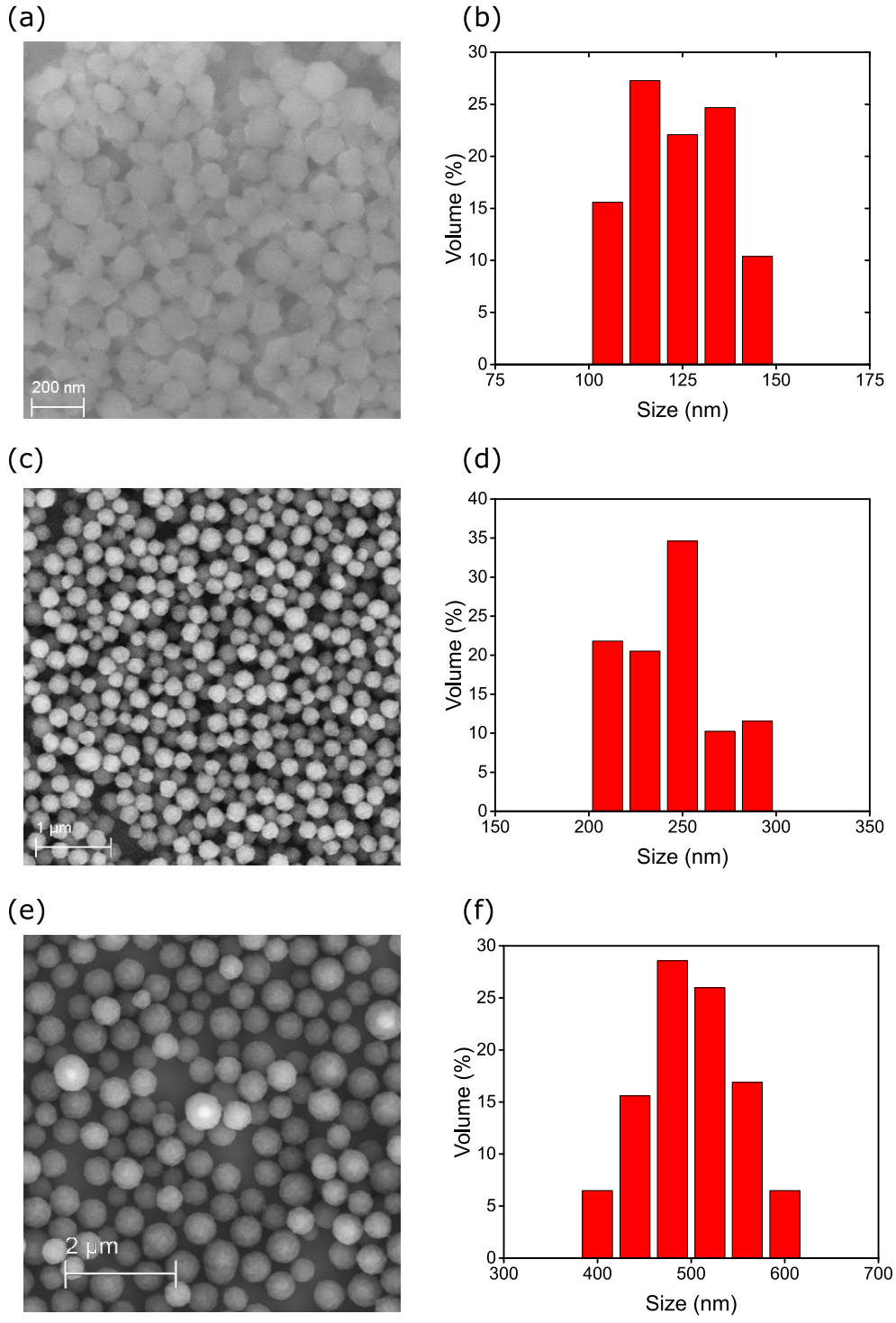

Figure 2.4. SEM and size distribution of LZU-1 nanocrystals. The size of monodisperse LZU-1 nanocrystals can be controlled from 112 ± 11 nm (a and b), 245 ± 25 nm (c and d), to 500 ± 52 nm (e and f) by altering the concentration of PVP. From the size distributions, it is clear that these particles are monodisperse (b, d and f).

Growth solvent of nanoparticle synthesis also plays an important role in determining the morphology. For example, with 1 mL toluene and ethanol mixture, a toluene fraction beyond 0.6 mL resulted in aggregated COFs, as the solution was not polar enough to dissolve PVP and disperse the polar nanocrystals; a toluene fraction between 0.6-0.3 mL usually afforded a clear solution or very low COF yield, since toluene behaved as an inhibitor of COF growth; only a toluene fraction below 0.3 mL yielded the hexagonal morphology of COF nanocrystals (Figure 2.5).

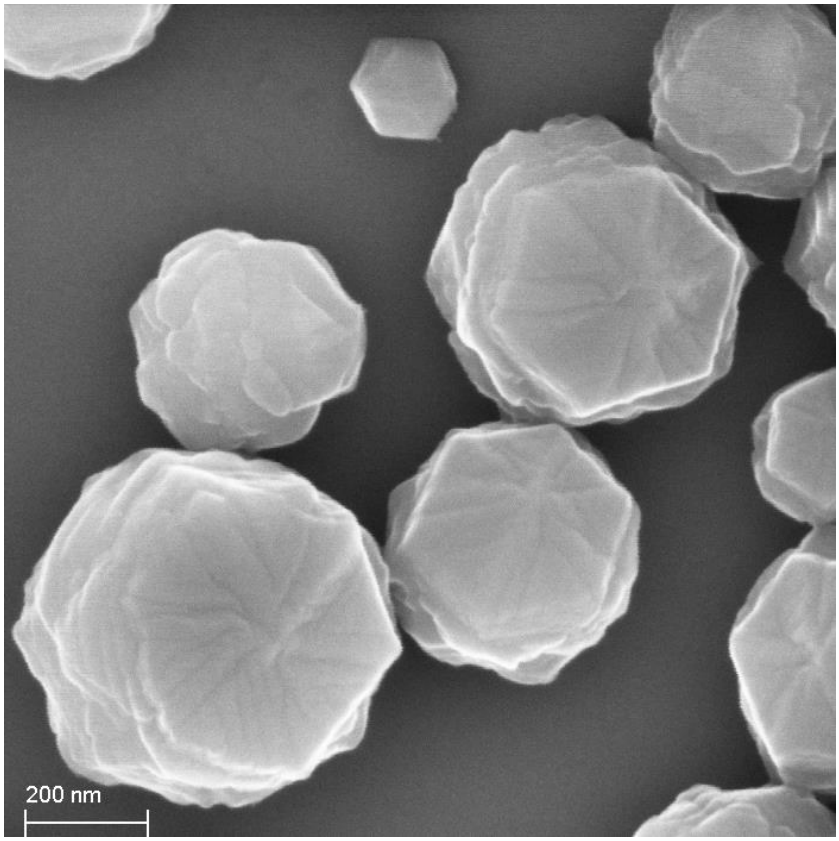

Figure 2.5. Hexagonal-shaped LZU-1 nanocrystals can be obtained by tuning the ratio of toluene in the growth solution.

The high crystallinity of these particles was confirmed by PXRD, and the resulting diffraction pattern was consistent with the simulated one (Figure 2.6). These particles were highly dispersible in polar solvents such as ethanol, methanol, and *N*,*N*-dimethylformamide, and they remained colloidally stable for weeks (Figure 2.7). High resolution TEM images further substantiated the crystallinity of the nanocrystals, where the 2.2 nm hexagonal pores of the LZU-1 nanocrystals were clearly observed (Figure 2.8).

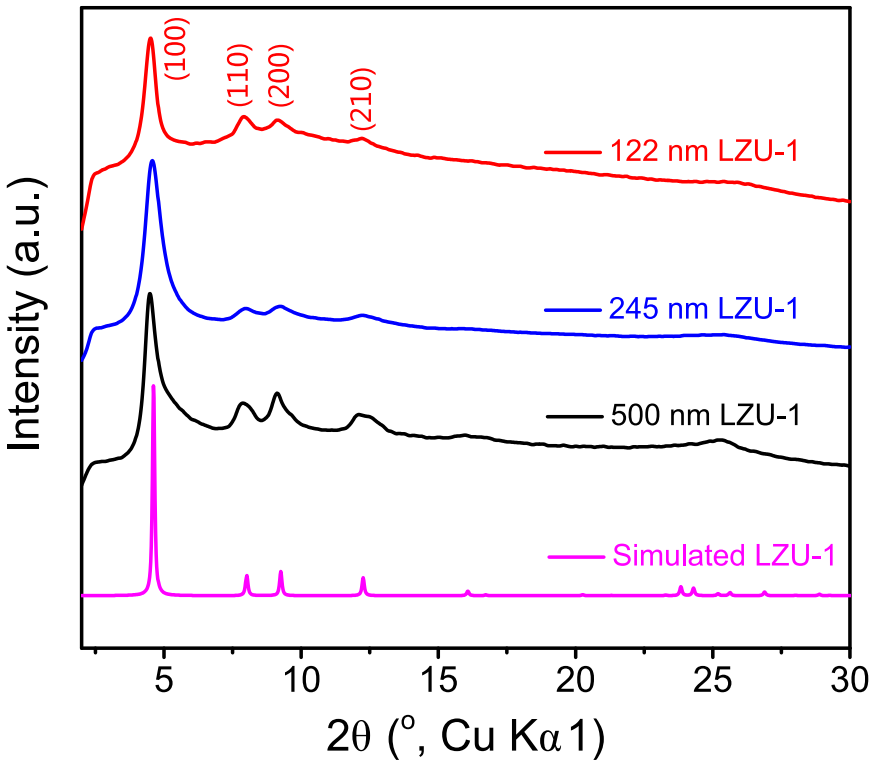

Figure 2.6. PXRD of COF-LZU-1 nanoparticles with different sizes, showing the high crystallinity the particles.

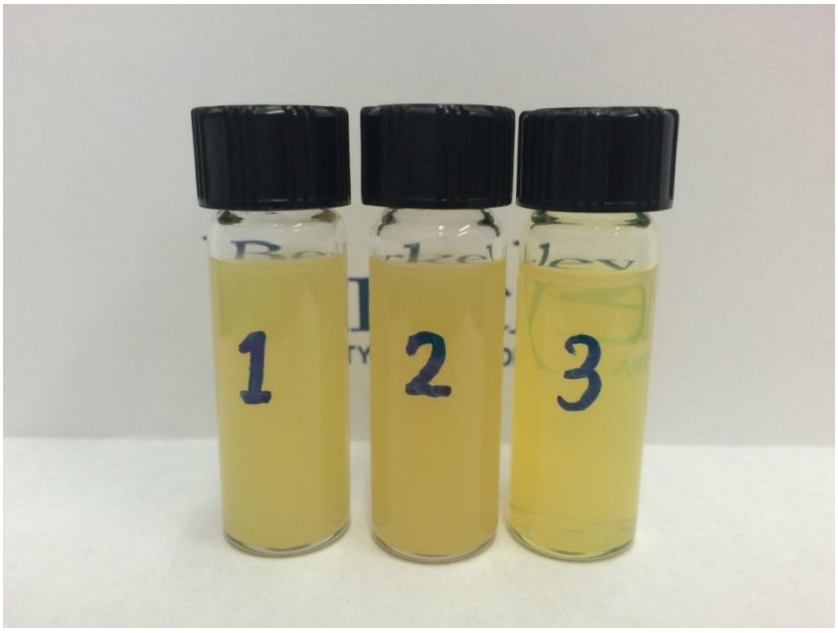

Figure 2.7. COF-LZU-1 nanoparticles dispersed in EtOH, where **1** for size of 112 nm, **2** for size of 245 nm, and **3** for size of 500 nm.

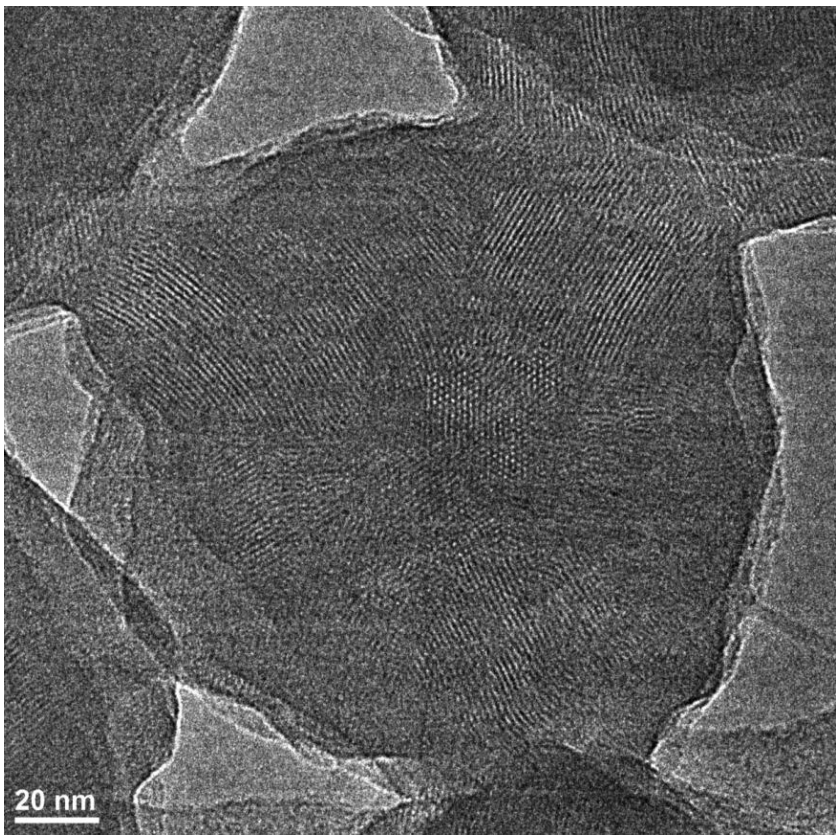

Figure 2.8. High resolution TEM revealed that LZU-1 nanocrystals were consist of several crystalline domains, as both one-dimensional channels (2.2 nm wide, perpendicular to electron beam) and hexagonal pores (2.2 nm diameter, parallel to electron beam) were observed in one particle.

Prepared LZU-1 nanocrystals displayed a high surface area of 729 m^2/g (Figure 2.9), which is more than 1.5 times that of the original report (457 m^2/g). This indicates that COF materials synthesized with this method have fewer structural defects.

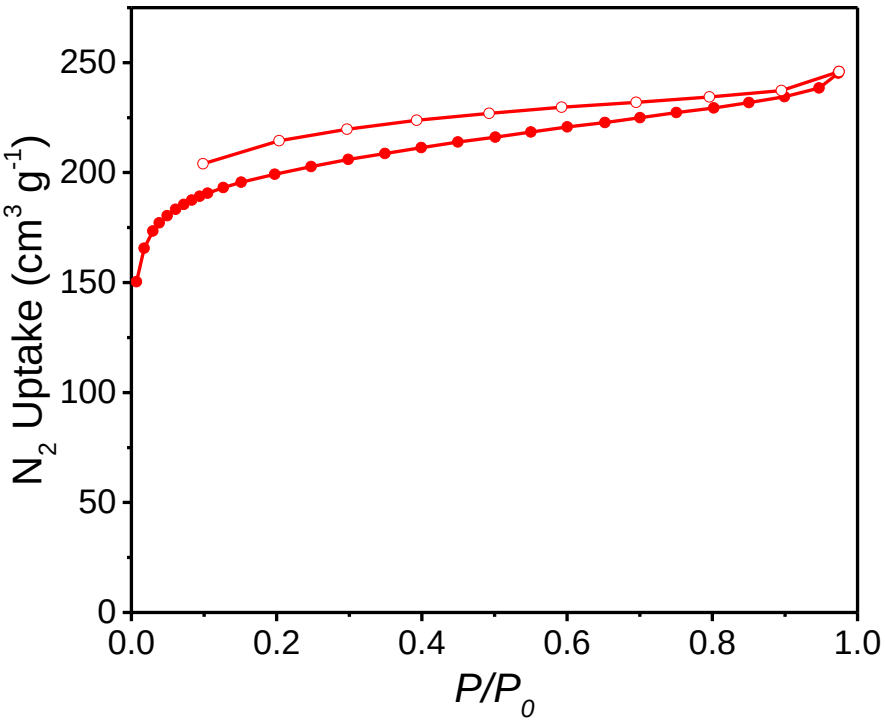

Figure 2.9. N_2 isotherm of 250 nm LZU-1 nanocrystals acquired at 77K.

2.3.2 Synthesis and Characterization of Other COF Nanoparticles

The homogenous synthetic method to produce COF nanocrystals developed here is highly generalizable. Two different COFs, Por-COF and TFPB-PDA COF, were successfully synthesized as monodisperse nanocrystals following this method (Scheme 2.2 and 2.3). The uniform morphology of the nanoparticles was confirmed by SEM images (Figure 2.10), and the crystallinity was confirmed by PXRD (Figure 2.11 and 2.12).

Scheme 2.2. Synthesis of Por-COF nanocrystals.

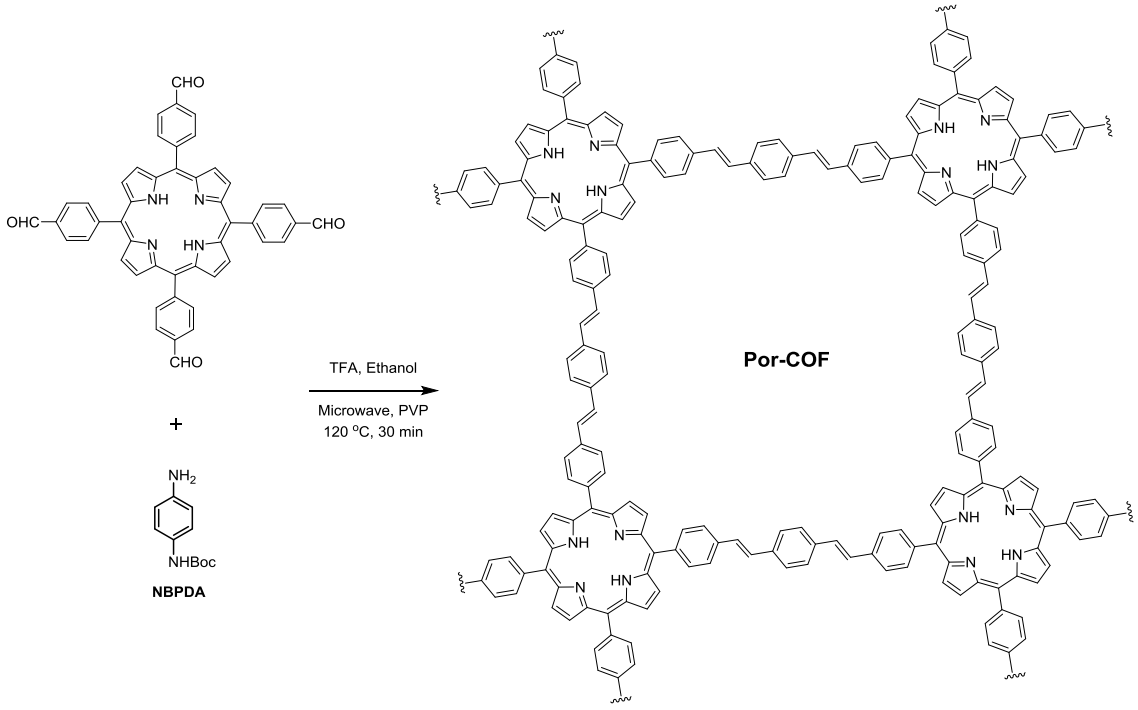

Scheme 2.3. Synthesis of TFPB-PDA COF nanocrystals.

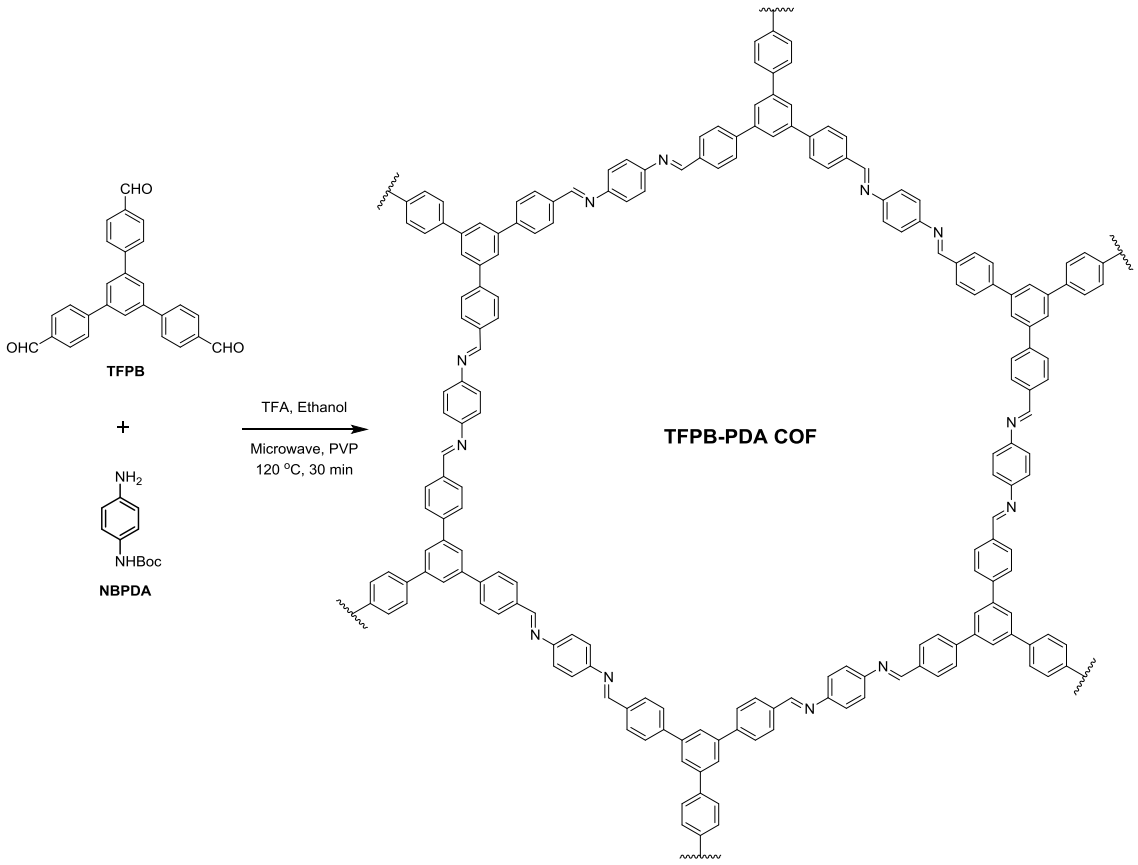

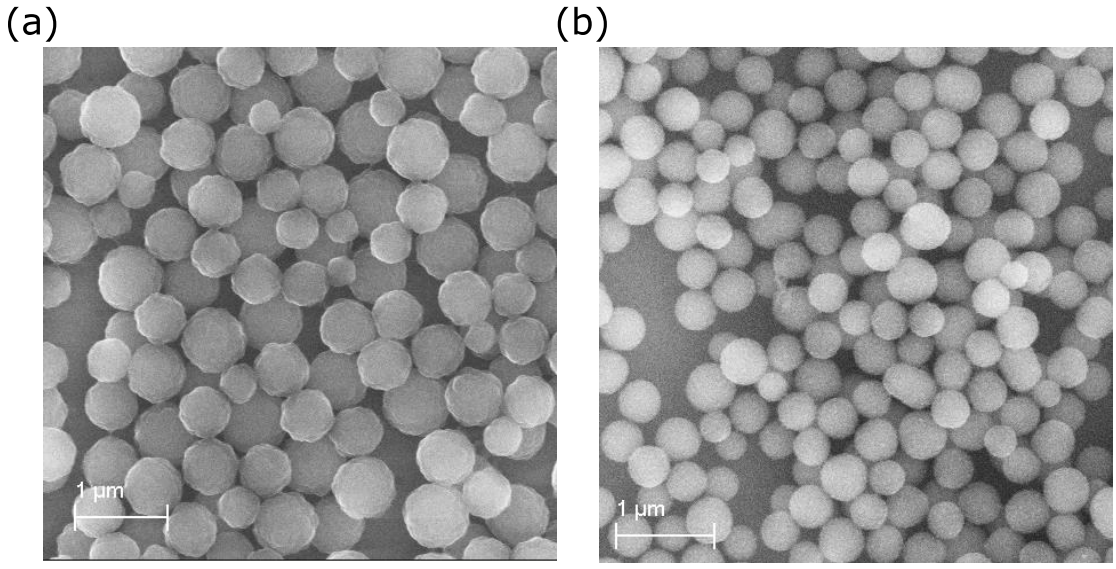

Figure 2.10. SEM images of (a) Por-COF and (b) TFPB-PDA COF nanoparticles.

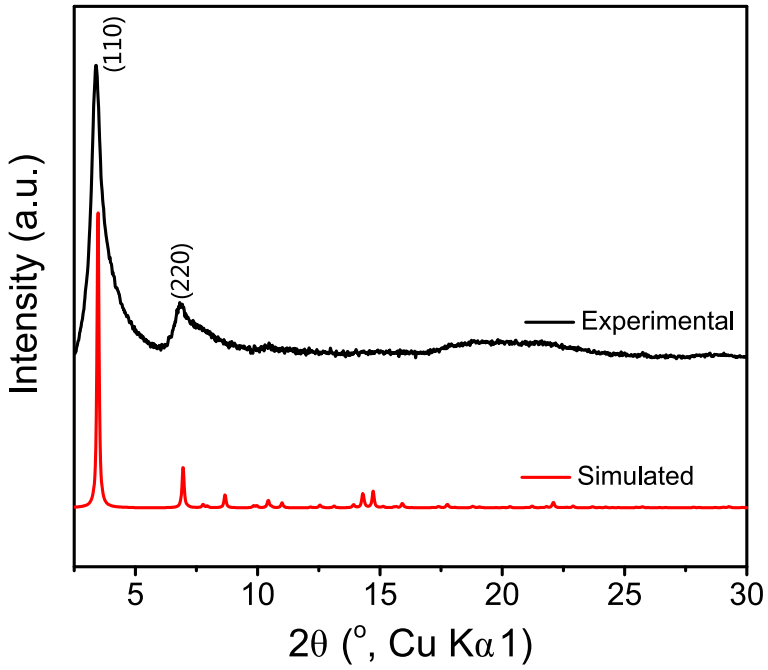

Figure 2.11. Simulated and experimental PXRD patterns of Por-COF nanoparticles.

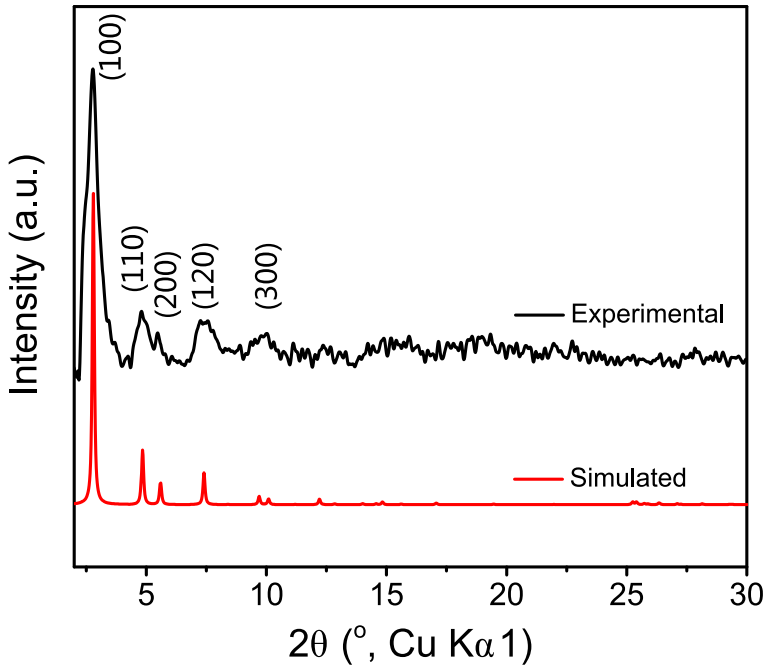

Figure 2.12. Simulated and experimental PXRD patterns of TFPB-PDA COF nanoparticles.

2.3.3 Applications of COF Nanoparticles

The successful synthesis of COF nanoparticles enables further processing and fabrication of these materials. For instance, uniform and porous COF nanocrystals can be used as well-defined processable building blocks in the preparation of COF-based mixed-matrix membranes, where PVDF and LZU-1 nanocrystals were dissolved or suspended in DMF and casted into free-standing thin films (Figure 2.13). As the COF nanoparticles were smaller than the wavelength of visible light, the membrane was transparent. SEM images of the membrane showed that COF nanoparticles maintained their uniform morphology and were encapsulated by PVDF fiber (Figure 2.14). The membrane also retained the porosity of the COF nanoparticles, as was confirmed by the N_2 uptake isotherm (Figure 2.15). The lower observed porosity resulted from the inclusion of the non-porous PVDF binder in the membrane.

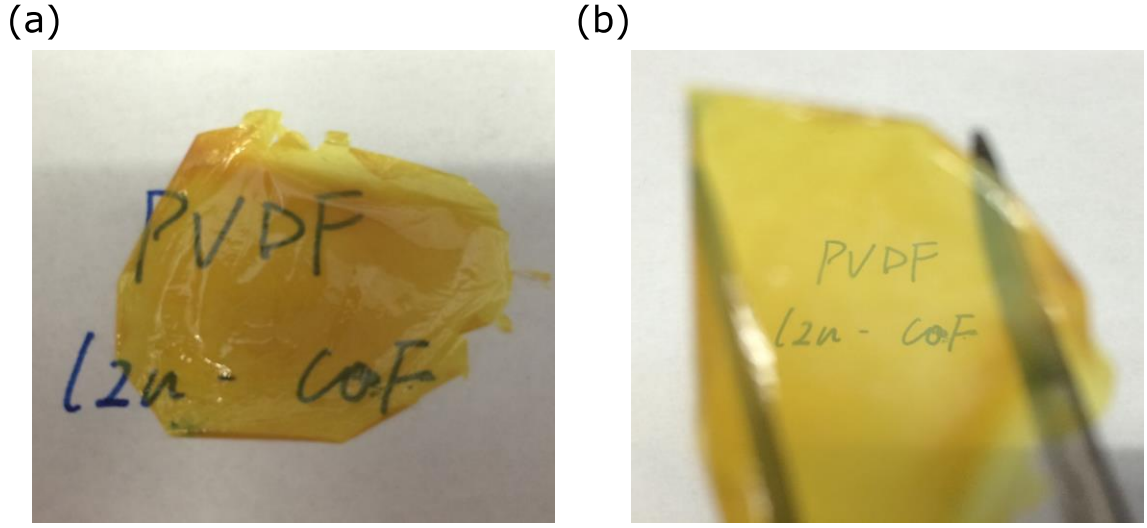

Figure 2.13. Images of COF-based mixed-matrix membranes. The membrane is transparent and free-standing.

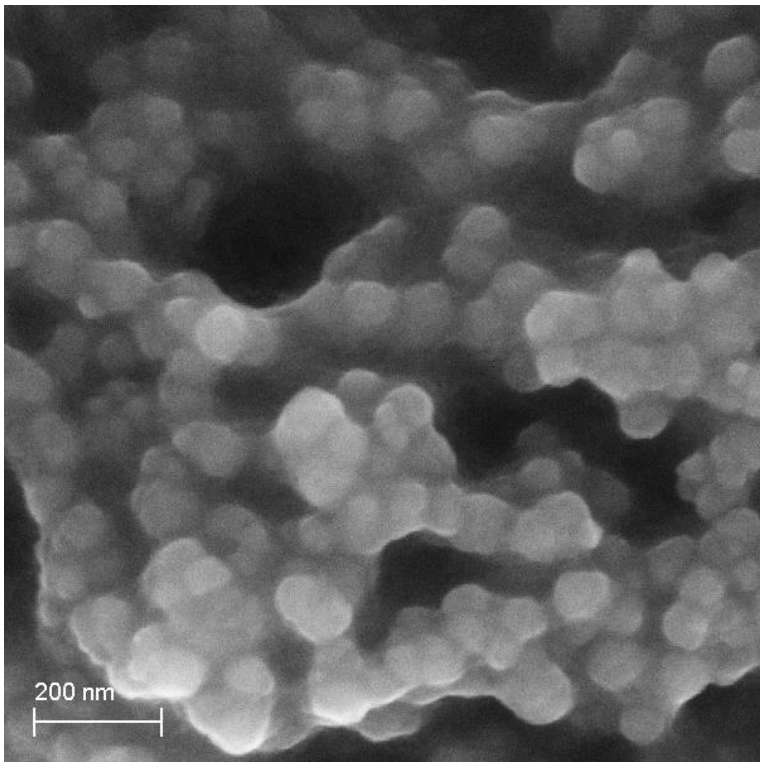

Figure 2.14. SEM image of COF-based mixed-matrix membrane.

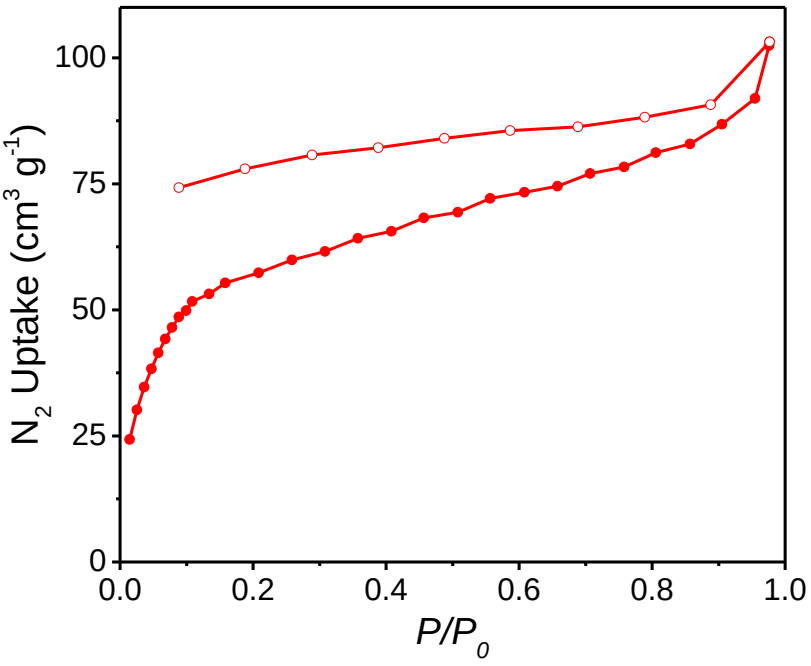

Figure 2.15. N_2 isotherm of COF-based mixed-matrix membrane.

2.4 Conclusion

In this chapter, a homogeneous synthetic route has been disclosed, where crystallites emerge from clear solutions without forming amorphous polyimine precipitates. The key feature of this route is the utilization of *tert*-butyloxycarbonyl (Boc) protected amine building blocks which are deprotected *in situ* and gradually nucleate to form a crystalline framework. This synthetic approach leads to the successful synthesis of monodisperse COF nanoparticles which maintain high crystallinity and porosity. The obtained COF nanoparticles can be further used as well-defined building blocks to form transparent porous mix-matrix membranes. This strategy holds promise for precise control over COF nucleation and crystal growth, and sheds light on the synthesis of COF materials with targeted morphology.

2.5 References

(1) Jiang, J.; Zhao, Y.; Yaghi, O. M. Covalent Chemistry beyond Molecules. *J. Am. Chem. Soc.* **2016**, *138* (10), 3255–3265.

(2) Umemura, A.; Diring, S.; Furukawa, S.; Uehara, H.; Tsuruoka, T.; Kitagawa, S. Morphology Design of Porous Coordination Polymer Crystals by Coordination Modulation. *J. Am. Chem. Soc.* **2011**, *133* (39), 15506–15513.

(3) Kuo, C.-H.; Tang, Y.; Chou, L.-Y.; Sneed, B. T.; Brodsky, C. N.; Zhao, Z.; Tsung, C.-K. Yolk–Shell Nanocrystal@ZIF-8 Nanostructures for Gas-Phase Heterogeneous Catalysis with Selectivity Control. *J. Am. Chem. Soc.* **2012**, *134* (35), 14345–14348.

(4) Lausund, K. B.; Nilsen, O. All-Gas-Phase Synthesis of UiO-66 through Modulated Atomic Layer Deposition. *Nat. Commun.* **2016**, *7*, 13578.

(5) Zhao, Y.; Kornienko, N.; Liu, Z.; Zhu, C.; Asahina, S.; Kuo, T.-R.; Bao, W.; Xie, C.; Hexemer, A.; Terasaki, O.; et al. Mesoscopic Constructs of Ordered and Oriented Metal–Organic Frameworks on Plasmonic Silver Nanocrystals. *J. Am. Chem. Soc.* **2015**, *137* (6), 2199–2202.

(6) Cavka, J. H.; Jakobsen, S.; Olsbye, U.; Guillou, N.; Lamberti, C.; Bordiga, S.; Lillerud, K. P. A New Zirconium Inorganic Building Brick Forming Metal Organic Frameworks with Exceptional Stability. *J. Am. Chem. Soc.* **2008**, *130* (42), 13850–13851.

(7) Furukawa, H.; Cordova, K. E.; O'Keeffe, M.; Yaghi, O. M. The Chemistry and Applications of Metal-Organic Frameworks. *Science* **2013**, *341* (6149), 1230444–1230444.

(8) Rungtaweevoranit, B.; Zhao, Y.; Choi, K. M.; Yaghi, O. M. Cooperative Effects at the Interface of Nanocrystalline Metal–Organic Frameworks. *Nano Res.* **2016**, *9* (1), 47–58.

(9) Smith, B. J.; Overholts, A. C.; Hwang, N.; Dichtel, W. R. Insight into the Crystallization of Amorphous Imine-Linked Polymer Networks to 2D Covalent Organic Frameworks. *Chem. Commun.* **2016**, *52* (18), 3690–3693.

(10) Uribe-Romo, F. J.; Hunt, J. R.; Furukawa, H.; Klöck, C.; O'Keeffe, M.; Yaghi, O. M. A Crystalline Imine-Linked 3-D Porous Covalent Organic Framework. *J. Am. Chem. Soc.* **2009**, *131* (13), 4570–4571.

(11) Xu, H.; Gao, J.; Jiang, D. Stable, Crystalline, Porous, Covalent Organic Frameworks as a Platform for Chiral Organocatalysts. *Nat. Chem.* **2015**, *7* (11), 905–912.

(12) Popp, N.; Homburg, T.; Stock, N.; Senker, J. Porous Imine-Based Networks with Protonated Imine Linkages for Carbon Dioxide Separation from Mixtures with Nitrogen and Methane. *J. Mater. Chem. A* **2015**, *3* (36), 18492–18504.

Chapter III. Synthesis of Highly Oriented COF Thin Films

3.1 Introduction

As an emerging class of materials, COFs have attracted much attention due to their intriguing structural merits.[1] However, the insoluble and unprocessable features of bulk COF powders have severely limited the practical application of such materials.[2] To address this challenge, many efforts have been devoted to the synthesis of thin films of two-dimensional COFs.[3–5] The diverse organic functionalities of COF films as well as their tunable morphology have endowed these materials with exceptional properties in the areas of energy storage,[6–12] membrane separation,[13–15] sensors,[16,17] and catalysts.[18–20]

The formation of COF thin film can be approached by either top-down or bottom-up strategy. In the top-down approach, COF thin films can be accessed by exfoliating COF crystallites into layered nets by soniation[21,22] or mechanical delamination.[23] This physical approach can be broadly applied to a wide range of COF materials, since it does not require any structural or chemical features of the materials. However, COF thin films obtained by this approach often have a wide distribution of thicknesses. Alternatively, COF thin films can be obtained by chemical exfoliation, where bulky substituents are introduced to the frameworks to set the layers apart and break the π-π interactions.[24] In this context, the thickness of the thin film can be carefully controlled, but specific functionalities are required to carry out such chemical transformation.

Another powerful approach to access COF thin films is the bottom-up strategy. In this method, the synthesis is carried out with a substrate introduced to the reaction system. COF thin films will nucleate and grow on the substrate, along with the formation of free bulky COF powders.[25] The advantage of this method is that it is applicable to a wide range of COF materials. On the other hand, the disadvantages are also obvious: there is little control over the thickness of the resulting film, and COF precipitates will form concurrently and contaminate the film.

To overcome this limitation, it is important to carefully control the rate of COF growth and avoid the formation of COF precipitates. Synthesis of imine COFs are generally conducted in heterogeneous suspensions.[26] Under these conditions, acids are preferred to increase the reversibility of imine bond formation and shorten reaction time, but at the

---

• Portions of this chapter have been previously published in:
Zhao, Y.*; Guo, L.*; Gándara, F.; Ma, Y.; Liu, Z.; Zhu, C.; Lyu, H.; Trickett, C. A.; Kapustin, E. A.; Terasaki, O.; Yaghi, O. M. A Synthetic Route for Crystals of Woven Structures, Uniform Nanocrystals, and Thin Films of Imine Covalent Organic Frameworks. *J. Am. Chem. Soc.* **2017**, *139* (37), 13166–13172.
*These authors contributed equally to this work.

same time, they also result in the formation of amorphous precipitates, altering the concentration of the growth solution and introducing undesired powder contamination onto the surface of the film. This heterogeneous nature of imine COF synthesis severely limits our access to high quality COF thin films. To address this challenge, a generalized homogeneous imine COF thin film synthesis is in high demand. In this context, the concentration of the starting materials in the growth solutions can be well-tuned by carefully altering reaction conditions, therefore allowing for control over the thickness of the obtained thin films.

3.2 Experimental Section

3.2.1 Methods and Materials

Chemicals. *p*-Phenylenediamine (PDA, purity ≥ 99 %), ethanol (anhydrous, purity ≥ 99.5 %), and triethylamine (TEA, purity ≥ 99.5 %) were obtained from Sigma-Aldrich. 1,3,5-Triformylbenzene (TFB, purity ≥ 98 %), 4-(*tert*-butoxycarbonylamino)-aniline (NBPDA, purity ≥ 97 %), and acetone (anhydrous, purity ≥ 99.8 %) were acquired from Acros Organics. Toluene (anhydrous purity ≥ 99.8%), glacial acetic acid (purity 100%), and trifluoroacetic acid (TFA, purity ≥ 99.7 %) were supplied from EMD Millipore Chemicals.

All reactions were performed under ambient laboratory conditions, and no precautions taken to exclude atmospheric moisture, unless otherwise specified.

Analytical techniques and instrument. Powder X-ray diffraction (PXRD) patterns were recorded using a Rigaku Miniflex 600 (Bragg-Brentano geometry, Cu K_α radiation λ = 1.54 Å) instrument. Attenuated total reflectance (ATR) FTIR spectra of neat samples were performed on a Bruker ALPHA Platinum ATR-FTIR Spectrometer equipped with a single reflection diamond ATR module. Scanning electron microscope (SEM) images were recorded on a Zeiss Gemini Ultra-55 analytical scanning electron microscope with accelerating voltage of 5 kV. Grazing-Incidence Wide-Angle X-ray Scattering (GIWAXS) patterns were acquired with a Pilatus 2 M (Dectris) instrument on beamline 7.3.3 at the ALS (λ = 1.24 Å). The incidence angle was held at 0.120° to optimize signal collection. Silver behenate was used for calibration. The Nika package for IGOR Pro (Wavemerics) was used to reduce the acquired 1D raw data to a 2D format.

3.2.2 Synthesis of COF-LZU-1 Thin Film

Synthesis of LZU-1 thin films with 190 nm thickness. The growth of LZU-1 thin film was realized by suspending the substrate into a heated growth solution at 100 ℃ for 1.5 h. The growth solution was prepared by dissolving TFB (5 mg, 0.03 mmol) and

NBPDA (10 mg, 0.05 mmol) in a solvent mixture of 2.25 mL toluene, 0.75 mL dioxane, and 0.6 mL TFA. The as-prepared thin films were washed with dioxane/TEA mixture and dried under a stream of nitrogen.

Synthesis of LZU-1 thin films with 260 nm thickness and 400 nm thickness. The synthesis of LZU-1 thin films with 260 nm and 400 nm thickness was carried out in a similar manner to that of thin films with 190 nm thickness. The reaction time was altered to 3 h and 6 h, respectively, to obtain thicker films.

3.3 Results and Discussion

COF-LZU-1 thin films can be synthesized on silicon substrates in hydrophobic aromatic solutions (Scheme 3.1). The LZU-1 thin films were synthesized by submerging the substrate in the growth solution for a given time, ranging from 1.5 h to 6 h at 100 ℃. The growth solution was prepared by dissolving NBPDA and TFB in 2.25 mL toluene, 0.75 mL dioxane, and 0.6 mL TFA. The high concentration of TFA is crucial to the formation of the film. Under these conditions, COF nanocrystals formed homogeneously and carried positive charge due to the protonation of their imine moieties, which favored their nucleation on the polar oxides (substrates and walls of the glassware). This resulted in the selective growth of COF thin films on the substrates (Figure 3.1).

Scheme 3.1. Synthetic scheme of COF-LZU-1 thin films.

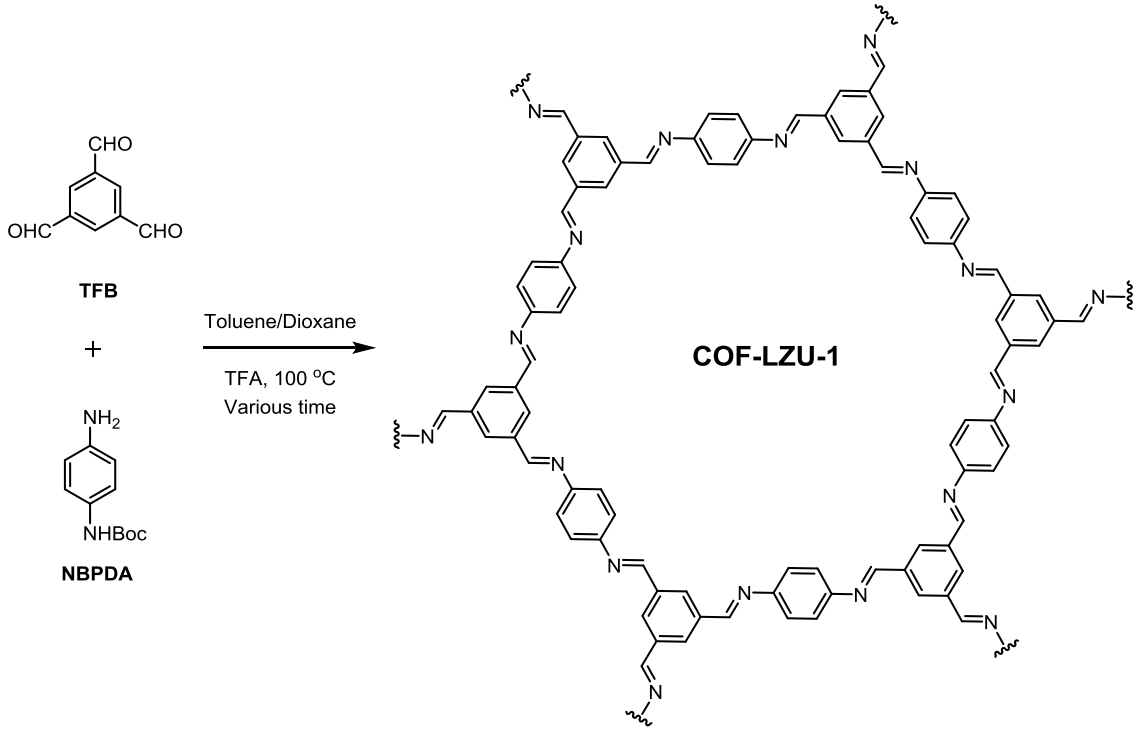

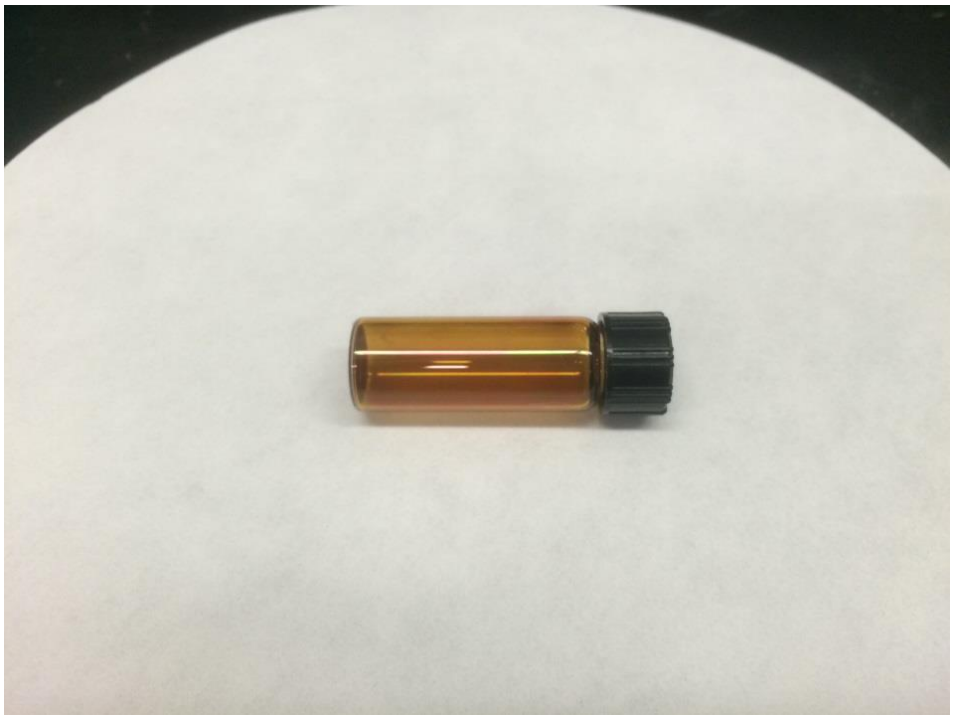

Figure 3.1. COF-LZU-1 thin film coated uniformly on the wall of the reaction vial.

The morphology of COF thin films was clearly observed at the edge of the substrate by SEM where the film was partially detached (Figure 3.2). Higher magnification SEM images revealed that the film was composed of the small crystallites with potentially similar orientation (Figure 3.3).

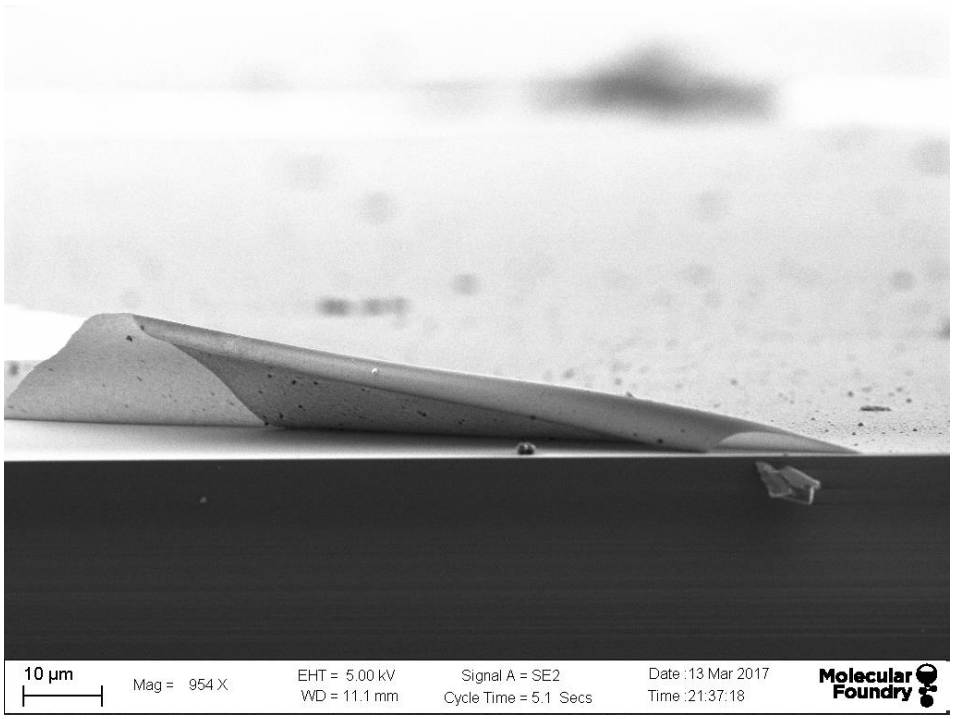

Figure 3.2. Uniform LZU-1 COF thin film formed on the silicon substrate.

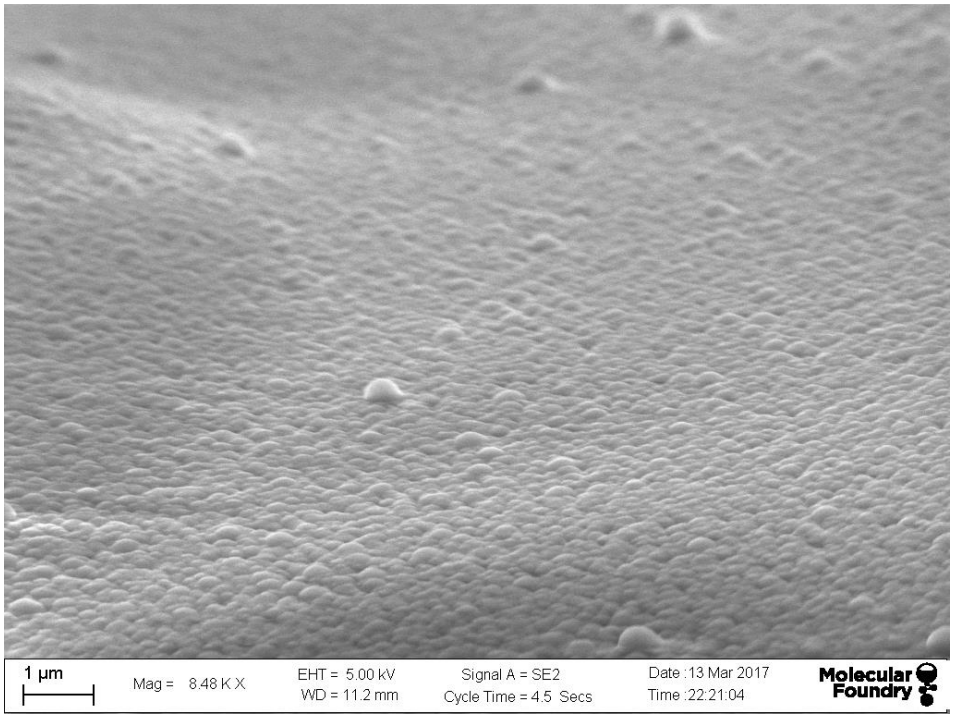

Figure 3.3. High magnification SEM image showing the obtained COF thin film was composed of small crystallites with similar orientation.

The crystallinity and orientation of the film were further characterized by Grazing-Incidence Wide-Angle X-ray Scattering (GIWAXS) measurements. This experiment showed that the crystallographic *c* axis runs perpendicular to the substrate (Figure 3.4). The derived diffraction pattern from GIWAXS measurement is consistent with the powder X-ray diffraction pattern of reported COF-LZU-1 powders.

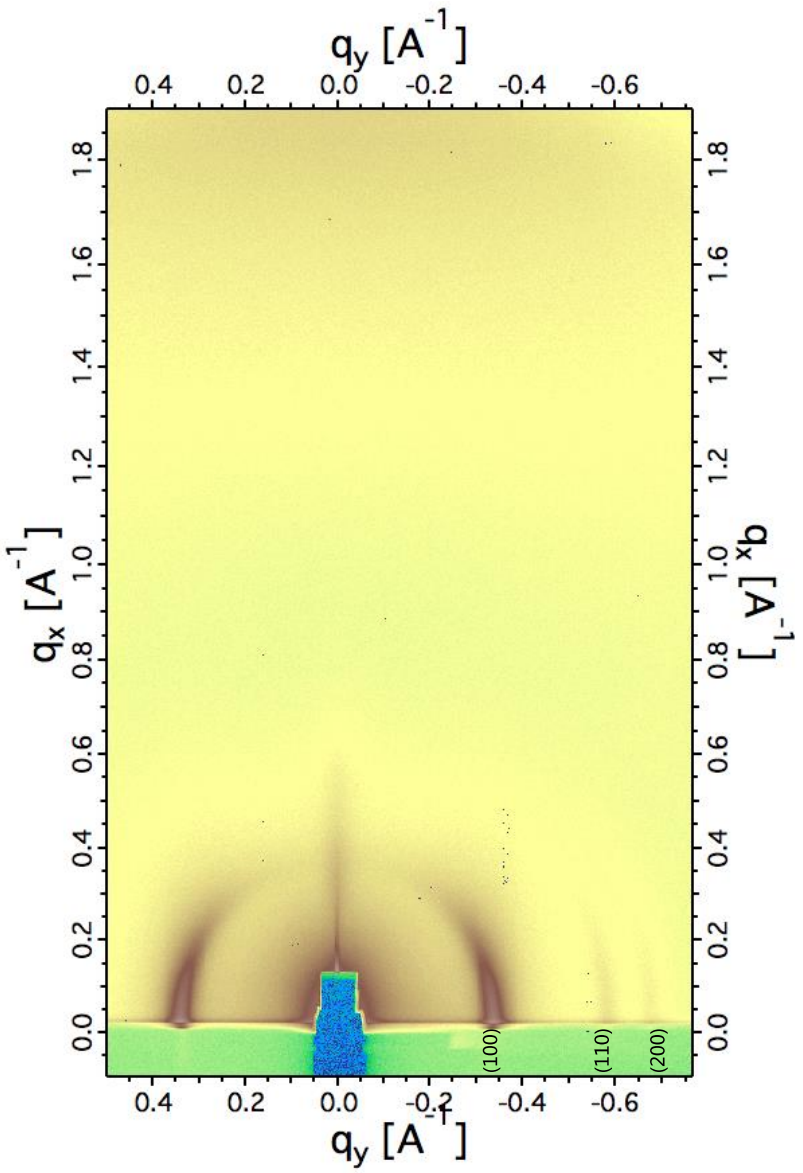

Figure 3.4. The crystallinity and orientation of the obtained COF thin film was confirmed by GIWAXS.

The thickness of the film can be tuned empirically by changing reaction time and the concentration of the growth solution. Longer reaction time will result in thicker films. For example, films with thickness of 190 nm were obtained by heating the growth solution for

1.5 h, films with thickness of 260 nm for 3 h, and films with thickness of 400 nm for 6 h. The thickness of the film was directly measured by cross-section SEM (Figure 3.5-3.7) and was also reflected by the color of the coated film as a result of thin film interference (Figure 3.8). It is interesting to note that modifying the amount of acid and temperature does not change the film thickness significantly.

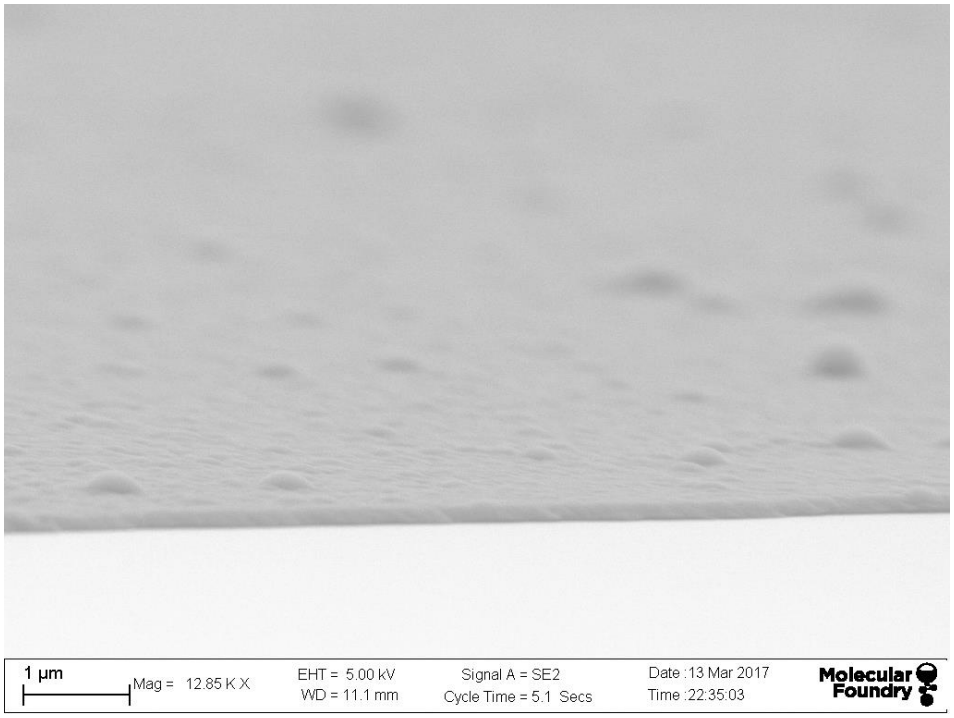

Figure 3.5. Cross-section SEM image of a COF thin film with a thickness of 190 nm.

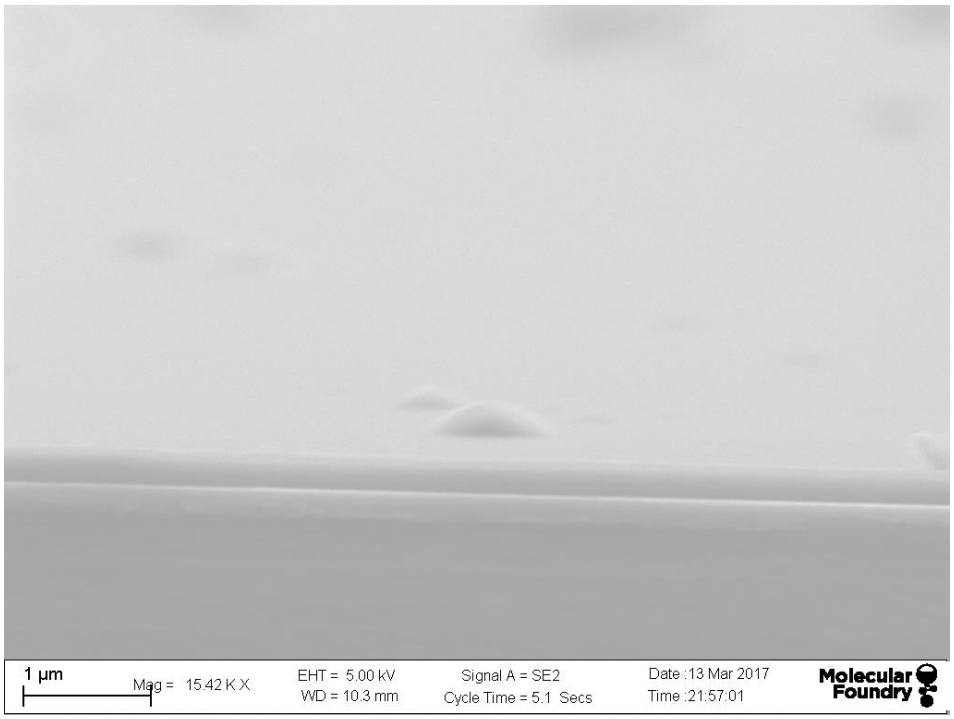

Figure 3.6. Cross-section SEM image of a thin film with thickness of 260 nm.

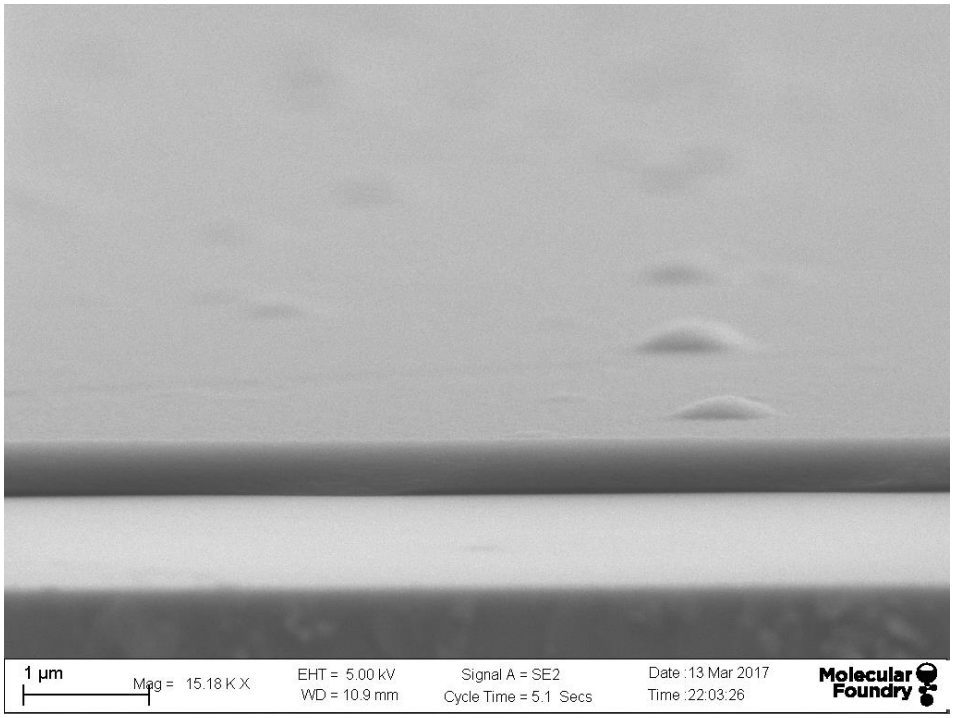

Figure 3.7. Cross-section SEM image of a thin film with thickness of 400 nm.

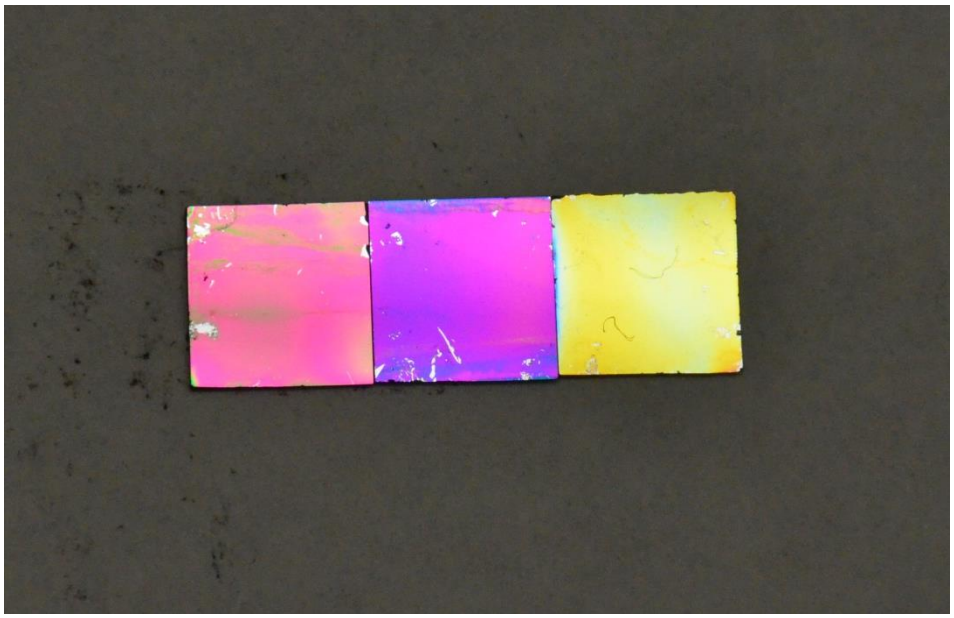

Figure 3.8. The difference in thickness of the thin films can be seen in the color of the coated silicon substrates. From left to right, the thicknesses of the films are 190 nm, 260 nm, and 400 nm, respectively.

It is also important to point out that in the synthesis of COF thin films, the substrate needs to be placed face-down in the solution to avoid collecting precipitated COF nuclei after prolonged heating. Besides, as-prepared thin films need to be immediately washed with slightly basic dioxane and ethanol solutions with small amounts of TEA added, and stored under inert atmosphere. The high concentration of TFA in the synthesis will remain on the surface of the as-synthesized thin films and will still function as a catalyst for the reversible imine bond formation. Exposing the unwashed films to ambient conditions would diminish the crystallinity of the film.

The high quality of the COF thin film gives rise to interesting chemical sensitive optical properties that indicate the porosity of these thin films. When COF thin films were exposed to organic vapor, a color change of the films occurred (Figure 3.9). This is a result of the change of overall refractive index upon adsorption of organic vapor, and this process is highly reversible, as when the vapor is removed, the color change is reversed. This phenomenon indicates the accessible porosity of the film, and can be best demonstrated by putting the thin film into vials containing organic solvents with different vapor pressures and observing if the film changes its color with respect to the liquid level.

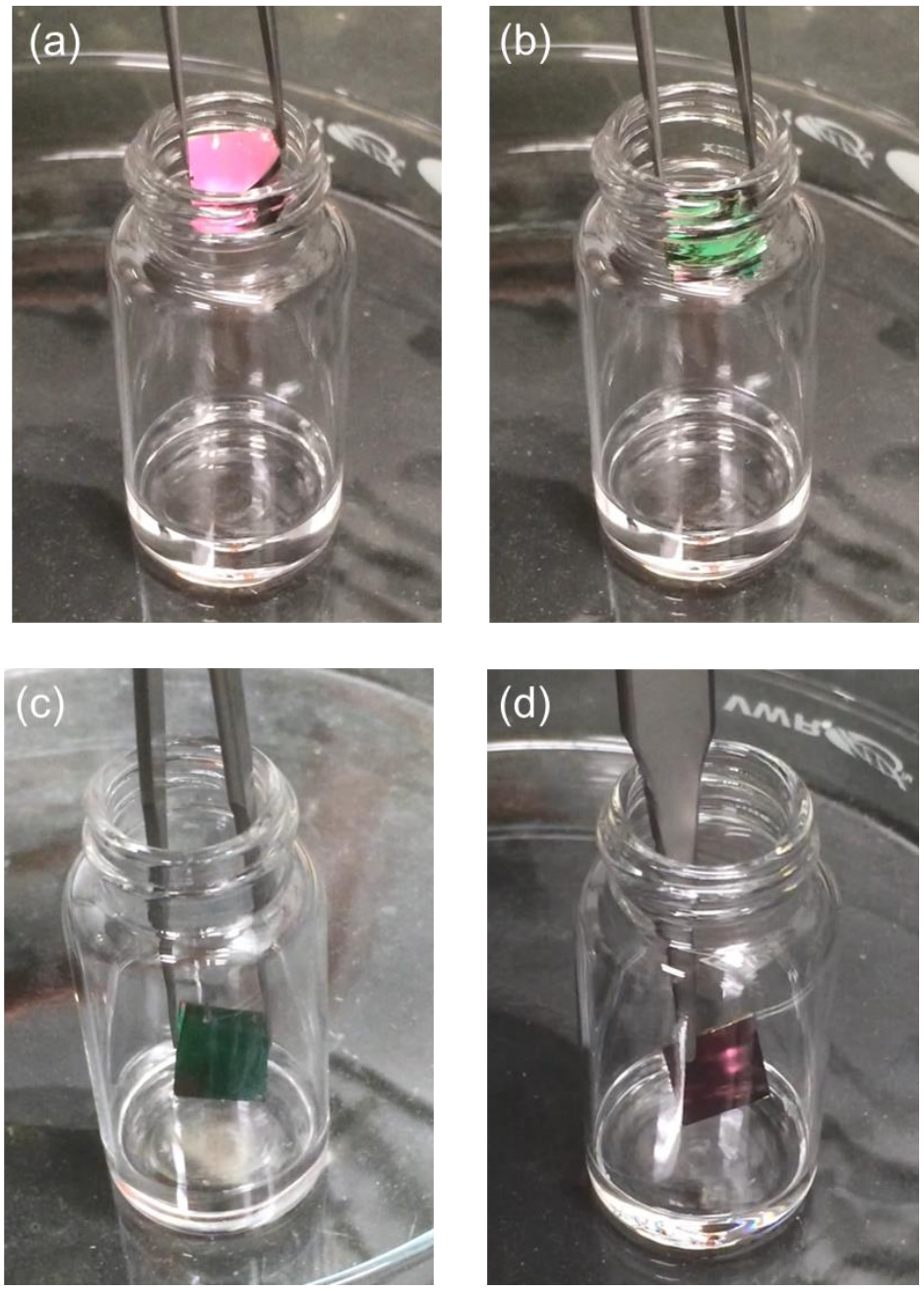

Figure 3.9. Gas adsorption triggered color change in LZU-1 thin film. The film was pink before exposure (a), and turned green after exposed to acetone (b) and methanol (c). As acetone has higher vapor pressure, the film turned green at the top of the vial, while for methanol the film only turned green after being closer to the liquid level. When ethylene glycol (d) was used, the film kept its original color due to the low vapor pressure of the liquid.

3.4 Conclusion

In this chapter, the homogeneous COF growth strategy was applied to successfully obtain unprecedented highly crystalline, oriented, and porous COF thin films. By using Boc-protected amino organic building blocks, COF thin films were able to grow from clear solutions. Highly acidic condition further facilitates the selective growth of thin films on the polar oxides in the reaction system. Smooth COF-LZU-1 thin films with different thicknesses were obtained and their crystallinity was confirmed by GIWAXS measurements. The obtained thin films were highly sensitive to volatile organic compounds. The utility of this thin film synthesis would greatly advance the impact of COF chemistry in optical and electronic applications.

3.5 References

(1) Yaghi, O. M.; Kalmutzki, M. J.; Diercks, C. S. *Introduction to Reticular Chemistry: Metal-Organic Frameworks and Covalent Organic Frameworks*; John Wiley & Sons, 2019.

(2) Kitagawa, S.; Matsuda, R. Chemistry of Coordination Space of Porous Coordination Polymers. *Coord. Chem. Rev.* **2007**, *21–24* (251), 2490–2509.

(3) Colson, J. W.; Woll, A. R.; Mukherjee, A.; Levendorf, M. P.; Spitler, E. L.; Shields, V. B.; Spencer, M. G.; Park, J.; Dichtel, W. R. Oriented 2D Covalent Organic Framework Thin Films on Single-Layer Graphene. *Science* **2011**, *332* (6026), 228–231.

(4) Spitler, E. L.; Colson, J. W.; Uribe‐Romo, F. J.; Woll, A. R.; Giovino, M. R.; Saldivar, A.; Dichtel, W. R. Lattice Expansion of Highly Oriented 2D Phthalocyanine Covalent Organic Framework Films. *Angew. Chem. Int. Ed.* **2012**, *51* (11), 2623–2627.

(5) Zwaneveld, N. A. A.; Pawlak, R.; Abel, M.; Catalin, D.; Gigmes, D.; Bertin, D.; Porte, L. Organized Formation of 2D Extended Covalent Organic Frameworks at Surfaces. *J. Am. Chem. Soc.* **2008**, *130* (21), 6678–6679.

(6) Chen, H.; Tu, H.; Hu, C.; Liu, Y.; Dong, D.; Sun, Y.; Dai, Y.; Wang, S.; Qian, H.; Lin, Z.; et al. Cationic Covalent Organic Framework Nanosheets for Fast Li-Ion Conduction. *J. Am. Chem. Soc.* **2018**, *140* (3), 896–899.

(7) Zha, Z.; Xu, L.; Wang, Z.; Li, X.; Pan, Q.; Hu, P.; Lei, S. 3D Graphene Functionalized by Covalent Organic Framework Thin Film as Capacitive Electrode in Alkaline Media. *ACS Appl. Mater. Interfaces* **2015**, *7* (32), 17837–17843.

(8) Montoro, C.; Rodríguez-San-Miguel, D.; Polo, E.; Escudero-Cid, R.; Ruiz-González, M. L.; Navarro, J. A. R.; Ocón, P.; Zamora, F. Ionic Conductivity and Potential Application for Fuel Cell of a Modified Imine-Based Covalent Organic Framework. *J. Am. Chem. Soc.* **2017**, *139* (29), 10079–10086.

(9) Cai, S.-L.; Zhang, Y.-B.; Pun, A. B.; He, B.; Yang, J.; Toma, F. M.; Sharp, I. D.; Yaghi, O. M.; Fan, J.; Zheng, S.-R.; et al. Tunable Electrical Conductivity in Oriented Thin Films of Tetrathiafulvalene-Based Covalent Organic Framework. *Chem. Sci.* **2014**, *5* (12), 4693–4700.

(10) Feldblyum, J. I.; McCreery, C. H.; Andrews, S. C.; Kurosawa, T.; Santos, E. J. G.; Duong, V.; Fang, L.; Ayzner, A. L.; Bao, Z. Few-Layer, Large-Area, 2D Covalent Organic Framework Semiconductor Thin Films. *Chem. Commun.* **2015**, *51* (73), 13894–13897.

(11) Medina, D. D.; Petrus, M. L.; Jumabekov, A. N.; Margraf, J. T.; Weinberger, S.; Rotter, J. M.; Clark, T.; Bein, T. Directional Charge-Carrier Transport in Oriented

Benzodithiophene Covalent Organic Framework Thin Films. *ACS Nano* **2017**, *11* (3), 2706–2713.

(12) Sun, B.; Zhu, C.-H.; Liu, Y.; Wang, C.; Wan, L.-J.; Wang, D. Oriented Covalent Organic Framework Film on Graphene for Robust Ambipolar Vertical Organic Field-Effect Transistor. *Chem. Mater.* **2017**, *29* (10), 4367–4374.

(13) Kandambeth, S.; Biswal, B. P.; Chaudhari, H. D.; Rout, K. C.; H, S. K.; Mitra, S.; Karak, S.; Das, A.; Mukherjee, R.; Kharul, U. K.; et al. Selective Molecular Sieving in Self-Standing Porous Covalent-Organic-Framework Membranes. *Adv. Mater.* **2017**, *29* (2), 1603945.

(14) Tong, M.; Yang, Q.; Ma, Q.; Liu, D.; Zhong, C. Few-Layered Ultrathin Covalent Organic Framework Membranes for Gas Separation: A Computational Study. *J. Mater. Chem. A* **2015**, *4* (1), 124–131.

(15) Kang, Z.; Peng, Y.; Qian, Y.; Yuan, D.; Addicoat, M. A.; Heine, T.; Hu, Z.; Tee, L.; Guo, Z.; Zhao, D. Mixed Matrix Membranes (MMMs) Comprising Exfoliated 2D Covalent Organic Frameworks (COFs) for Efficient CO2 Separation. *Chem. Mater.* **2016**, *28* (5), 1277–1285.

(16) Das, G.; Biswal, B. P.; Kandambeth, S.; Venkatesh, V.; Kaur, G.; Addicoat, M.; Heine, T.; Verma, S.; Banerjee, R. Chemical Sensing in Two Dimensional Porous Covalent Organic Nanosheets. *Chem. Sci.* **2015**, *6* (7), 3931–3939.

(17) Wang, P.; Kang, M.; Sun, S.; Liu, Q.; Zhang, Z.; Fang, S. Imine-Linked Covalent Organic Framework on Surface for Biosensor. *Chin. J. Chem.* **2014**, *32* (9), 838–843.

(18) Yadav, R. K.; Kumar, A.; Park, N.-J.; Kong, K.-J.; Baeg, J.-O. A Highly Efficient Covalent Organic Framework Film Photocatalyst for Selective Solar Fuel Production from CO2. *J. Mater. Chem. A* **2016**, *4* (24), 9413–9418.

(19) Diercks, C. S.; Lin, S.; Kornienko, N.; Kapustin, E. A.; Nichols, E. M.; Zhu, C.; Zhao, Y.; Chang, C. J.; Yaghi, O. M. Reticular Electronic Tuning of Porphyrin Active Sites in Covalent Organic Frameworks for Electrocatalytic Carbon Dioxide Reduction. *J. Am. Chem. Soc.* **2018**, *140* (3), 1116–1122.

(20) Sick, T.; Hufnagel, A. G.; Kampmann, J.; Kondofersky, I.; Calik, M.; Rotter, J. M.; Evans, A.; Döblinger, M.; Herbert, S.; Peters, K.; et al. Oriented Films of Conjugated 2D Covalent Organic Frameworks as Photocathodes for Water Splitting. *J. Am. Chem. Soc.* **2018**, *140* (6), 2085–2092.

(21) Uribe-Romo, F. J.; Doonan, C. J.; Furukawa, H.; Oisaki, K.; Yaghi, O. M. Crystalline Covalent Organic Frameworks with Hydrazone Linkages. *J. Am. Chem. Soc.* **2011**, *133* (30), 11478–11481.

(22) Bunck, D. N.; Dichtel, W. R. Bulk Synthesis of Exfoliated Two-Dimensional Polymers Using Hydrazone-Linked Covalent Organic Frameworks. *J. Am. Chem. Soc.* **2013**, *135* (40), 14952–14955.

(23) Chandra, S.; Kandambeth, S.; Biswal, B. P.; Lukose, B.; Kunjir, S. M.; Chaudhary, M.; Babarao, R.; Heine, T.; Banerjee, R. Chemically Stable Multilayered Covalent Organic Nanosheets from Covalent Organic Frameworks via Mechanical Delamination. *J. Am. Chem. Soc.* **2013**, *135* (47), 17853–17861.

(24) Khayum, M. A.; Kandambeth, S.; Mitra, S.; Nair, S. B.; Das, A.; Nagane, S. S.; Mukherjee, R.; Banerjee, R. Chemically Delaminated Free-Standing Ultrathin Covalent Organic Nanosheets. *Angew. Chem. Int. Ed.* **2016**, *55* (50), 15604–15608.

(25) Lin, S.; Diercks, C. S.; Zhang, Y.-B.; Kornienko, N.; Nichols, E. M.; Zhao, Y.; Paris, A. R.; Kim, D.; Yang, P.; Yaghi, O. M.; Chang, C. J. Covalent Organic Frameworks Comprising Cobalt Porphyrins for Catalytic CO_2 Reduction in Water. *Science* **2015**, *349* (6253), 1208–1213.

(26) Bisbey, R. P.; DeBlase, C. R.; Smith, B. J.; Dichtel, W. R. Two-Dimensional Covalent Organic Framework Thin Films Grown in Flow. *J. Am. Chem. Soc.* **2016**, *138* (36), 11433–11436.

Chapter IV. Design, Synthesis, and Characterization of Woven COF-112

4.1 Introduction

4.1.1 Woven Crystalline COFs

Weaving is a traditional method of textile production, where two distinct sets of threads are interlaced at a certain angle to form a fabric or cloth. On the molecular level, this design can be realized in woven crystalline COFs, where infinite one-dimensional covalently linked molecular chains are held together by mechanical entanglement (Figure 4.1).[1–3] Because the chains are interlaced *via* metal templates and cross at points of registry, they possess many degrees of freedom upon demetallation, allowing for enormous spatial deviations to take place without deteriorating overall structure. The reticular synthesis of woven crystalline COFs not only greatly expands the scope of COF chemistry by enabling successful construction of atomically defined woven materials, but also provides a powerful strategy to synthesize materials with exceptional mechanical properties and dynamics that have not been achieved before.

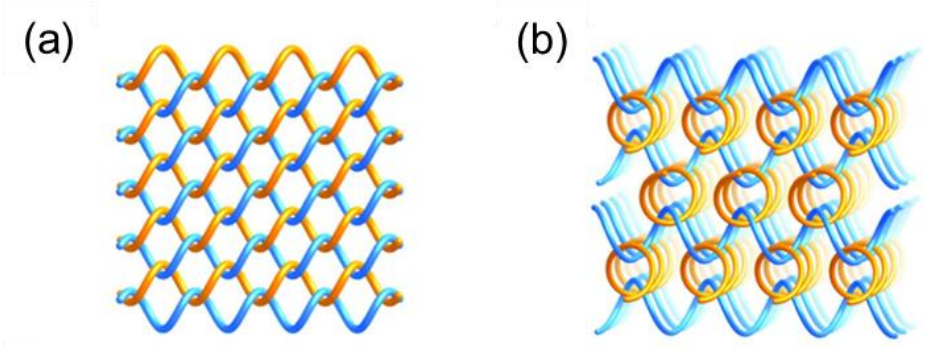

Figure 4.1. Illustrations of weaving threads into (a) a two-dimensional nets and (b) a three-dimensional framework. Adapted with permission from ref 1. Copyright 2016 AAAS.

• Portions of this chapter have been previously published in:
Zhao, Y.*; Guo, L.*; Gándara, F.; Ma, Y.; Liu, Z.; Zhu, C.; Lyu, H.; Trickett, C. A.; Kapustin, E. A.; Terasaki, O.; Yaghi, O. M. A Synthetic Route for Crystals of Woven Structures, Uniform Nanocrystals, and Thin Films of Imine Covalent Organic Frameworks. *J. Am. Chem. Soc.* **2017**, *139* (37), 13166–13172.
*These authors contributed equally to this work.

4.1.2 Design Principle of Woven Structures

To design a woven framework, one would need long covalently linked molecules (*i.e.*, infinite one-dimensional chains), which serve as backbones of the framework, and metal templates, which bring these molecular threads together. Toward this end, metal templates are a powerful tool for the synthesis of woven crystalline COFs. Similar to the synthesis of discrete interlocking molecules (*e.g.*, knots, catenanes, and rotaxanes),[4–11] organic ligands are pre-organized into a certain orientation and are stitched together with strong covalent bonds into two-dimensional and three-dimensional crystalline COFs (Figure 4.2).[12] The geometry of the metal complex (directionality of the points of extension, length of the ligand, etc.) has a profound influence on the underlying structure of the framework, and elaborate design of woven COFs is required beyond conducting the synthesis.

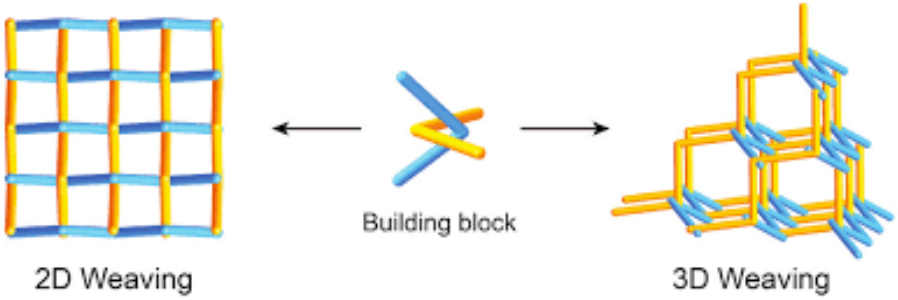

Figure 4.2. Synthesis of 2D and 3D woven frameworks by linking woven molecular building units.

4.1.3 The First Woven COF

The first woven COF, COF-505, was constructed from aldehyde functionalized copper(I)-bisphenanthroline tetrafluoroborate, $Cu(PDB)_2(BF_4)$, and benzidine (BZ), by imine condensation reactions (Figure 4.3).[1] COF-505 can be reversibly demetallated (with strong chelating reagents) and remetallated, rendering different elastic behaviors.

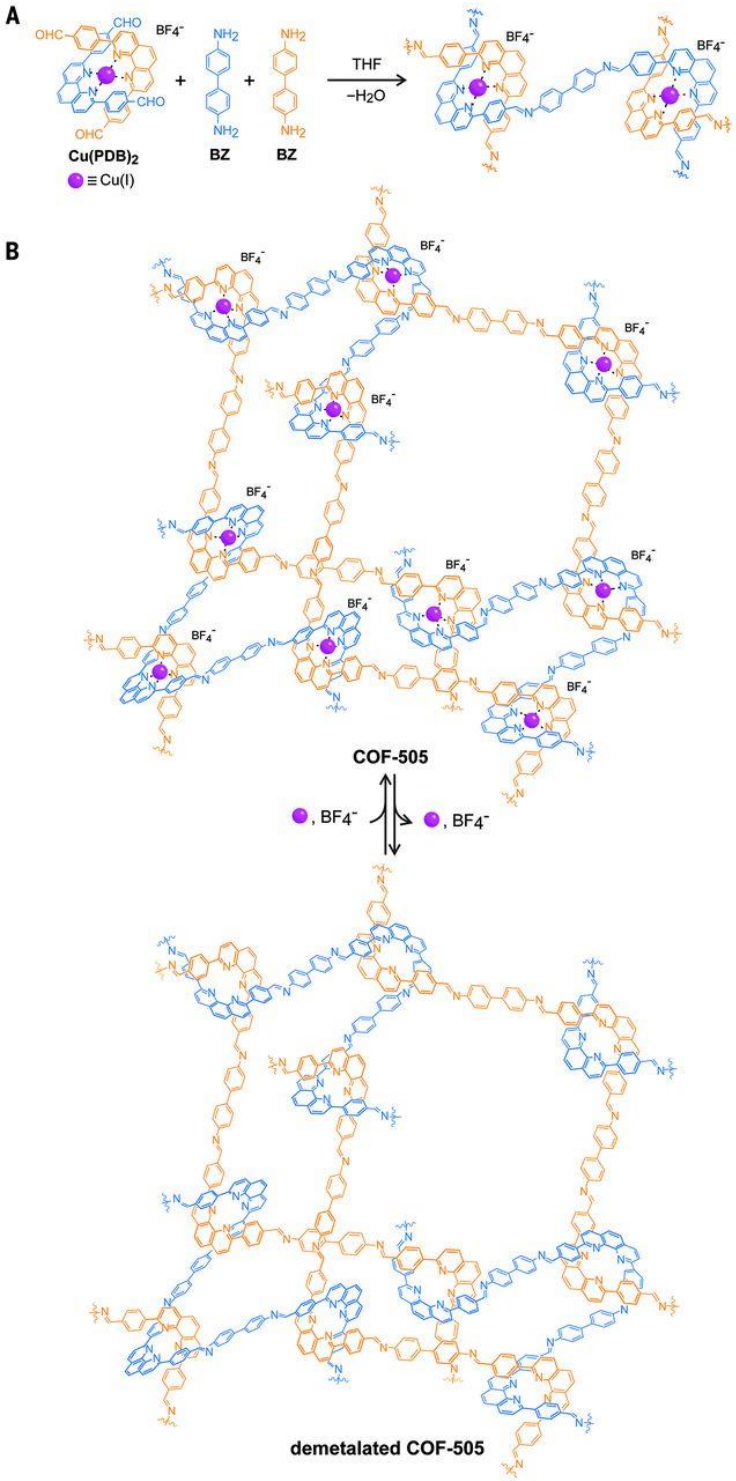

Figure 4.3. Synthesis of COF-505. COF-505 was constructed from organic threads using copper (I) as a template (a) to make an extended weaving structure (b), which can be subsequently demetallated and remetallated. Adapted with permission from ref 1. Copyright 2016 AAAS.

In COF-505, the secondary building unit copper *bis*-phenanthroline complex possesses a dihedral angle (between the two phenanthroline rings) of 57 °, which is probably due to the π- π interactions between the phenanthroline and its neighboring phenyl planes.[13] This highly distorted tetrahedral coordination geometry of copper(I) complex directs the polyimine chains to be helical. These chiral helices are propagating along [110] and [–110] directions, resulting in an overall racemic interpenetrating framework.

4.1.4 Design of COF-112

Herein, a woven crystalline COF constructed from less distorted secondary building units is designed (Scheme 4.1). Cobalt bis(diiminopyridine) complexes [$Co(DIP)_2$] are selected as the tetrahedral building unit, given that its dihedral angles (between the two pyridine rings) are close to the ideal angle of 90 °.[14,15] The higher symmetry of this metal complex results in a more symmetrical arrangement of the organic threads to afford an ideal woven structure based on the diamond topology. Since diiminopyridine (DIP) ligands can be synthesized by imine condensation from *p*-phenylenediamine (PDA) and 2,6-pyridinedicarboxaldehyde (PCBA), PDA, PCBA, and $Co(BF_4)_2$ $6H_2O$ are employed as starting materials to construct an extended non-interpenetrated framework.

Scheme 4.1. The conventional heterogeneous, homogeneous (one-pot), and metal-complex route for COF-112.

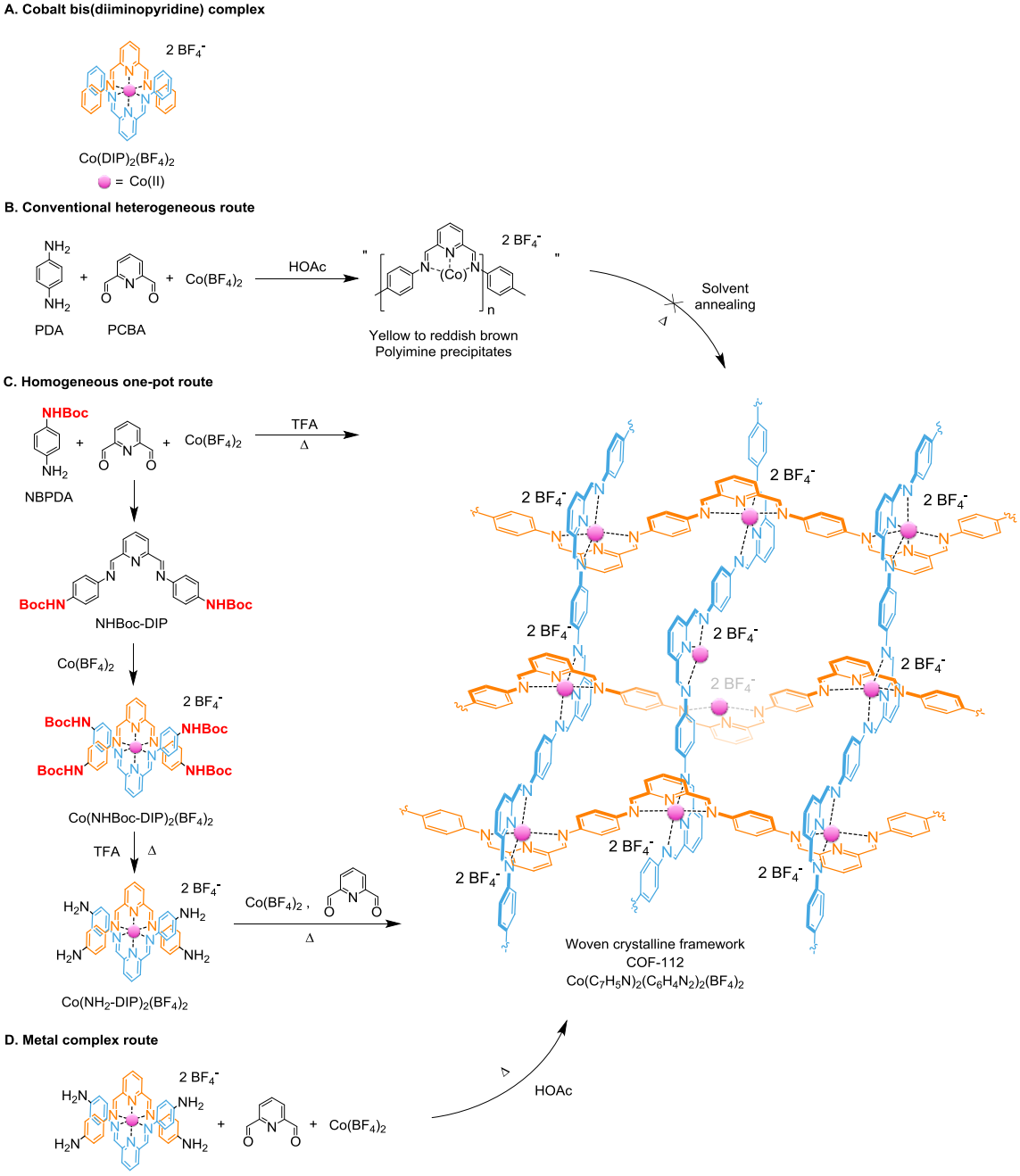

4.2 Experimental Section

4.2.1 Methods and Materials

Chemicals. $Co(BF_4)_2$ $6H_2O$ (purity ≥ 99 %), $Fe(BF_4)_2$ $6H_2O$ (purity ≥ 97 %), and ethanol (anhydrous, purity ≥ 99.5 %) were obtained from Sigma-Aldrich. Isopropanol (anhydrous, purity ≥ 99.8 %) and 4-(t*ert*-butoxycarbonylamino)-aniline (NBPDA, purity ≥ 97 %) were purchased from Acros Organics. 2,6-Pyridinedicarboxaldehyde (PCBA, purity ≥ 98 %) was obtained from TCI. Toluene (anhydrous purity ≥ 99.8%), acetonitrile (purity ≥ 99.8%), glacial acetic acid (purity 100%), and trifluoroacetic acid (TFA, purity ≥ 99.7 %) were purchased from EMD Millipore Chemicals.

All reactions were performed under ambient laboratory conditions and no precautions taken to exclude atmospheric moisture, unless otherwise specified. Pyrex glass tubes, charged with reagents and flash frozen with liquid N_2, were evacuated using a Schlenk line by fitting the open end of the tube inside a short length of standard rubber hose that was further affixed to a ground glass tap, which could be closed to insulate this assembly from dynamic vacuum when the desired internal pressure was reached. Tubes were sealed under the desired static vacuum using an oxygen propane torch.

Analytical techniques and instrument. Gas adsorption experiments (up to 760 torr) were carried out on a Quantachrome AUTOSORB-1 automatic volumetric instrument. Ultrahigh-purity-grade N_2 and He gases were used in all adsorption measurements. The N_2 (77 K) isotherms were measured using a liquid nitrogen bath (77 K). The backbone density of the COF-112 was measured by pycnometry on a Quantachrome-UPYC 1200e V5.04 instrument using He gas. Powder X-ray diffraction (PXRD) patterns were recorded using a Rigaku Miniflex 600 (Bragg-Brentano geometry, Cu K_α radiation λ = 1.54 Å) instrument. Solution ^{1}H NMR spectra were acquired on a Bruker AVB-400 and AV-600 NMR spectrometer. Elemental microanalyses (EA) were performed in the Microanalytical Laboratory of the College of Chemistry at UC Berkeley, using a Perkin Elmer 2400 Series II CHNS elemental analyzer. The amount of Co, Fe and B in COF-112 was analyzed by an ICP−AES spectroscometer with Optima 7000 DV (PerkinElmer) instrument. Attenuated total reflectance (ATR) FTIR spectra of neat samples were performed on a Bruker ALPHA Platinum ATR-FTIR Spectrometer equipped with a single reflection diamond ATR module. Scanning electron microscope (SEM) images were recorded on a Zeiss Gemini Ultra-55 analytical scanning electron microscope with accelerating voltage of 5 kV. Transmission electron microscopy (TEM) was performed on a cold field emission JEM-2100F instrument equipped with a DELTA C_s corrector. Optical refractive index was measured using ellipsometer (Gaertner Scientific Corporation). Single crystal X-ray diffraction data was collected using synchrotron radiation on beamline 11.3.1 at the Advanced Light Source (ALS) at Lawrence Berkeley National Lab (LBNL), equipped with

a Bruker Photon 100 CMOS area detector using synchrotron radiation (16 keV). Samples were mounted on MiTeGen® kapton loops and placed in a 100 K nitrogen cold stream unless otherwise specified.

4.2.2 Synthesis

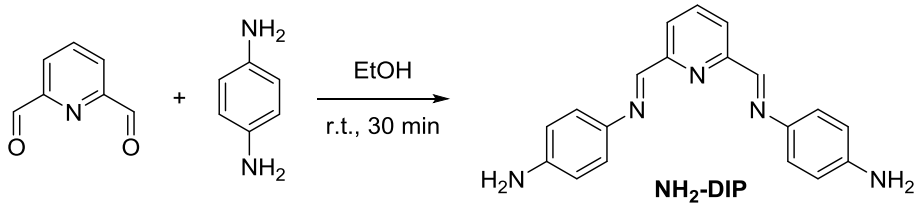

Synthesis of 2,6-pyridinedicarboxaldhydebis-(*p*-aminophenylimine) (NH_2-DIP). 2,6-Pyridinedicarboxaldehyde (270 mg, 2 mmol) was dissolved in 16 mL of anhydrous isopropyl alcohol under nitrogen. This solution was added dropwise into 1,4-benzenediamine (648 mg, 6 mmol) in 16 mL of ethanol. The mixture was stirred for 30 minutes and filtered. The precipitate was washed with ethanol thoroughly and dried to give compound **NH_2-DIP** (518 mg, 82%). ^{1}H NMR (400 MHz, d-DMSO) δ 8.64 (s, 2H), 8.11 (d, 3J = 7.6 Hz, 2H), 7.98 (t, ^3J = 8.0 Hz, 1H), 7.25 (d, ^3J = 8.8 Hz, 4H), 6.62 (d, ^3J = 8.4 Hz, 4H), 5.43 (s, 4H). HRMS (ESI$^+$) for $[C_{19}H_{18}N_5]^+$ (M+H$^+$): m/z Calcd. 316.1557, found 316.1557.

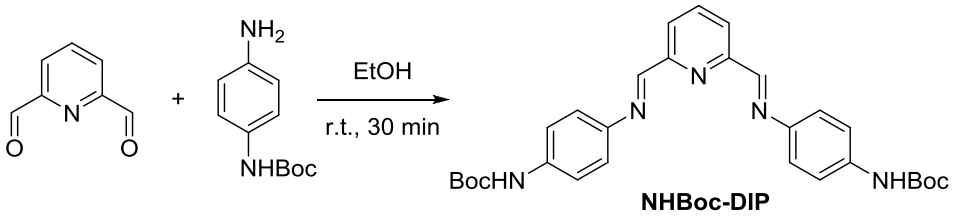

Synthesis of 2,6-pyridinedicarboxaldhydebis-(*p*-aminophenylimine) (NHBoc-DIP). 2,6-Pyridinedicarboxaldehyde (128 mg, 0.95 mmol) was dissolved in 5 mL of isopropyl alcohol purged with nitrogen. This solution was added dropwise into 4-(*tert*-butoxycarbonylamino)-aniline (396 mg, 1.90 mmol) in 5 mL of ethanol. The mixture was stirred for 30 minutes and filtered. The precipitate was washed with ethanol thoroughly and dried to give compound **NHBoc-DIP** (387.0 mg, 79%). ^{1}H NMR (600 MHz, d-acetone δ 8.71 (s, 2H), 8.56 (s, 2H), 8.30 (d, ^3J = 7.8 Hz, 2H), 8.01 (t, ^3J = 7.8 Hz, 1H), 7.67 (d, ^3J = 8.4 Hz, 4H), 7.40 (d, ^3J = 8.4 Hz, 4H), 1.50 (s, 18H). HRMS (ESI$^+$) for $[C_{29}H_{33}O_4N_5]^+$ (M+H$^+$): *m*/*z* Calcd 516.2605, found 516.2611.

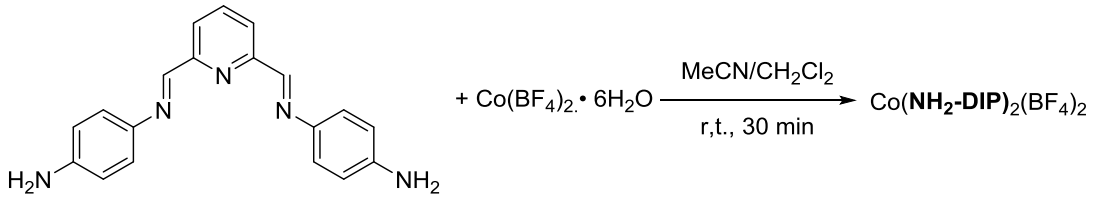

Synthesis of [Co(NH$_2$-DIP)$_2$(BF$_4$)$_2$]. $Co(BF_4)_2{\cdot}6H_2O$ (102.2 mg, 0.3 mmol) was dissolved in 5 mL of MeCN and added to a solution of NH_2-DIP (188.2 mg, 0.6 mmol) in 5 mL of CH_2Cl_2, affording a dark brown solution, which was stirred under N_2 at room temperature for 30 min. The solution was then concentrated under vacuum to afford the analytically pure title compound as a dark brown solid (258 mg, quantitative). HRMS (ESI^+) for $[C_{38}H_{34}N_{10}Co_1]^{2+}$ *m/z* Calcd 344.6144, found 343.1152.

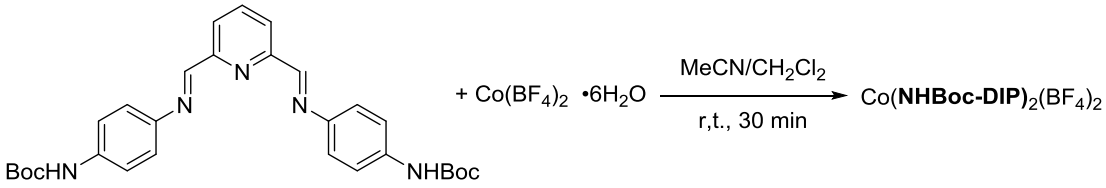

Synthesis of [Co(NHBoc-DIP)$_2$(BF$_4$)$_2$]. $Co(BF_4)_2{\cdot}6H_2O$ (128 mg, 0.375 mmol) was dissolved in 5 mL of MeCN and added to a solution of NHBoc-DIP (387 mg, 0.75 mmol) in 5 mL of CH_2Cl_2, affording a dark brown solution, which was stirred under N_2 at room temperature for 30 min. The solution was then concentrated under vacuum to afford an analytically pure title compound as a dark brown solid (473.0 mg, quantitative). HRMS (ESI^+) for $[C_{58}H_{66}O_8N_{10}Co_1]^{2+}$ *m/z* Calcd 544.7193, found 544.7194.

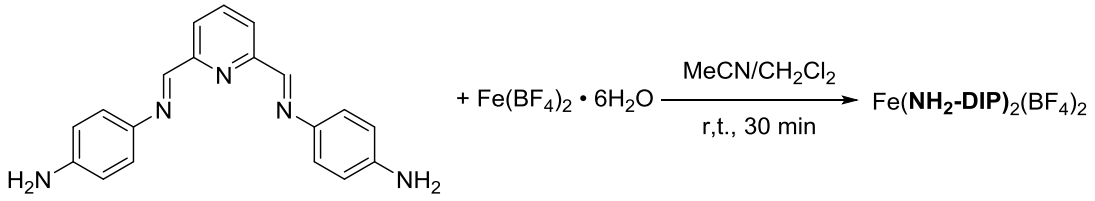

Synthesis of [Fe(NH$_2$-DIP)$_2$(BF$_4$)$_2$]. $Fe(BF_4)_2{\cdot}6H_2O$ (101.2 mg, 0.3 mmol) was dissolved in 5 mL of MeCN and added to a solution of NH_2-DIP (188.2 mg, 0.6 mmol) in 5 mL of CH_2Cl_2, affording a dark solution, which was stirred under N_2 at room temperature for 30 min. The solution was then concentrated under vacuum to afford the title compound as a dark brown solid (256.0 mg, quantitative). HRMS (ESI^+) for $[C_{38}H_{34}N_{10}Fe]^{2+}$ *m/z* Calcd 343.1153, found 343.1152.

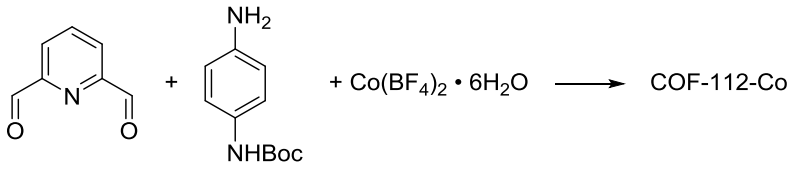

One-pot homogeneous synthesis route to COF-112-Co. A Pyrex tube measuring 10 × 8 mm (o.d × i.d) was charged with 2,6-pyridinedicarboxaldehyde (5.4 mg, 0.04 mmol), 4-(*tert*-butoxycarbonylamino)-aniline (8.3 mg, 0.04 mmol), $Co(BF_4)_2{\cdot}6H_2O$ (6.8 mg, 0.02 mmol), 0.3 mL of anhydrous MeCN, 0.4 mL of anhydrous toluene, and 0.05 mL of aqueous trifluoroacetic acid solution (trifluoroacetic acid: water (v/v) = 1:4). The tube was flash frozen at 77 K (liquid N_2 bath), evacuated to an internal pressure of 50 mTorr and flame sealed. Upon sealing, the length of the tube was reduced to 18-20 cm. The mixture was heated to 85 ℃ for 48 h, yielding brown solids at the bottom of the tube, which were isolated by centrifugation and washed with anhydrous acetone and dried at 120 ℃ under 50 mTorr for 12 h. This material was insoluble in water and common organic solvents such as hexanes, methanol, acetone, tetrahydrofuran, *N*,*N*-dimethylformamide, and dimethyl sulfoxide, indicating the formation of an extended structure. The composition of COF-112 was studied combining ICP-AES and elemental analysis techniques: $C_{26}H_{18}N_6Co_1B_2F_8{\cdot}2H_2O$: Calcd.: C, 45.72; H, 3.25; N, 12.30; Co, 8.63; B, 3.17; F, 22.25; O, 4.68%. Found: C, 45.57; H, 3.81; N, 12.05; Co, 8.41; B, 3.14%.

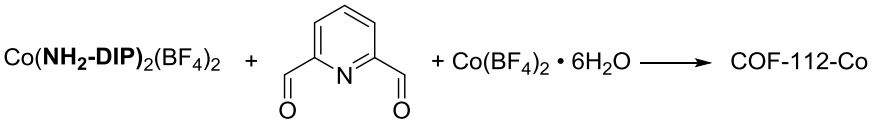

Metal-complex synthetic route to COF-112-Co with $Co(NH_2\text{-}DIP)_2(BF_4)_2$. A Pyrex tube measuring 10 × 8 mm (o.d × i.d) was charged with $Co(\mathbf{NH_2\text{-}DIP})_2(BF_4)_2$ (8.6 mg, 0.01 mmol), 2,6-pyridinedicarboxaldehyde (2.7 mg, 0.02 mmol), $Co(BF_4)_2{\cdot}6H_2O$ (3.4 mg, 0.01 mmol), 0.4 mL of anhydrous MeCN, 0.6 mL of anhydrous toluene, and 0.1 mL of 6 M aqueous acetic acid solution. The tube was flash frozen at 77 K (liquid N_2 bath), evacuated to an internal pressure of 50 mTorr and flame sealed. Upon sealing, the length of the tube was reduced to 18-20 cm. The mixture was heated to 120 ℃ for 72 h, yielding brown solids at the bottom of the tube. The solids were isolated by centrifugation and washed with anhydrous acetone and dried at 120 ℃ under 50 mTorr for 12 h. This material was insoluble in water and common organic solvents such as hexanes, methanol, acetone, tetrahydrofuran, *N*,*N*-dimethylformamide, and dimethyl sulfoxide, indicating the formation of an extended structure.

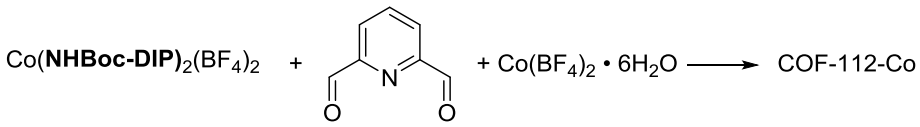

Homogeneous synthesis of COF-112-Co with Boc-protected complex $Co(NHBoc\text{-}DIP)_2(BF_4)_2$. A Pyrex tube measuring 10 × 8 mm (o.d × i.d) was charged with $Co(NHBoc\text{-}DIP)_2(BF_4)_2$ (12.6 mg, 0.01 mmol), 2,6-pyridinedicarboxaldehyde (2.7 mg, 0.02 mmol), $Co(BF_4)_2{\cdot}6H_2O$ (3.4 mg, 0.01 mmol), 0.3 mL of anhydrous MeCN, 0.4 mL of anhydrous toluene, and 0.05 mL of aqueous trifluoroacetic acid solution (trifluoroacetic acid: water (v/v) = 1:4). The tube was flash frozen at 77 K (liquid N_2 bath), evacuated to an internal pressure of 50 mTorr and flame sealed. Upon sealing, the length of the tube was reduced to 18-20 cm. The mixture was heated to 100 ℃ for 48 h yielding brown solids at the bottom of the tube which was isolated by centrifugation and washed with anhydrous acetone and dried at 120 ℃ under 50 mTorr for 12 h. This material was insoluble in water and common organic solvents such as hexanes, methanol, acetone, tetrahydrofuran, *N*,*N*-dimethylformamide, and dimethyl sulfoxide, indicating the formation of an extended structure.

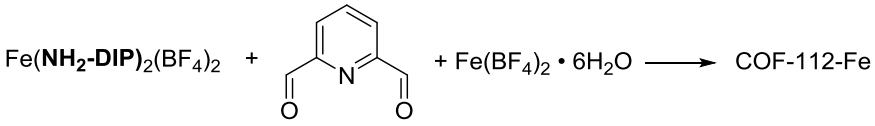

Synthesis of COF-112-Fe. A Pyrex tube measuring 10 × 8 mm (o.d × i.d) was charged with $Fe(NH_2\text{-}DIP)_2(BF_4)_2$ (8.6 mg, 0.01 mmol), 2,6-pyridinedicarboxaldehyde (2.7 mg, 0.02 mmol), $Fe(BF_4)_2{\cdot}6H_2O$ (3.3 mg, 0.01 mmol), 0.4 mL of anhydrous EtOH, 0.6 mL of anhydrous toluene, and 0.1 mL of 6 M aqueous acetic acid solution. The tube was flash frozen at 77 K (liquid N_2 bath), evacuated to an internal pressure of 50 mTorr and flame sealed. Upon sealing, the length of the tube was reduced to 18-20 cm. The mixture was heated at 120 ℃ for 72 h yielding black solids at the bottom of the tube which was isolated by centrifugation and washed with anhydrous acetone and dried at 120 ℃ under 50 mTorr for 12 h. This material was insoluble in water and common organic solvents such as hexanes, methanol, acetone, tetrahydrofuran, *N*,*N*-dimethylformamide, and dimethyl sulfoxide, indicating the formation of an extended structure. The composition of COF-112-Fe was studied combining ICP-AES and elemental analysis techniques: $C_{26}H_{18}N_6Fe_1B_2F_8{\cdot}H_2O$: Calcd.: C, 45.18; H, 3.05; N, 12.70; Fe, 8.44; B, 3.27; F, 22.96; O, 2.42%. Found: C, 47.03; H, 3.68; N, 12.15; Fe, 8.95; B, 3.07%.

4.3 Results and Discussion

4.3.1 Synthesis and Characterization of COF-112

A conventional one-pot COF synthesis was initially set up with PDA, PCBA and $Co(BF_4)_2 \cdot 6H_2O$ as starting materials (Scheme 4.1B). However, this yielded no crystalline products, despite testing a wide range of synthetic conditions. Frequently, the formation of yellow precipitates, which quickly turned reddish brown, was observed. This indicates that imine condensation had proceeded to afford polyimine precipitates, before all DIP sites were coordinated by cobalt ions. Since non-metallated polyimine threads can be crystallized and prefer to pack in a parallel manner, which is dramatically different from that of the targeted woven framework, it is speculated and observed that defect correction with conventional solvent annealing is insufficient to afford crystalline products. Consequently, to obtain the target crystalline woven COF, the formation of polyimine precipitates needs to be avoided to allow the metal DIP complexes to direct the propagation and entanglement of the polyimine chains. Toward this end, 4-(*tert*-butoxycarbonylamino)aniline (NBPDA), of which one of the two amine groups in PDA is protected with Boc groups, was employed as the starting material. NBPDA can form DIP ligands and the corresponding cobalt complexes rapidly at room temperature (Scheme 4.1C), yet avoid the precipitation of the polyimine observed in the heterogeneous route.

The one-pot homogeneous synthesis of COF-112 was thus carried out with NBPDA, PCBA, and $Co(BF_4)_2$ as starting materials in a solvent mixture of acetonitrile and toluene with trifluoroacetic acid as the catalyst for imine condensation and the reagent for deprotection of the Boc groups. The reaction started with a clear solution without polyimine precipitates in the heterogeneous imine COF synthesis. This clear solution was heated in a sealed Pyrex tube to 85 °C for 48 h, yielding reddish brown microcrystals. In this synthetic route, NBPDA and PCBA first underwent imine condensation to form the Boc-protected diiminopyridine ligand (NHBoc-DIP, Scheme 4.1C). This ligand rapidly bound cobalt ions to form $Co(NHBoc\text{-}DIP)_2(BF_4)_2$ complexes, giving the solution a red color. While being heated, crystalline solids emerged from this red solution, as the *in situ* deprotected amine groups reacted with the remaining PCBA to form the interlacing one-dimensional polyimine chains and the COF-112 structure. In this homogeneous route to synthesize COF-112, the assembly of the molecular threads is directed by the metal complex leading to successful crystallization. This is in contrast with the heterogeneous route, where polyimine chains formed prior to metal complexation (Scheme 4.1B). To further compare the homogeneous and heterogeneous synthesis routes, deprotected amine intermediate $[Co(NH_2\text{-}DIP)_2(BF_4)_2]$ of the homogeneous route was used to react with PCBA and cobalt ions in the synthesis similar to that leading to COF-505 (Scheme 4.1D).

This metal-complex route also afforded crystalline COF-112, indicating that the initial cobalt complex formation in the homogeneous one-pot route is the key to obtaining crystalline frameworks.

The completeness of the imine condensation to synthesize COF-112 was assessed by FT-IR spectroscopy, where no vibrational modes were observed for any unreacted amines, aldehydes, and Boc protecting groups (Figure 4.4). The presence of DIP was supported by comparing the IR spectra with $Co(NH_2\text{-}DIP)_2(BF_4)_2$ (Figure 4.5). Solid state UV-Vis spectroscopy of COF-112 showed almost identical absorption with $[Co(NH_2\text{-}DIP)_2(BF_4)_2]$ (Figure 4.6). Inductively coupled plasma atomic emission spectroscopy (ICP-AES), along with elemental analysis further confirmed the composition of COF-112.

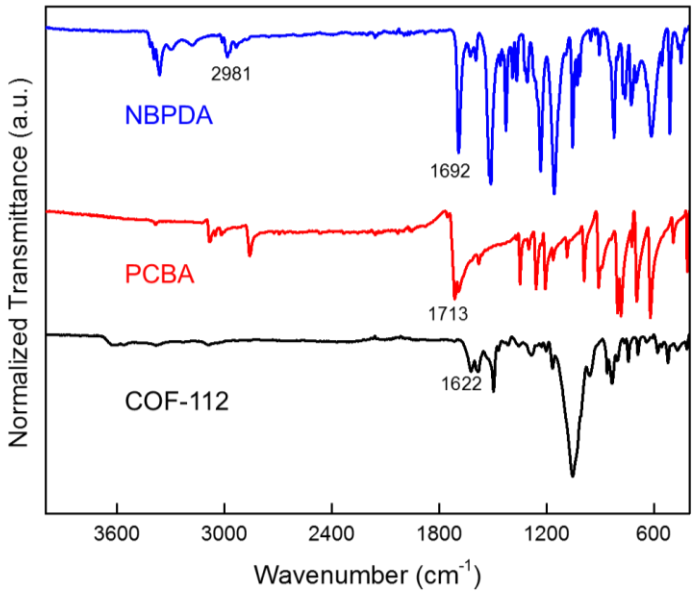

Figure 4.4. FT-IR spectra of COF-112 and its starting material. It is clear that Boc groups (characteristic C=O stretching band at 1692 cm^{-1} and C-H stretching band at 2981 cm^{-1}) and amine groups (N-H absorbance bands beyond 3000 cm^{-1}) in NBPDA, and aldehyde groups in PCBA (C=O absorbance band at 1713 cm^{-1}) are absent in COF-112.

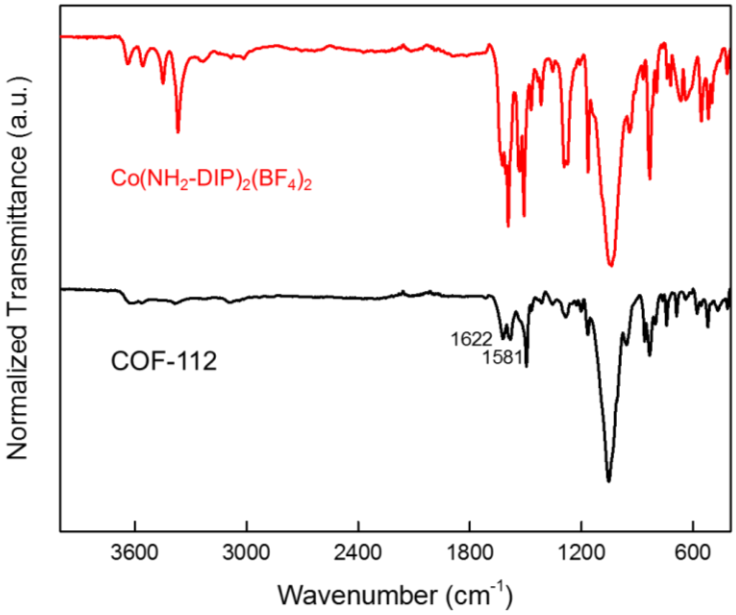

Figure 4.5. FT-IR spectra of COF-112 and $Co(NH_2\text{-}DIP)_2(BF_4)_2$. Two compounds display similar vibrational modes, where in COF-112 the vibrational mode of N-H stretching (beyond 3200 cm^{-1}) disappeared and that of imine bond (1622 cm^{-1}) strengthened, both consistent with their slight structural difference.

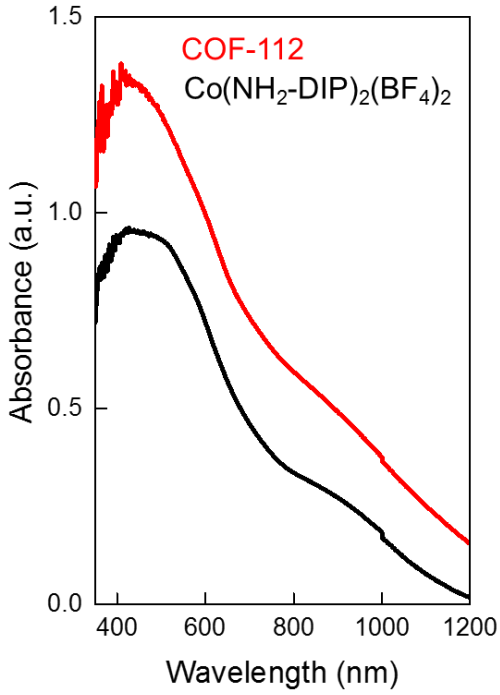

Figure 4.6. The UV-Vis spectra of COF-112 and $Co(NH_2\text{-}DIP)_2(BF_4)_2$, showing almost identical absorption due to ligand to metal charge transfer.

The crystal structure of COF-112 was solved by a combination of X-ray and electron crystallographic studies (Figure 4.7). One three-dimensional electron diffraction tomography dataset was collected from a submicron crystal by using a goniometer tilt of 3 ° and an electron-beam tilt of 0.3 ° (Figure 4.7a, b and c). From the reconstruction of the reciprocal lattice, two of unit cell parameters were uniquely determined, while the third one remained uncertain due to insufficient reflections and possible twinning. Subsequently, the PXRD pattern of COF-112 was indexed confirming an orthorhombic lattice and providing the third cell parameter. Pawley refinement was then conducted with the data from the PXRD pattern, resulting in unit cell parameters a = 19.74 Å, b = 25.13 Å, and c = 12.26 Å. The first four strong reflections in the PXRD pattern could be indexed as (111), (220), (131), and (040). The observed reflection conditions from electron diffraction and PXRD patterns were summarized as hkl: $h+k$, $h+l$, $k+l$ = 2n; 0kl: k, l = 2n&$k+l$ = 4n. This indicated an *F*-center Bravais lattice and the most likely space group of *Fdd2*. Two HRTEM images of COF-112 were taken along the [-101] and [0-11] incidences (Figure 4.7d and e). The Fourier analysis of these images after imposing the space group symmetry indicated the positions of the cobalt centered complexes, which was consistent with that given by the electron density map reconstructed by applying the charge flipping method with the reflection intensities extracted from the PXRD pattern (Figure 4.7f). Moreover, with the unit cell and space group determined, the position of cobalt atoms can also be confirmed from the measured sample density of 1.4 g/cm^3. This indicated one unit cell had only eight cobalt atoms, and their coordinates could be determined from the Wyckoff positions. The detailed construction process of COF-112 model can be found in the Appendix.

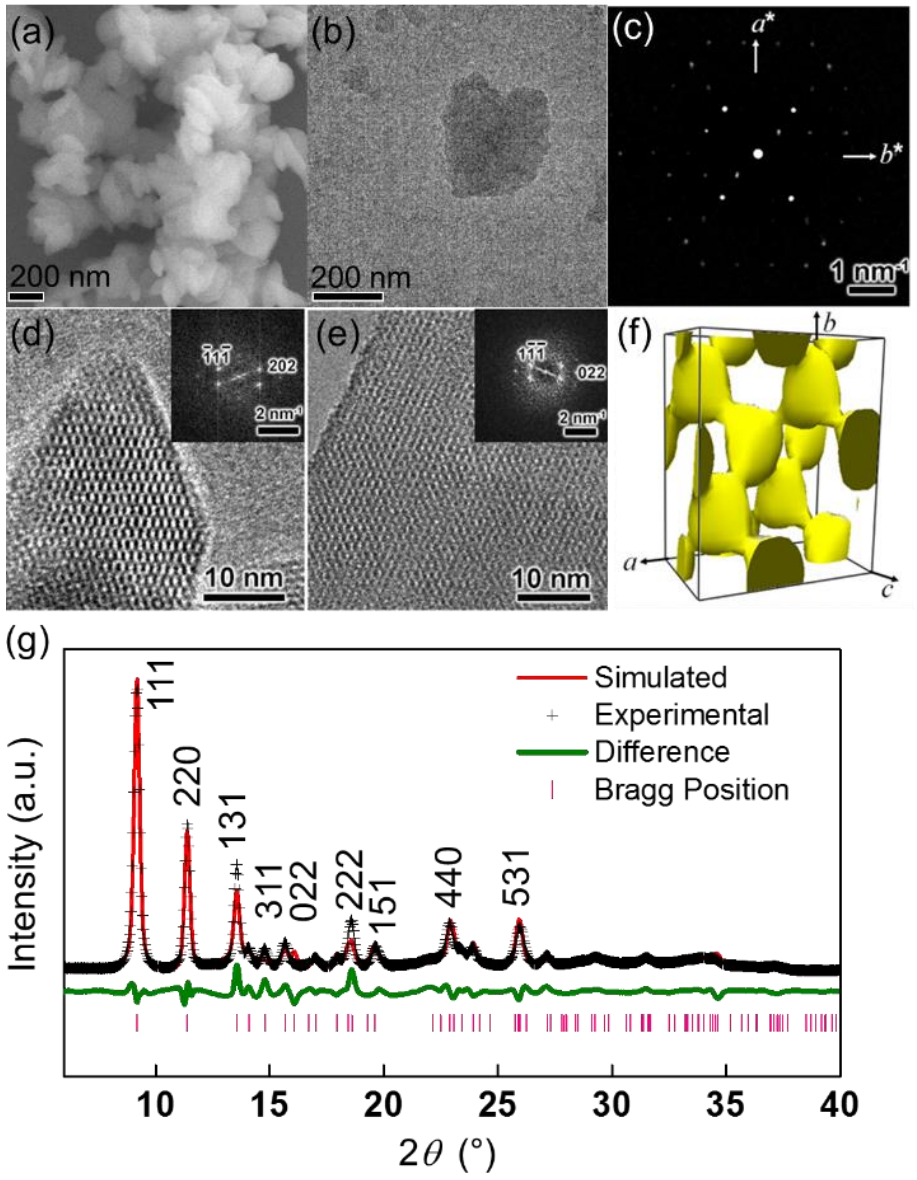

Figure 4.7. Structural determination of COF-112. (a) COF-112 crystals were 200 nm in size, as observed by SEM. 3D-EDT study (b) and (c) gave the unit cell parameters *a* and *b*, from which the unit cell could be determined by Pawley refinement of the PXRD pattern. High resolution TEM images (d) and (e) were combined to give cobalt positions by Fourier analysis (f). COF-112 structural model was thus built and optimized by Rietveld refinement with R_p and R_{wp} values of 1.66% and 2.48%, respectively (g).

The structure of the COF-112 consists of two sets of one-dimensional zig-zag polyimine chains, which propagate linearly along [110] and [-110] directions of the crystal and weave at the coordinated cobalt ions as point of registry at regular intervals of 1.6 nm (Figure 4.8). This structure is an ideal example of molecular weaving, which represents one of the simplest three-dimensional woven structures as it involves only two sets of

threads that are straight and parallel, and only one point of registry. COF-112 is a non-interpenetrated framework with **dia** topology, with $Co(DIP)_2^{2+}$ complexes serving as tetrahedral building units. The two sets of polyimine chains cross at an angle of 77.3 °, close to the 80 ° dihedral angle between the two pyridine rings in the $Co(NH_2\text{-}DIP)_2(BF_4)_2$ complex, thus supporting our initial design principle that the coordination geometry of the metal template would direct the propagation of the molecular threads.

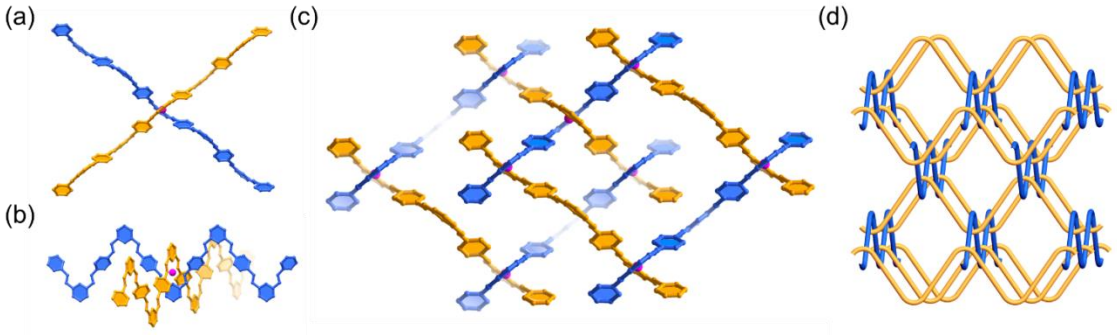

Figure 4.8. The structure of COF-112. (a) COF-112 is composed of two sets of interlacing polyimine threads (marked blue and orange for their different propagating directions) crossing at 77.3 °angle (a). The threads are woven with cobalt(II) ions as points of registry at regular intervals of 1.6 nm (b), which form a three-dimensional framework (c) that represents a simple 3D woven network (d). Additional parallel threads are omitted for clarity in (c).

4.3.2 Generality of Homogeneous Synthesis Strategy

The generality of this newly developed homogeneous synthetic route for imine COF synthesis is proved by the successful synthesis of COF-112-Fe, an isostructural framework of COF-112-Co. The resulted crystalline product was fully characterized by FT-IR spectroscopy (Figure 4.9), elemental analysis, powder X-ray diffraction (Figure 4.10), and SEM microscopy (Figure 4.11).

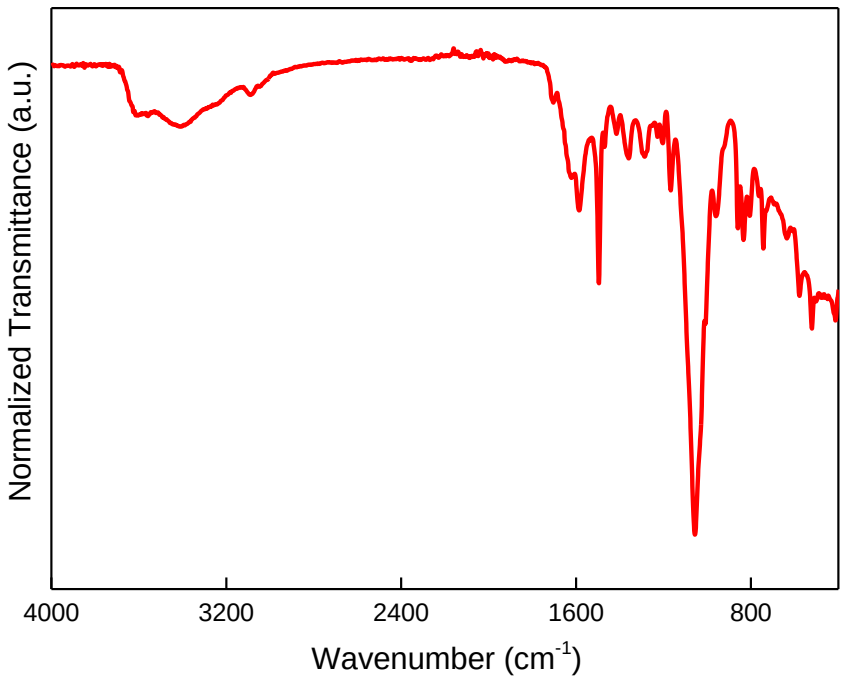

Figure 4.9. FT-IR spectrum of COF-112-Fe.

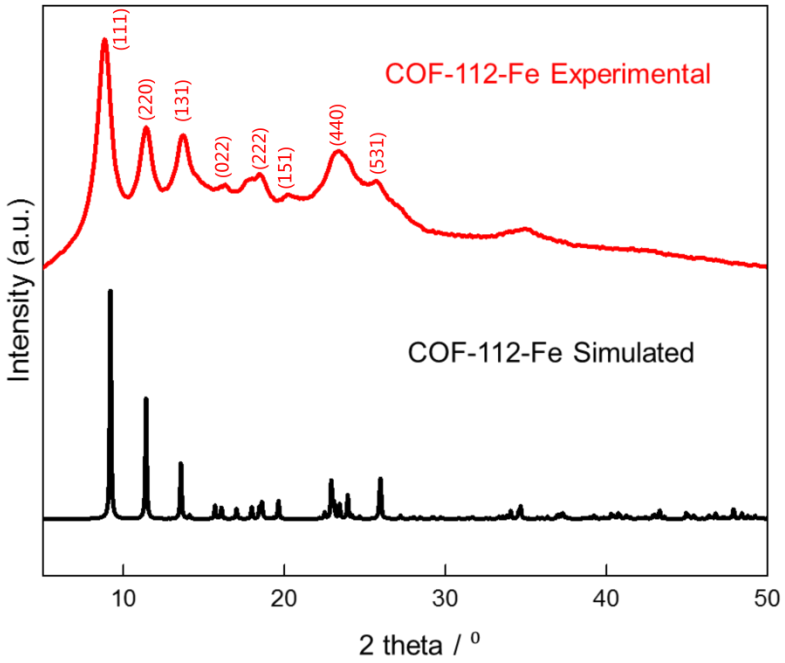

Figure 4.10. The simulated and experimental PXRD patterns of COF-112-Fe.

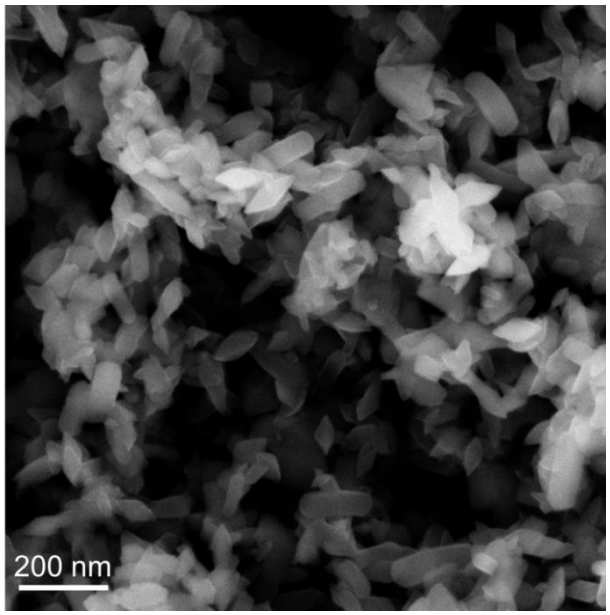

Figure 4.11. SEM image of COF-112-Fe.

4.4 Conclusion

In this study, a three-dimensional woven crystalline framework COF-112 was designed and successfully synthesized. Amine-functionalized Co(DIP) served as the metal template and was linked by 2,6-pyridinedicarboxaldehyde to yield an ideal woven structure based on the diamond topology. COF-112 serves as an ideal example of molecular weaving, which represents one of the simplest three-dimensional woven structures as it involves only two sets of threads that are straight and parallel and one point of registry. Although preliminary attempts to demetallate COF-112 were unsuccessful, it should be mentioned that the threads throughout the structure are not interrupted by metal ions, their persistence in the structure is fundamentally independent of the threads. To conclude, COF-112 framework is an example of constructing a highly complex structure from simple building blocks, where metal coordination and imine condensation reactions take place coherently in a one-pot reaction enabled by a homogenized imine COF synthetic route.

4.5 References

(1) Liu, Y.; Ma, Y.; Zhao, Y.; Sun, X.; Gándara, F.; Furukawa, H.; Liu, Z.; Zhu, H.; Zhu, C.; Suenaga, K.; Oleynikov, P.; Alshammari, A. S.; Zhang, X.; Terasaki, O.; Yaghi, O. M. Weaving of Organic Threads into a Crystalline Covalent Organic Framework. *Science* **2016**, *351* (6271), 365–369.

(2) Liu, Y.; Ma, Y.; Yang, J.; Diercks, C. S.; Tamura, N.; Jin, F.; Yaghi, O. M. Molecular Weaving of Covalent Organic Frameworks for Adaptive Guest Inclusion. *J. Am. Chem. Soc.* **2018**, *140* (47), 16015–16019.

(3) Liu, Y.; Diercks, C. S.; Ma, Y.; Lyu, H.; Zhu, C.; Alshmimri, S. A.; Alshihri, S.; Yaghi, O. M. 3D Covalent Organic Frameworks of Interlocking 1D Square Ribbons. *J. Am. Chem. Soc.* **2019**, *141* (1), 677–683.

(4) Dietrich-Buchecker, C. O.; Sauvage, J. P.; Kern, J. M. Templated Synthesis of Interlocked Macrocyclic Ligands: The Catenands. *J. Am. Chem. Soc.* **1984**, *106* (10), 3043–3045.

(5) Dietrich‐Buchecker, C. O.; Sauvage, J.-P. A Synthetic Molecular Trefoil Knot. *Angew. Chem. Int. Ed. Engl.* **1989**, *28* (2), 189–192.

(6) Chichak, K. S. Molecular Borromean Rings. *Science* **2004**, *304* (5675), 1308–1312.

(7) Wood, C. S.; Ronson, T. K.; Belenguer, A. M.; Holstein, J. J.; Nitschke, J. R. Two-Stage Directed Self-Assembly of a Cyclic [3]Catenane. *Nat. Chem.* **2015**, *7* (4), 354–358.

(8) Ponnuswamy, N.; Cougnon, F. B. L.; Pantoş, G. D.; Sanders, J. K. M. Homochiral and *Meso* Figure Eight Knots and a Solomon Link. *J. Am. Chem. Soc.* **2014**, *136* (23), 8243–8251.

(9) Beves, J. E.; Danon, J. J.; Leigh, D. A.; Lemonnier, J.-F.; Vitorica‐Yrezabal, I. J. A Solomon Link through an Interwoven Molecular Grid. *Angew. Chem. Int. Ed.* **2015**, *54* (26), 7555–7559.

(10) Ayme, J.-F.; Beves, J. E.; Leigh, D. A.; McBurney, R. T.; Rissanen, K.; Schultz, D. A Synthetic Molecular Pentafoil Knot. *Nat. Chem.* **2012**, *4* (1), 15–20.

(11) Leigh, D. A.; Pritchard, R. G.; Stephens, A. J. A Star of David Catenane. *Nat. Chem.* **2014**, *6* (11), 978–982.

(12) Liu, Y.; Yaghi, O. M. Metal Coordination as a Template Strategy to Make Resilient Woven Materials. *Bull. Jpn. Soc. Coord. Chem.*, **2018**, *71* (0), 12–17.

(13) Miller, M. T.; Gantzel, P. K.; Karpishin, T. B. Structures of the Copper(I) and Copper(II) Complexes of 2,9-Diphenyl-1,10-Phenanthroline: Implications for Excited-State Structural Distortion. *Inorg. Chem.* **1998**, *37* (9), 2285–2290.

(14) Vance, A. L.; Alcock, N. W.; Heppert, J. A.; Busch, D. H. An Octahedral Template Based on a New Molecular Turn: Synthesis and Structure of a Model Complex and a Reactive, Diphenolic Ligand and Its Metal Complexes. *Inorg. Chem.* **1998**, *37* (26), 6912–6920.

(15) Leigh, D. A.; Lusby, P. J.; Teat, S. J.; Wilson, A. J.; Wong, J. K. Y. Benzylic Imine Catenates: Readily Accessible Octahedral Analogues of the Sauvage Catenates. *Angew. Chem. Int. Ed.* **2001**, *40* (8), 1538–1543.

4.6 Appendix

4.6.1 Construction of COF-112 Structural Model

With the unit cell and cobalt center determined, model of the structure can be built rigorously. The single crystal structure of the secondary building unit $Co(NH_2\text{-}DIP)_2(BF_4)_2$ motif was obtained (Table 4.1), with the torsion angle between the pyridine rings (highlighted in orange) in $Co(NH_2\text{-}DIP)_2(BF_4)_2$ being 80 º (Figure 4.12 and 4.13). The single crystal structure of $Co(NH_2\text{-}DIP)_2(BF_4)_2$ provides evidence for the model construction of COF-112.

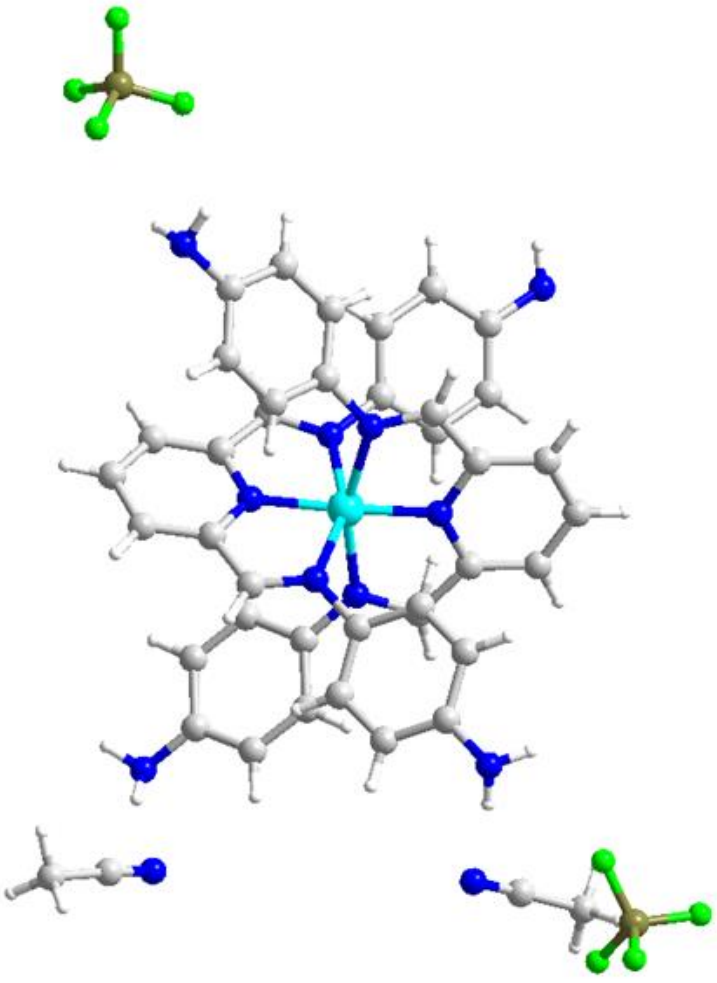

Figure 4.12. Single crystal structure of $Co(NH_2\text{-}DIP)_2(BF_4)_2$.

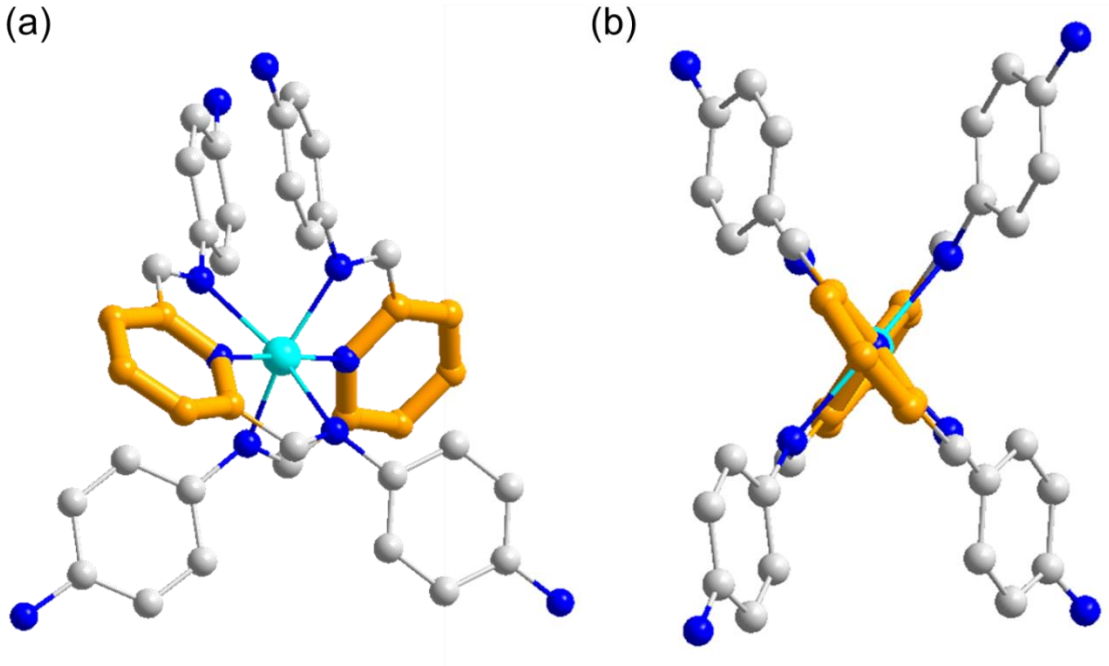

Figure 4.13. The torsion angle between the pyridine rings (highlighted in orange) in $Co(NH_2\text{-}DIP)_2(BF_4)_2$ is 80°, rendering the complex a more ideal tetrahedron (a) and directing the angle between the polyimine chains (b). The two images are this complex viewed in different orientations.

Table 4.1. Crystal data and structure determination for **[Co(NH_2-DIP)$_2$(BF_4)$_2$].**

Compound	**Co(NH_2-DIP)$_2$(BF_4)$_2$**
Chemical formula	$C_{42}H_{40}B_2CoF_8N_{12}$
Formula mass	945.41
Crystal system	triclinic
Space group	*P*-1
λ (Å)	0.7749(1)
a (Å)	12.1126(16)
b (Å)	14.208(2)
c (Å)	15.083(2)
α (°)	113.528(4)
β (°)	90.375(4)
γ (°)	112.600(4)
Z	2
V (Å^3)	2157.7(5)
Temperature (K)	100(2)
Size /mm^3	0.030 × 0.020 × 0.010
Density (g/cm^{-3})	1.455
Measured reflections	3913
Unique reflections	2898
Parameters	586
Restraints	66
R_{int}	0.1378
θ range (°)	2.10-21.71
R_1, wR_2	0.0810, 0.2050
S (GOF)	1.026
Max/min res. dens. (e/Å^3)	0.47/-0.56

The cobalt ions have four nearest neighbors at a distance of 8.55 Å arranged in tetrahedral geometry, which is consistent with the determined chemical composition and the presence of the $Co(DIP)_2$ motif. Taking the cobalt atom in the center of the unit cell as a reference, the four neighboring cobalt ions are arranged diagonally; thus it is clear that the molecular thread would propagate along one of the diagonal direction and fix the connectivity of the framework (Figure 4.14).

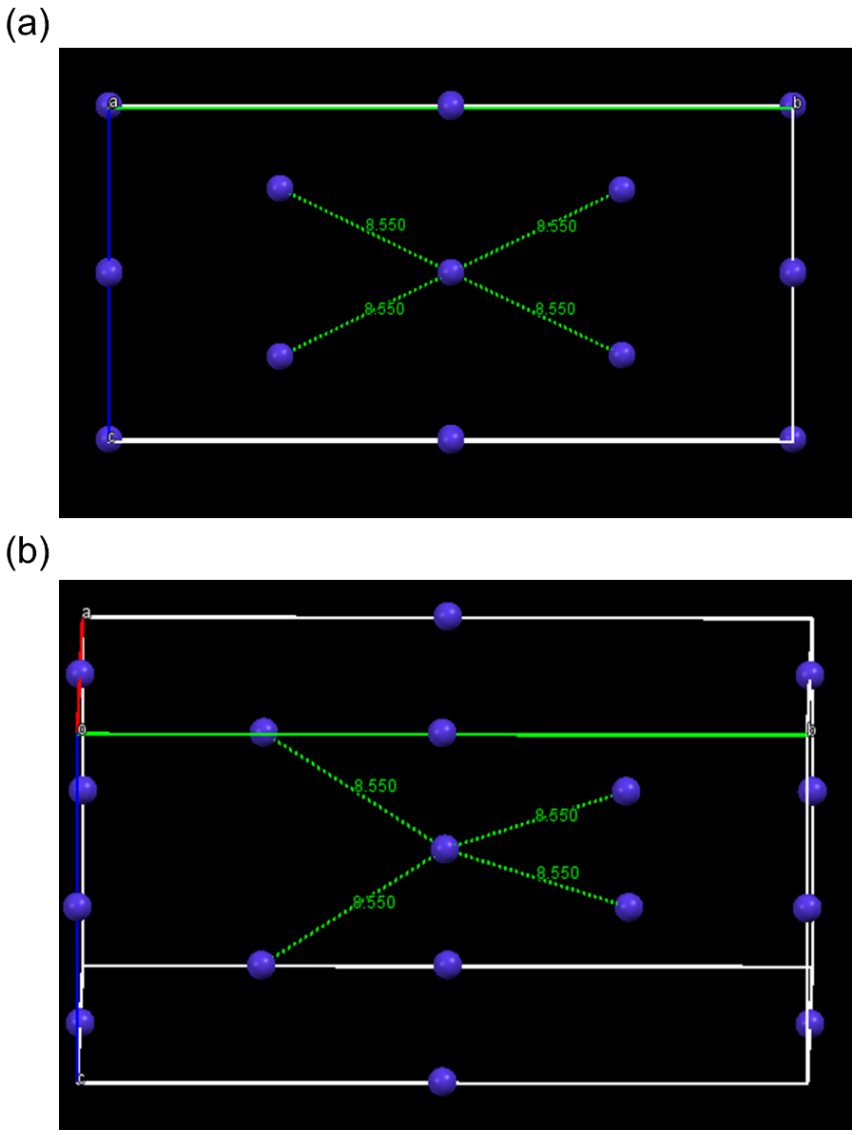

Figure 4.14. The position of the cobalt atoms viewing along *a* axis (a) showing the four nearest neighbors in tetrahedral geometry (b). The nearest cobalt ions should be connected through a PDA unit as their distance is in good agreement with the molecular model, and their tetrahedral spatial arrangement is consistent with the $-NH_2$ position in $Co(NH_2\text{-}DIP)_2$ complex.

Considering the *Fdd2* symmetry, the pyridine unit of the DIP ligand would be coordinating to a cobalt atom along *c* axis, as otherwise more than two pyridine units per cobalt ion would be generated by a space group symmetry operation. The orientation of these pyridine ring is fixed in the diagonal direction, which is the orientation determined by the connectivity (Figure 4.15).

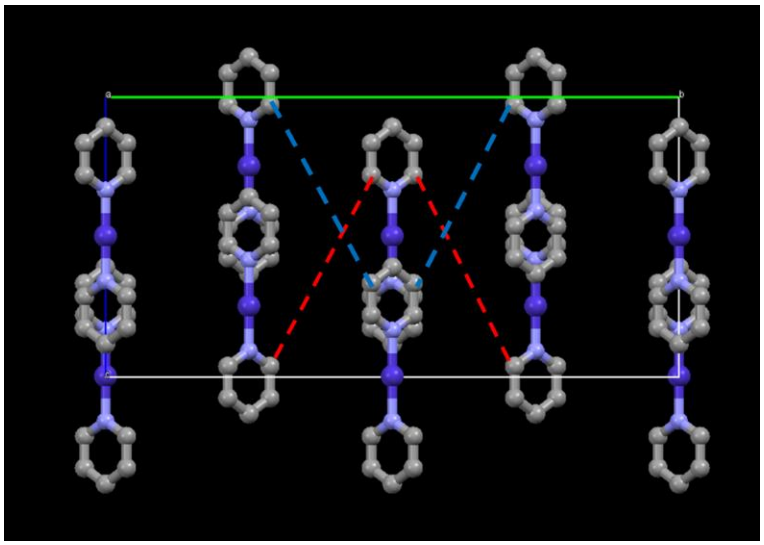

Figure 4.15. The position of the pyridine units. The *Fdd2* symmetry requires them to be vertical, and the connectivity (red and blue dash line, the pyridine rings linked by same color line are connected by a PDA unit) requires the connected pyridine rings to be in plane, thus restricting them in the diagonal [011] planes.

From the location of the neighboring cobalt atoms and the determined pyridine positions, the loci of the other four nitrogen atoms can be ascertained (diagonal direction), and thus the overall PCBA units has been concluded (Figure 4.16).

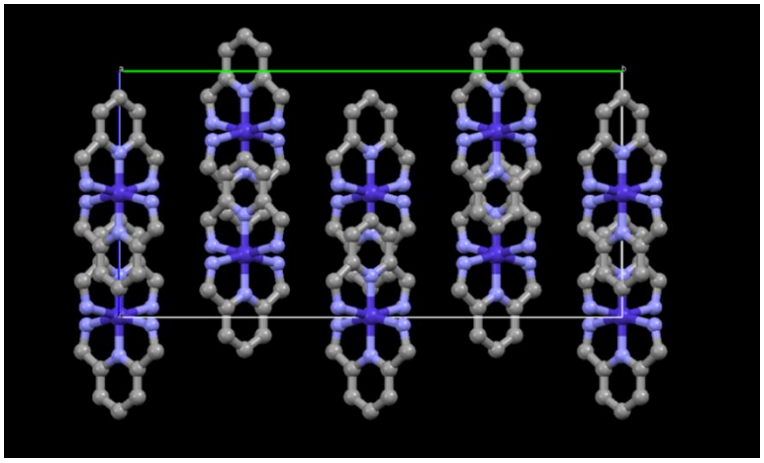

Figure 4.16. The position of PCBA units in COF-112.

The PDA unit then can be determined to be in plane with the two cobalt centers and linking the PCBA units. With PCBA and PDA unit positioned, the structure model of COF-112 is obtained (Figure 4.17). The BF_4 counter ions are then filled in the framework and refined by Rietveld refinement.

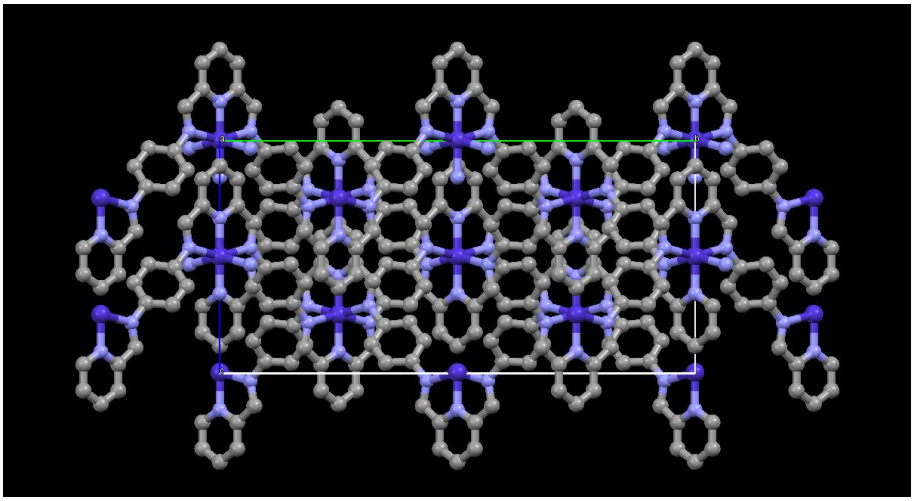

Figure 4.17. The structure model of the COF-112 framework.

Additionally, the structural characterization process has sufficient redundancy to derive this COF-112 structure model using different methods. In the cobalt position determination process, the position of cobalt per unit cell can be determined by sample density. With the determined unit cell dimension and density of 1.4 g/cc, eight cobalt ions are in one unit cell. Even without using the *Fdd2* symmetry determined from XRD, merely assuming the very apparent F centering, the choice of cobalt position can be significantly narrowed down (F centered orthorhombic cell all have high symmetry with multiplicity of arbitrary point being 16, thus cobalt has to be on a special Wyckoff position). And the fact that one cobalt atom has four closest non-coplanar neighbors [the $Co(DIP)_2$ complex is four connected and the phenyl rings are extending from the cobalt center in a tetrahedral manner] would give only one plausible cobalt position and the dd2 symmetry can be unambiguously fixed. All other F centered orthorhombic space group would contradict the basic geometry of the $Co(DIP)_2$ complex and thus contradict the COF composition determined through IR, EXAFS, EA, and ICP measurements.

With the cobalt position fixed, any topology other than diamond (connect the cobalt atoms differently through DIP ligand) would give a severely distorted DIP unit, and even models with the diamond topology but a different way of connection (essentially exchanging the *c* axis with another axis under *Fdd2* symmetry) would significantly distort the DIP ligand. It is worth noting that this possibility was initially ruled out by powder X-ray diffraction pattern indexing.

Chapter V. Post-Synthetic Modifications of a Carboxyl-Functionalized Covalent Organic Framework

5.1 Introduction

Covalent organic frameworks (COFs) are made by stitching together molecular building units through covalent bonds into crystalline extended structures.[1,2] The high porosities and large surface areas of these frameworks have motivated researchers to investigate their application to areas such as gas storage and separation,[3–6] heterogeneous catalysis,[7–12] ion conductivity,[13–18] and sensing.[19–21] Generally, to design a COF for a particular application, a specific chemical functionality needs to be introduced into the framework's pores to optimize its interactions with guest species. The introduction of functional groups can be effected both pre-synthetically by modifying the molecular building units,[22,23] or post-synthetically by modifying the organic backbone of the framework.[24–32] In this context, pre-synthetic modification of COFs is limited because it can interfere with the COF forming reaction. Post-synthetic modification provides higher versatility, with click chemistry currently being the most widely-used protocol.[8,33–37] However, conducting such copper-catalyzed azide-alkyne cycloaddition (CuAAC) reactions on COFs generally requires anaerobic handling, involves heterogeneous Cu(I) catalysts that need to be removed from the pores of the framework, and is incompatible with molecules featuring chelating functionalities, all of which greatly limit the generality of this approach. As such, a more general strategy for post-synthetic modification of COFs is highly desirable.

Against this backdrop, a new COF, termed COF-616, has been developed with its backbone functionalized with carboxyl groups that serve as orthogonal handles for facile post-synthetic functionalization reactions. Specifically, the carboxylic acid groups of COF-616 are found to be amenable to post-synthetic amidation, esterification, and thioesterification reactions under mild conditions, with high yields and an easy work-up protocol (Scheme 5.1). These new post-synthetic modification reactions allow for a large variety of functionalities to be introduced into the framework. To demonstrate the versatility of this approach, a series of sulfur and nitrogen-rich substrates were introduced into the framework and tested as heavy metal ion adsorbents. Such modification is incompatible with copper-assisted click reactions due to the strong chelating ability of these payloads.

Scheme 5.1. Newly-developed post-synthetic modification reactions for a carboxyl-functionalized COF.

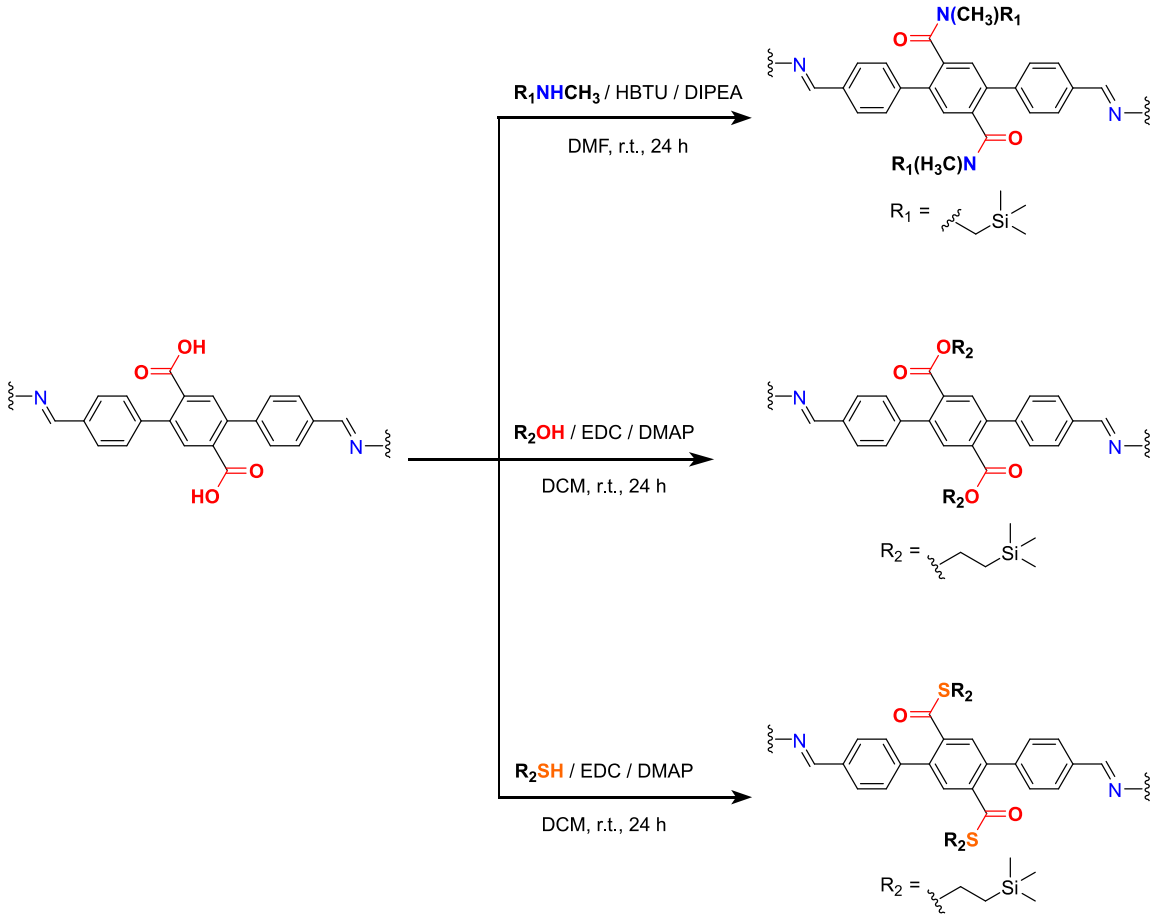

5.2 Experimental Section

5.2.1 Methods and Materials

Chemicals. Thionyl chloride (purity ≥ 97 %), trifluoromethanesulfonic anhydride (purity ≥ 99 %), trimethyl orthoformate (purity ≥ 99 %), (chloromethyl)trimethylsilane (purity ≥ 98 %), 2-(trimethylsilty)ethanol (purity ≥ 98 %), 1,4-dithiothreitol (purity ≥ 97 %), 2-(methythio)ethanol (purity ≥ 99 %), toluene (anhydrous purity ≥ 99.8%), 2-imidazolecarboxaldehyde (purity ≥ 97 %), THF (purity ≥ 99.8%), methylamine (33% in absolute EtOH), 1,4,8,11-tetraazacyclotetradecane (purity ≥ 98%), HBTU (purity ≥ 98%), *N*,*N*-diisopropylethylamine (purity ≥ 99 %), 4-(dimethylamino)pyridine (purity ≥ 99 %), and glacial acetic acid (purity 100%) were obtained from Sigma-Aldrich. 2,5-Dihydroxyterephthalic acid (purity ≥ 98 %) and lithium hydroxide anhydrous (purity ≥ 98 %) were purchased from TCI. 4-Formylphenylboronic acid (purity ≥ 98 %),

2-trimethylsilylethanol (purity ≥ 99 %), *N*-(3-dimethylaminopropyl)-*N*′-ethylcarbodiimide hydrochloride (purity ≥ 99 %), and tetrakis(triphenylphosphine) palladium(0) (purity ≥ 98 %) were acquired from Oakwood Chemicals. Toluene (anhydrous purity ≥ 99.8%) and THF (purity ≥ 99.8%) were supplied from EMD Millipore Chemicals. 4PE[38] and *N*,*N*-bis(2-((2-(ethylthio)ethyl)thio)ethyl)amine (NS4')[39] were prepared according to a reported procedure.

All reactions were performed under ambient laboratory conditions, with no precautions taken to exclude atmospheric moisture, unless otherwise specified. Pyrex glass tubes, charged with reagents and flash frozen with liquid N_2, were evacuated using a Schlenk line by fitting the open end of the tube inside a short length of standard rubber hose that was further affixed to a ground glass tap which could be closed to insulate this assembly from dynamic vacuum when the desired internal pressure was reached. Tubes were sealed under the desired static vacuum using an oxygen propane torch.

Analytical techniques and instrument. Powder X-ray diffraction data for unit cell determination were collected using a Bruker D8-Advance θ-θ diffractometer in parallel beam geometry employing Cu Kα1 line focused radiation at 1600 W (40 kV, 40 mA) power and equipped with a position sensitive detector. Samples were mounted on zero background sample holders by dropping powders from a wide-blade spatula and then leveling the sample with a razor blade. Gas adsorption experiments (up to 760 torr) were carried out on a Quantachrome AUTOSORB-1 automatic volumetric instrument and Micromeritics 3Flex Surface Characterization Analyzer. Ultrahigh-purity-grade N_2 was used in all adsorption measurements. The N_2 (77 K) isotherms were measured using a liquid nitrogen bath (77 K). Solution ^{1}H NMR spectra were acquired on a Bruker AV-600 NMR spectrometer. Elemental microanalyses (EA) were performed in the Microanalytical Laboratory of the College of Chemistry at UC Berkeley, using a Perkin Elmer 2400 Series II CHNS elemental analyzer. Inductively coupled plasma atomic emission spectroscopy was performed on an Agilent 7500ce ICP-AES using the helium collision gas mode. Attenuated total reflectance (ATR) FTIR spectra of neat samples were performed on a Bruker ALPHA Platinum ATR-FTIR Spectrometer equipped with a single reflection diamond ATR module. Samples for SEM study were prepared by dropcasting the samples from a MeOH suspension onto a 1 cm^2 silicon wafer. SEM images were recorded on a Quanta™ 3D FEG scanning electron microscope with an accelerating voltage of 5 kV and a working distance of 10 mm.

5.2.2 Synthesis

Synthesis of 3P-COOH.

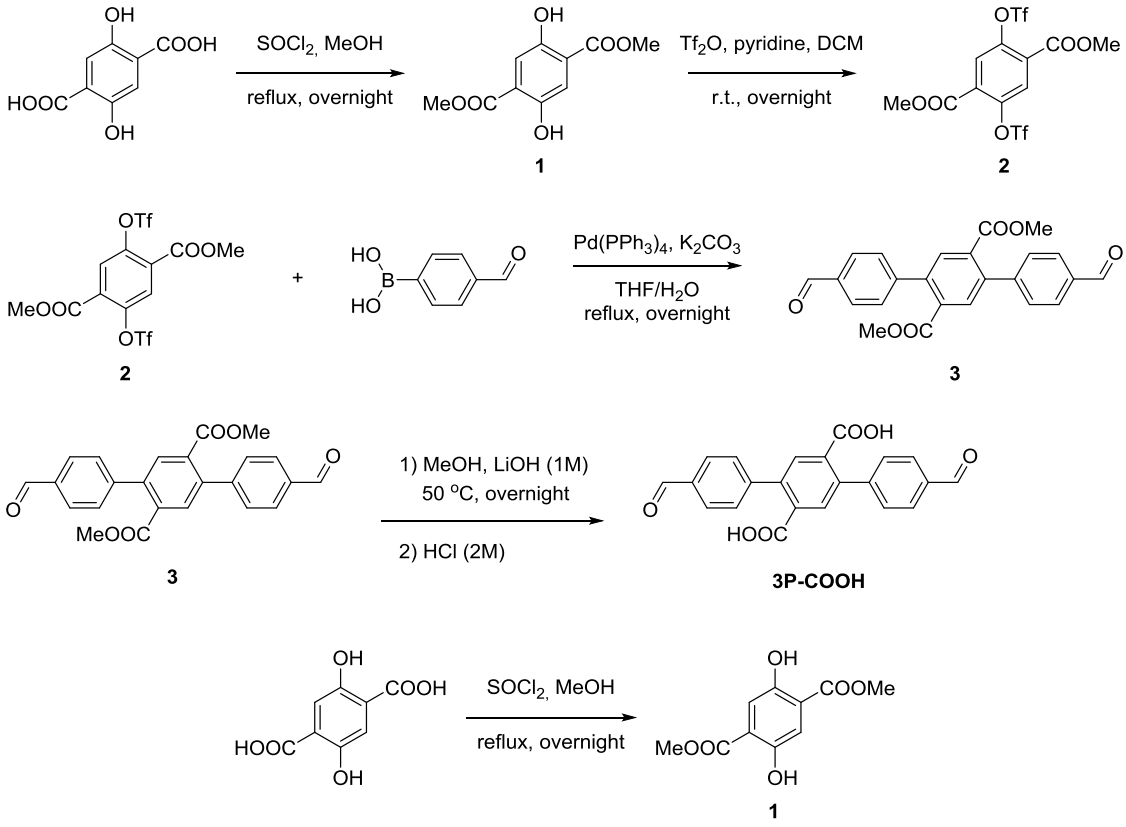

1. To a flask containing 2,5-dihydroxyterephthalic acid (2.0 g, 10 mmol) in methanol (anhydrous, 40 mL) cooled in an ice/water bath was added thionyl chloride (9 mL, 124 mmol) dropwise. The mixture was warmed to room temperature and then refluxed under N_2 overnight. After cooling to room temperature, the organic solvent was removed. Crude product **1** was afforded as a dark yellow solid (ca. 2.1 g) and was used directly in the next step without further purification. This compound is characterized elsewhere.[40]

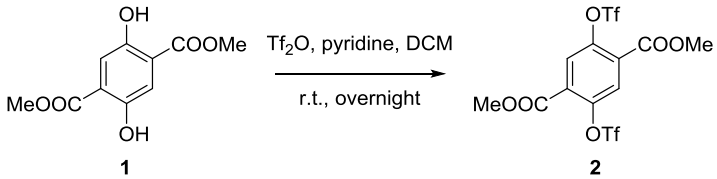

2. To a flask containing **1** (1.45 g, 6.4 mmol) and pyridine (1.3 mL, 16.5 mmol) in DCM (anhydrous, 16 mL) cooled in an ice/water bath was added trifluoromethanesulfonic anhydride (3.2 mL, 19 mmol) dropwise. The mixture was warmed to room temperature and stirred overnight. Upon completion of the reaction, the organic solvent was removed. The

mixture was quenched with aq HCl (1M, 50 mL) and extracted by DCM three times. The organic phase was then dried by Na_2SO_4 and concentrated to afford **2** as a light brown solid. The crude residue was purified by column chromatography (EtOAc-hexanes) to afford **2** (2.92 g, 5.95 mmol, 88% yield over two steps) as a white solid. ^{1}H NMR (600 MHz, $CDCl_3$) δ 8.00 (s, 2H), 4.02 (s, 6H). ^{13}C NMR (151 MHz, $CDCl_3$) δ 161.95, 146.62, 129.68, 127.44, 119.84, 117.72, 53.71.

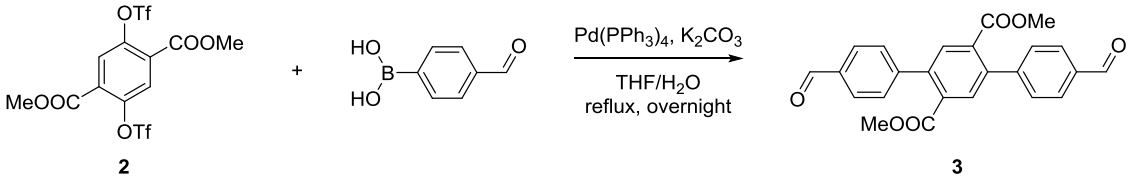

2 **3**

3. In a typical synthesis, a three-neck round-bottom flask was charged with **2** (5.3 g, 10.8 mmol), 4-formylphenylboronic acid (4.1 g, 27 mmol), and potassium carbonate (5.8 g, 42.0 mmol) in a water (50 mL) and THF (100 mL) mixture. The mixture was degassed for 30 minutes with N_2 and under vigorous stirring. To this solution was added $Pd(PPh_3)_4$ (5.0 g, 4.3 mmol) and the mixture was heated to reflux overnight. THF was removed under vacuum and the mixture was further extracted with DCM (3 x 150 mL). The combined organic phases were washed with water, brine, and dried with sodium sulfate. Evaporation of the solvent afforded crude product, which was purified by column chromatography (EtOAc: hexanes (v/v) = 1:3) to give a white powder (2.9 g, 7.2 mmol, 67%). ^{1}H NMR (600 MHz, $(CD_3)_2SO$) δ 10.09 (s, 2H), 8.01 (d, *J* = 8.0 Hz, 4H), 7.89 (s, 2H), 7.63 (d, J = 7.8 Hz, 4H), 3.65 (s, 6H). ^{13}C NMR (151 MHz, $(CD_3)_2SO$) δ 192.79, 166.80, 144.85, 139.83, 135.39, 133.07, 131.59, 129.49, 129.06, 52.44.

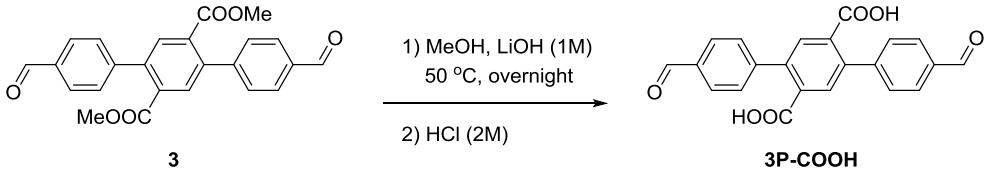

3 **3P-COOH**

3P-COOH. To a solution of **3** (1.4 g, 3.6 mmol) in MeOH (50 mL) cooled in an ice/water bath, was added dropwise an aqueous solution of LiOH (1M, 50 mL) dropwise, and the mixture was warmed to 50 °C and stirred overnight. MeOH was removed under reduced pressure, and the residue was acidified to pH 1, resulting in precipitation. The solid was filtered, washed with water, and dried under vacuum to afford **3P-COOH**, used without further purification (1.2 g, 3.2 mmol, 88%). ^{1}H NMR (600 MHz, $(CD_3)_2SO$) δ 13.34 (s, 1H), 10.08 (s, 1H), 7.99 (d, J = 8.1 Hz, 2H), 7.82 (s, 1H), 7.65 (d, J = 8.0 Hz, 2H). ^{13}C NMR (151 MHz, $(CD_3)_2SO$) δ 192.81, 167.99, 145.59, 139.61, 135.29, 134.07, 131.42, 129.38, 129.20, 39.93, 39.80, 39.66, 39.52, 39.38, 39.24, 39.10. HRMS (ESI^-) for $[C_{22}H_{13}O_6]^-$ ($M\text{-}H^-$): m/z Calcd. 373.0718, found 373.0715.

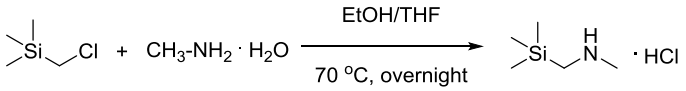

Synthesis of *N*-methyl-1-(trimethylsilyl)methanaminium chloride. (Chloromethyl)trimethylsilane (558 μL, 4 mmol) and methylamine (33 wt. % in ethanol solution, 1.81 mL, 24 mmol) were added to an EtOH/THF (1.6 mL/3.2 mL) solvent mixture in a pressure vessel. The mixture was heated to 70 °C overnight. Upon completion of the reaction, it was cooled down to room temperature, and an excess of methanolic HCl was added. The solvent was removed under vacuum to yield the product (428.7 mg, 57 %). ^{1}H NMR (600 MHz, MeOD) δ 2.74 (s, 3H), 2.51 (s, 2H), 0.21 (s, 9H). ^{13}C NMR (151 MHz, MeOD) δ 41.21, 38.16, -2.60. HRMS (ESI^{+}) for $[C_5H_{16}NSi]^{+}$ (M+H^{+}): m/z Calcd.118.1047, found 118.1046.

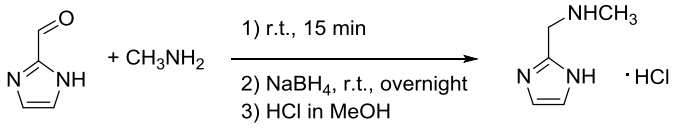

Synthesis of 1-(1H-imidazol-2-yl)-*N*-methylmethanaminium chloride. To a solution of 2-imidazolecarboxaldehyde (192.2 mg, 2 mmol) in EtOH was added methylamine (33 wt. % in ethanol solution, 8 mL). After stirring at room temperature for 15 minutes, the solution was cooled to 0 ℃, prior to the portion-wise addition of sodium borohydride (227 mg, 6 mmol, 3 eq). The resulting solution was stirred at room temperature overnight, followed by addition of an excess of methanolic HCl. The solvent was removed under vacuum to yield the product (130.0 mg, 44%). ^{1}H NMR (600 MHz, MeOD) δ 7.73 (s, 2H), 4.69 (s, 2H), 2.86 (s, 3H). ^{13}C NMR (151 MHz, MeOD) δ 122.25, 42.37, 33.94. HRMS (ESI^{+}) for $[C_5H_{10}N_3]^{+}$ (M+H^{+}): m/z Calcd.112.0869, found 112.0869.

Synthesis of COF-616. To an oven-dried Pyrex tube measuring 10 × 8 mm (o.d × i.d) were added 3P-COOH (13.5 mg, 0.036 mmol, 2 eq), 4PE (7.1 mg, 0.18 mmol), glacial acetic acid (10 μL), butanol (120 μL), and 1,2-dichlorobenzene (180 μL). The tube was flash frozen at 77 K (liquid N_2 bath). After two freeze-pump-thaw cycles, the system was evacuated to an internal pressure of 70 mTorr and flame sealed, reducing the tube length to approximately 15 cm. After heating to 100 ℃ for 48 h, a precipitate formed at the bottom of the tube, which was isolated by filtration and washed with an excess of DMF, then MeOH in a Soxhlet extractor for two days. The wet solid was washed five times with liquid CO_2. The system was then heated up to 45 ℃ to bring about the supercritical state of CO_2 and slowly bled to ambient pressure. Finally, the chamber with the product was evacuated at 30 mTorr and at 50 ℃ for 6 h and 100 ℃ for 24 h to yield COF-616 as a yellow-orange powder. Elemental analysis of COF-616: Calcd for $C_{35}H_{24}N_2O_4{\cdot}H_2O$: C, 75.8%; H, 4.7%; N, 5.1%; O, 14.4%. Found: C, 74.2%; H, 5.1%; N, 5.2%; O, 15.5%.

Synthesis of COF-616-CON(CH_3)R_1 (R_1 = trimethylsilylmethyl). *N*-methyl-1-(trimethylsilyl)methanaminium chloride (8.3 mg, 0.054 mmol, 3 eq), HBTU (20.5 mg, 0.054 mmol, 3 eq), and DIPEA (18.8 μL, 0.108 mmol, 3 eq) were dissolved in DMF (1 mL), and COF-616 (5 mg, 0.018 mmol -COOH) was then added to the solution. The mixture was allowed to react in a shaker at room temperature for 24 h. The product was then filtered, washed with an excess of DMF and MeOH in a Soxhlet extractor, and eventually evacuated under vacuum at 50 ^{o}C for 24 h. The conversion yield is 95% as confirmed by ^{1}H NMR spectroscopy of the digested sample. Elemental analysis of COF-616-CON(CH_3)R_1: Calcd for $C_{44.5}H_{48.7}N_{3.9}O_{2.1}Si_{1.9}$: C, 73.8%; H, 6.7%; N, 7.5%; O, 4.6%; Si, 7.3%. Found: C, 73.2%; H, 6.3%; N, 7.4%.

Synthesis of COF-616-COOR_2 (R_2 = 2-(trimethylsilyl)ethyl). *N*-methyl-1-2-(trimethylsilyl)ethanol (34.4 μL, 0.24 mmol, 6 eq), EDC·HCl (23 mg, 0.120 mmol, 3 eq), and DMAP (45 mg, 0.368 mmol, 9 eq) were dissolved in DCM, and COF-616 (11.1 mg, 0.04 mmol -COOH) was then added to the solution. The mixture was allowed to react in a shaker at room temperature for 24 h. The product was filtered, washed with an excess of DCM, and MeOH in a Soxhlet extractor, and eventually evacuated under vacuum at 50 ^{o}C for 24 h. The conversion yield is 74% as confirmed by ^{1}H NMR spectroscopy of the digested sample. Elemental analysis of COF-616-COOR_2: Calcd for $C_{42.5}H_{42}N_2O_4Si_{1.5}$: C, 74.5%; H, 6.1%; N, 4.1%; O, 9.3%; Si, 6.1%. Found: C,70.0%; H, 6.1%; N, 4.5%.

Synthesis of COF-616-COSR_2 (R_2 = 2-(trimethylsilyl)ethyl). 2-(Trimethylsilyl) ethanethiol (57 μL, 0.36 mmol, 9 eq), EDC·HCl (23 mg, 0.120 mmol, 3 eq), and DMAP (45 mg, 0.368 mmol, 9 eq) were dissolved in DCM, and COF-616 (11.1 mg, 0.04 mmol -COOH) was then added to the solution. The mixture was allowed to react in a shaker at room temperature for 24 h. The product was filtered, washed with an excess of DCM, and MeOH in a Soxhlet extractor, and eventually evacuated under vacuum at 50 ^{o}C for 24 h. The conversion yield is 63.3% as confirmed by ^{1}H NMR spectroscopy of the digested sample. Elemental analysis of COF-616-COSR_2: Calcd for $C_{41}H_{38.4}N_2O_{2.8}Si_{1.2}S_{1.2}$: C, 73.0%; H, 5.8%; N, 4.1%; O, 6.2%; Si, 5.0%, S, 5.7%. Found: C, 73.0%; H, 5.1%; N, 4.7%, S, 5.7%.

Synthesis of COF-616-NS4'. *N*,*N*-bis(2-((2-(ethylthio)ethyl)thio)ethyl)amine (NS4') (17 mg, 0.054 mmol, 3 eq), HBTU (20.5 mg, 0.054 mmol, 3 eq), and DIPEA (18.8 μL, 0.108 mmol, 3 eq) were dissolved in DMF, and COF-616 (5 mg, 0.018 mmol –COOH) was then added to the solution. The mixture was allowed to react in a shaker at room temperature for 24 h. The product was filtered, washed with an excess of DMF, and MeOH in a Soxhlet extractor, and eventually evacuated under vacuum at 50 ^{o}C for 24 h. The conversion yield is 100% as confirmed by ^{1}H NMR spectroscopy of the digested sample. Elemental analysis of COF-616-NS4': Calcd for $C_{59}H_{74}N_4O_2S_8$: C, 62.9%; H, 6.6%; N, 5.0%; O, 2.8%; S, 22.7%. Found: C, 59.4%; H, 7.1%; N, 4.9%, S, 21.3%.

Synthesis of COF-616-CY. 1,4,8,11-Tetraazacyclotetradecane (Cyclam) (11 mg, 0.054 mmol, 3 eq), HBTU (20.5 mg, 0.054 mmol, 3 eq), and DIPEA (18.8 μL, 0.108 mmol, 3 eq) were dissolved in DMF, and COF-616 (5 mg, 0.018 mmol –COOH) was then added to the solution. The mixture was allowed to react in a shaker at room temperature for 24 h. The product was filtered, washed with an excess of DMF, and MeOH in a Soxhlet extractor, and eventually evacuated under vacuum at 50 °C for 24 h. The conversion yield is 64.3% as confirmed by ^{1}H NMR spectroscopy of the digested sample. Elemental analysis of COF-616-CY: Calcd for $C_{48}H_{53}N_{7.2}O_{2.7} \cdot (H_2O)_{3.4}$: C, 68.9%; H, 7.2%; N, 13.0%; O, 11.7%. Found: C, 68.9%; H, 6.8%; N, 11.2%.

Synthesis of COF-616-IMD. 1-(1H-imidazol-2-yl)-*N*-methylmethanaminium chloride (IMD) (6 mg, 0.054 mmol, 3 eq), HBTU (20.5 mg, 0.054 mmol, 3 eq), and DIPEA (18.8 μL, 0.108 mmol, 3 eq) were dissolved in DMF, and COF-616 (5 mg, 0.018 mmol –COOH) was then added to the solution. The mixture was allowed to react in a shaker at room temperature for 24 h. The product was filtered, washed with an excess of DCM, and MeOH in a Soxhlet extractor, and eventually evacuated under vacuum at 50 °C for 24 h. The conversion yield is 65% as confirmed by ^{1}H NMR spectroscopy of the digested sample.

Synthesis of COF-616-MTE. 2-(Methylthio)ethanol (MTE) (20.9 μL, 0.24 mmol, 12 eq), EDC·HCl (23 mg, 0.120 mmol, 6 eq), and DMAP (45 mg, 0.368 mmol, 18 eq) were dissolved in DCM, and COF-616 (11.1 mg, 0.02 mmol) was then added to the solution. The mixture was allowed to react in a shaker at room temperature for 24 h. The product was filtered, washed with an excess of DCM, and MeOH in a Soxhlet extractor, and eventually evacuated under vacuum at 50 °C for 24 h. The conversion yield is 67% as confirmed by ^{1}H NMR spectroscopy of the digested sample. Elemental analysis of COF-616-MTE: Calcd for $C_{38.9}H_{31.8}N_2O_4S_{1.3}$: C, 73.9%; H, 5.0%; N, 4.4%; O, 10.1%, S, 6.6%. Found: C, 69.4%; H, 5.6%; N, 4.3%, S, 5.1%.

Synthesis of COF-616-DTT. Dithiothreitol (DTT) (37 mg, 0.24 mmol, 12 eq), EDC·HCl (23 mg, 0.120 mmol, 6 eq), and DMAP (45 mg, 0.368 mmol, 18 eq) were dissolved in DCM, and COF-616 (11.1 mg, 0.02 mmol) was then added to the solution. The mixture was allowed to react in a shaker at room temperature for 24 h. The product was filtered, washed with an excess of DCM, and MeOH in a Soxhlet extractor, and eventually evacuated under vacuum at 50 °C for 24 h. The conversion yield is 59% as confirmed by ^{1}H NMR spectroscopy of the digested sample. Elemental analysis of COF-616-DTT: Calcd for $C_{42.2}H_{38.4}N_2O_{5.8}S_{3.6}$: C, 64.9%; H, 4.9%; N, 3.6%; O, 11.9%, S, 14.7%. Found: C, 63.6%; H, 6.3%; N, 4.7%, S, 14.6%.

5.3 Results and Discussion

5.3.1 Synthesis and Characterization of COF-616.

COF-616 was synthesized from *p*-terphenyl-2',5'-dicarboxylic acid-4,4''-dicarboxaldehyde (3P-COOH) and 1,1,2,2-tetraphenylethene (4PE) under solvothermal reaction conditions in a mixture of butanol and 1,2-dichlorobenzene (DCB), using glacial acetic acid as a catalyst (Figure 5.1). The mixture was sealed in a Pyrex tube and heated to 100 ^{o}C for 2 days. COF-616 was obtained by filtration as a yellow microcrystalline powder, which was found to be insoluble in common organic solvents such as alcohols, acetone, dichloromethane, tetrahydrofuran (THF), *N*,*N*-dimethylformamide (DMF), and *N*-methyl-2-pyrrolidionone (NMP).

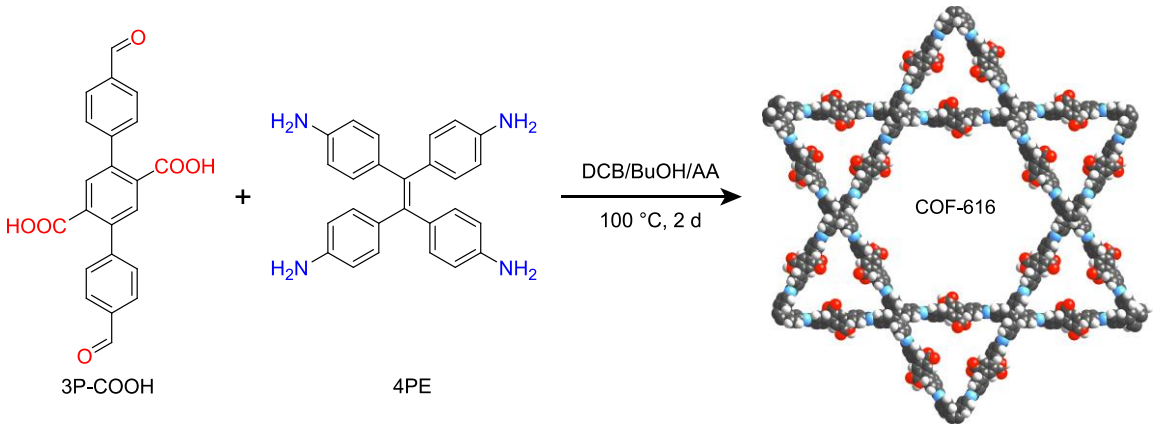

Figure 5.1. Synthetic scheme of COF-616. Color code: H, white; C, gray; N, blue; O, red.

The completeness of the reaction was confirmed by Fourier Transform Infrared (FT-IR) spectroscopy: a characteristic imine stretching vibration at 1621 cm^{-1} emerged, and the disappearance of both the characteristic aldehyde absorption band at 1682 cm^{-1} and the amine absorption band at 3500-3150 cm^{-1} was observed in the corresponding spectra (Figure 5.2). As a result of increased conjugation in the framework, the carbonyl stretching band of the carboxylic acid functional groups is redshifted from 1723 cm^{-1} in the starting material 3P-COOH, to 1696 cm^{-1} in COF-616. This is consistent with what is observed for a molecular analogue (Figure 5.3).

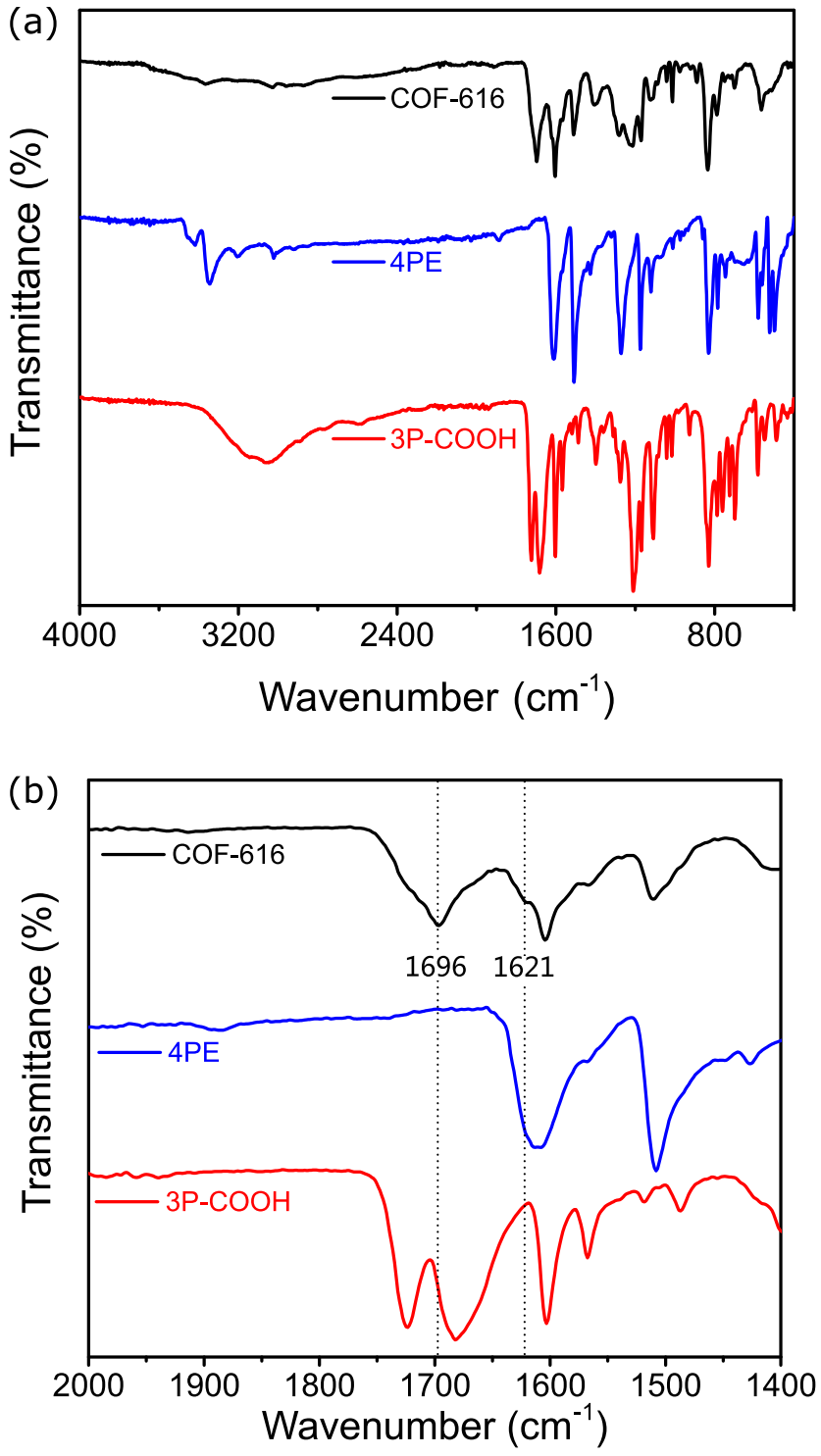

Figure 5.2. FT-IR spectra of COF-616 and comparison to the starting materials 4PE and 3P-COOH, respectively.

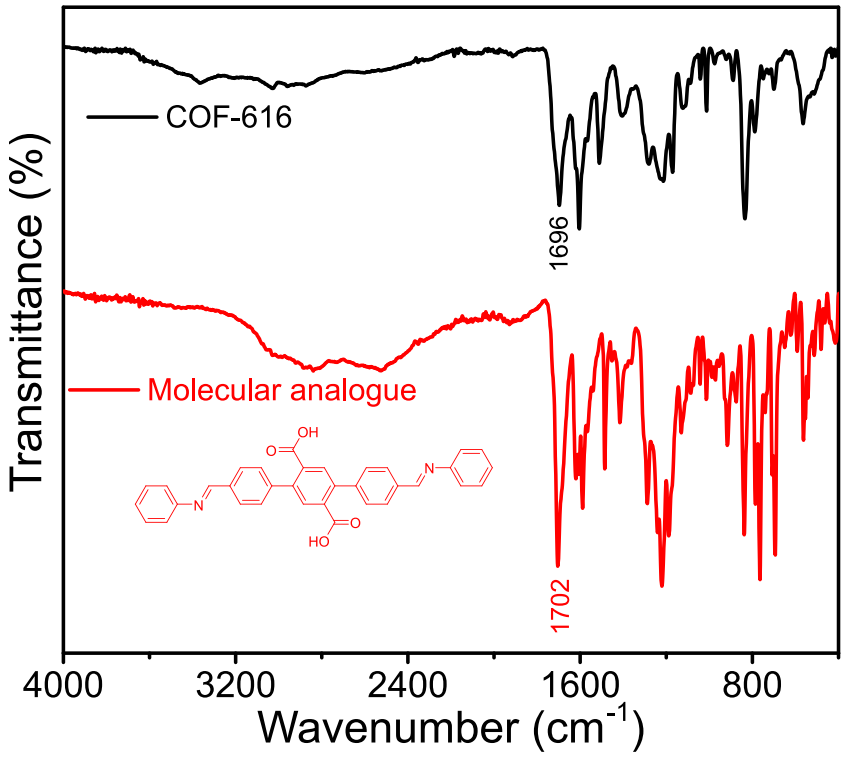

Figure 5.3. FT-IR spectra of COF-616 and its molecular analogue.

The thermal stability of COF-616 was evaluated by thermogravimetric analysis and no significant weight loss was observed until 310 ^{o}C under an N_2 atmosphere (Figure 5.4). The chemical formula of activated COF-616 was determined by elemental analysis and was found to be consistent with the expected elemental composition (Calcd for $C_{35}H_{24}N_2O_4 \cdot H_2O$: C, 75.80%; H, 4.73%; N, 5.06%; O, 14.42%. Found: C, 74.18%; H, 5.11%; N, 5.25%; O, 15.46%).

Scanning electron microscopy (SEM) images of COF-616 showed that all particles displayed a homogeneous morphology, consisting of aggregated flake-shaped crystals (Figure 5.5). The crystallinity of COF-616 was confirmed by powder X-ray diffraction (PXRD) and the framework was found to crystalize in the hexagonal space group *P*6 (Figure 5.6). Structural modeling of COF-616 was carried out in the Materials Studio 8.0 software package and the theoretical models were optimized by the Forcite module. Pawley refinements of the PXRD pattern were done in the Reflex module using data from 1.75 to 50 °, and yielded unit cell parameters of $a = b = 55.038(56)$ Å, and $c = 3.930(21)$ Å with good agreement factors ($R_p = 2.55$ %, $R_{wp} = 3.69$ %) (Table 5.1 in Appendix). The activated COF-616 sample was analyzed by N_2 sorption at 77 K. Brunauer−Emmett−Teller (BET) surface areas of COF-616 was calculated to be 397 m^2/g (Figure 5.7-5.9).

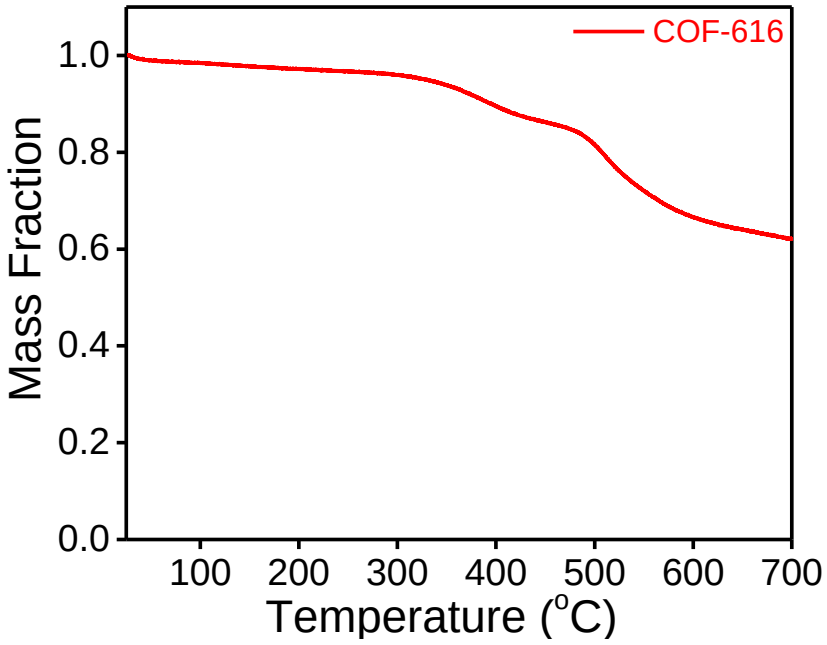

Figure 5.4. TGA trace for the COF-616 under an N_2 atmosphere.

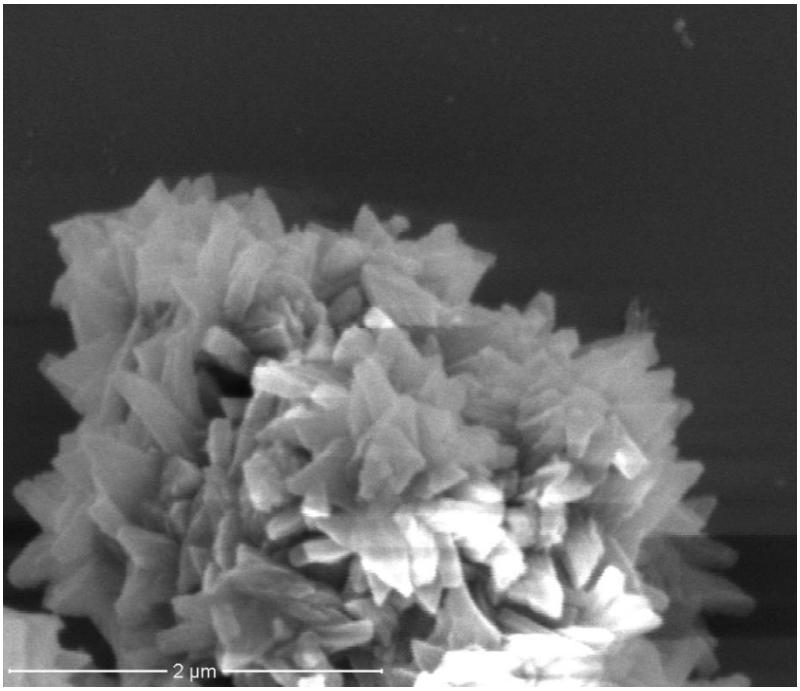

Figure 5.5. SEM image of COF-616 powder. The crystallites of COF-616 are of flake-shape with size of 1 µm.

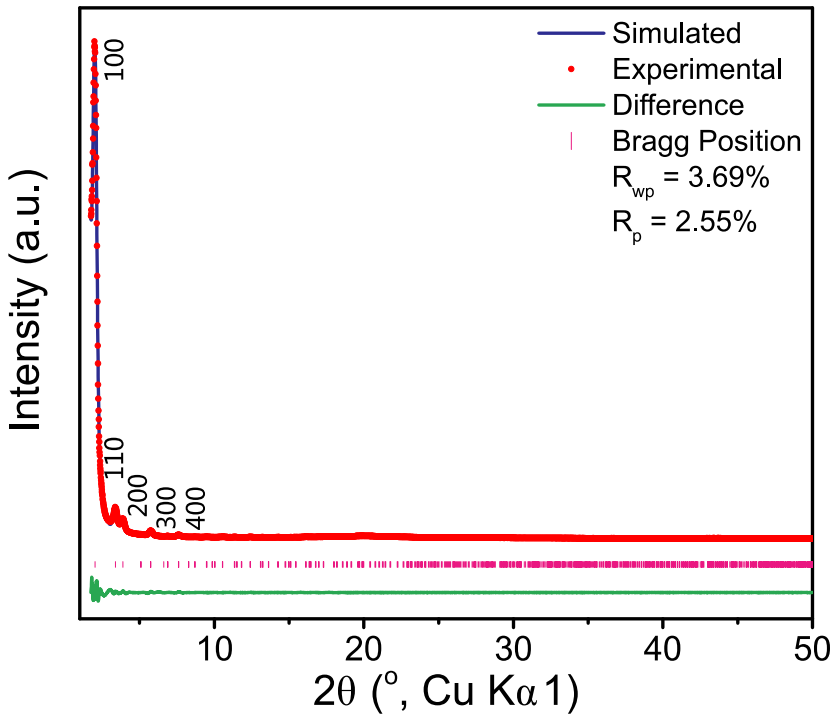

Figure 5.6. PXRD pattern and Pawley refinement of COF-616.

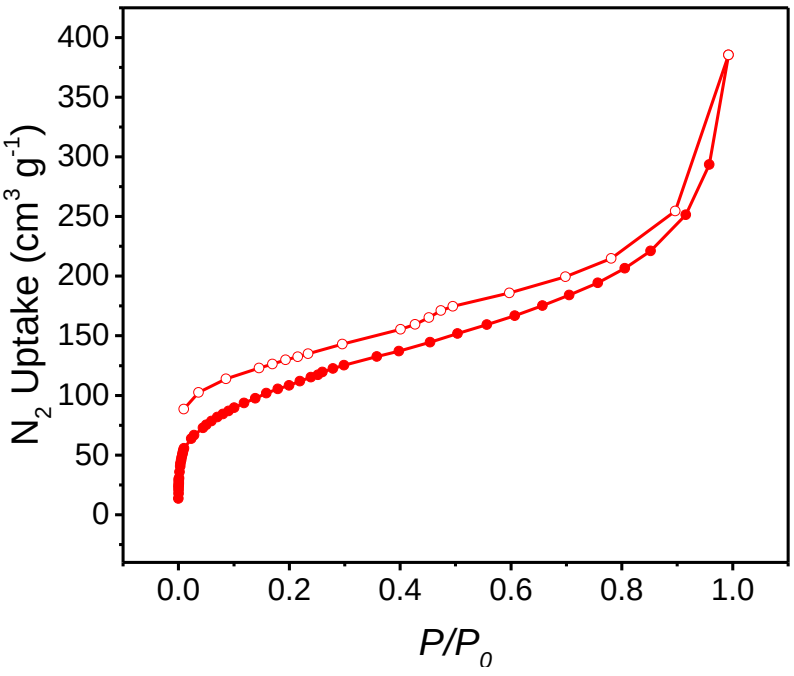

Figure 5.7. N_2 adsorption isotherm of COF-616 acquired at 77 K.

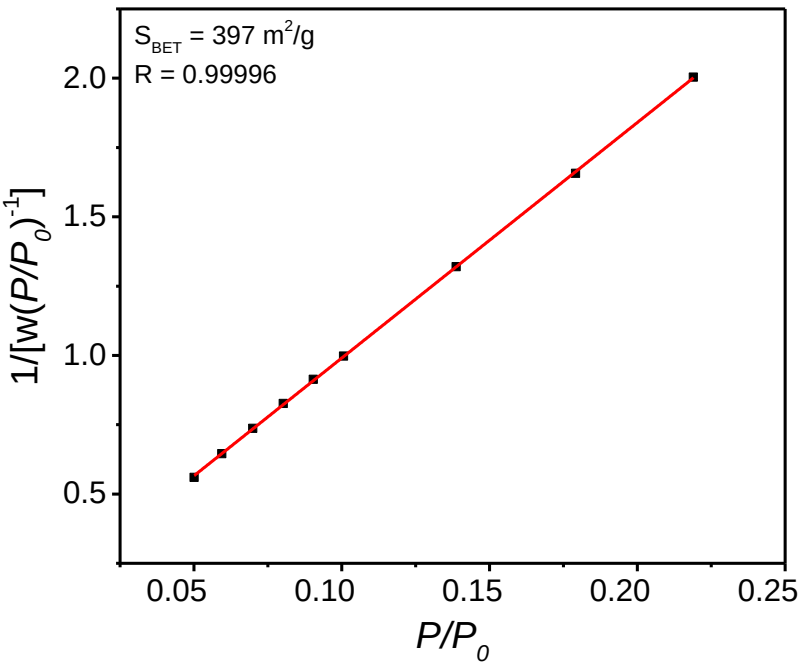

Figure 5.8. BET plot for COF-616.

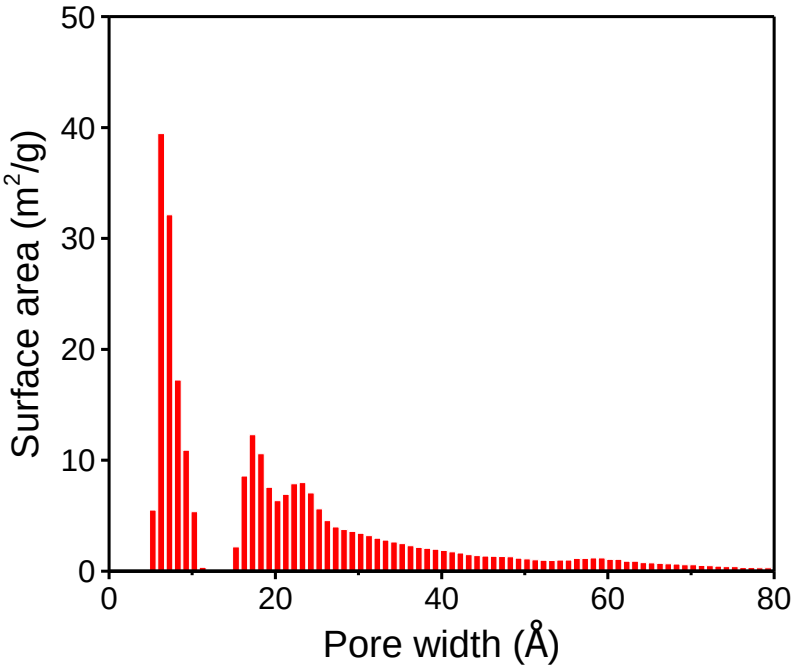

Figure 5.9. Pore size distribution histogram of COF-616 calculated from DFT fitting of the adsorption branch of the N_2 adsorption isotherm acquired at 77 K with a fitting error of 0.79% using a slit/cylinder pores, QSDFT adsorption branch model.

5.3.2. Post-Synthetic Modifications for COF-616

Carboxyl groups are prominent functionalities in synthetic organic chemistry as they can be converted into various derivatives through activation followed by nucleophilic substitution reactions. This type of transformation is widely used in heterogeneous solid-phase peptide synthesis, and, as such, holds promise as a mild and effective toolbox for post-synthetically introducing complex payloads onto carboxylic acid functionalized COFs. Amide coupling on COF-616 was performed using uronium salts as coupling reagents.[41–43] While primary amines are not suitable for this post-synthetic modification due to off-pathway transimination reactions with the linkages of the framework,[44] secondary amines are great candidates to append organic moieties onto COFs. *N*-methyl-1-(trimethylsilyl)methanamine was selected as a model compound (Scheme 5.1). To carry out the post-synthetic modification, COF-616 was added to a solution of *N*-methyl-1-(trimethylsilyl) methanamine, hexafluorophosphate benzotriazole tetramethyl uronium (HBTU), and *N*,*N*-diisopropylethylamine (DIPEA) in DMF, and the mixture was allowed to react at room temperature for 24 h. The amidated product, COF-616-CON(CH_3)R_1 (R_1 = trimethylsilyl)methyl), was obtained by filtration, washed with an excess of DMF, and methanol in a Soxhlet extractor, and eventually evacuated under dynamic vacuum. Near-quantitative conversion (95%) of carboxyl groups to amides was confirmed by the appearance of characteristic peaks (δ = -0.09 ppm for trimethylsilyl group) in the ^{1}H NMR spectrum of the digested sample (Figure 5.10-5.12). This was further supported by FT-IR spectroscopy, where the modified product exhibited the emergence of a characteristic C=O amide absorbance band (1648 cm^{-1}) and the disappearance of the C=O (1696 cm^{-1}) carboxyl stretching vibration of the carboxylic acid precursor (Figure 5.13). The PXRD pattern and SEM micrographs demonstrated that COF-616-CON(CH_3)R_1 retained its crystallinity throughout the post-synthetic modification process (Figure 5.14 and 5.15).

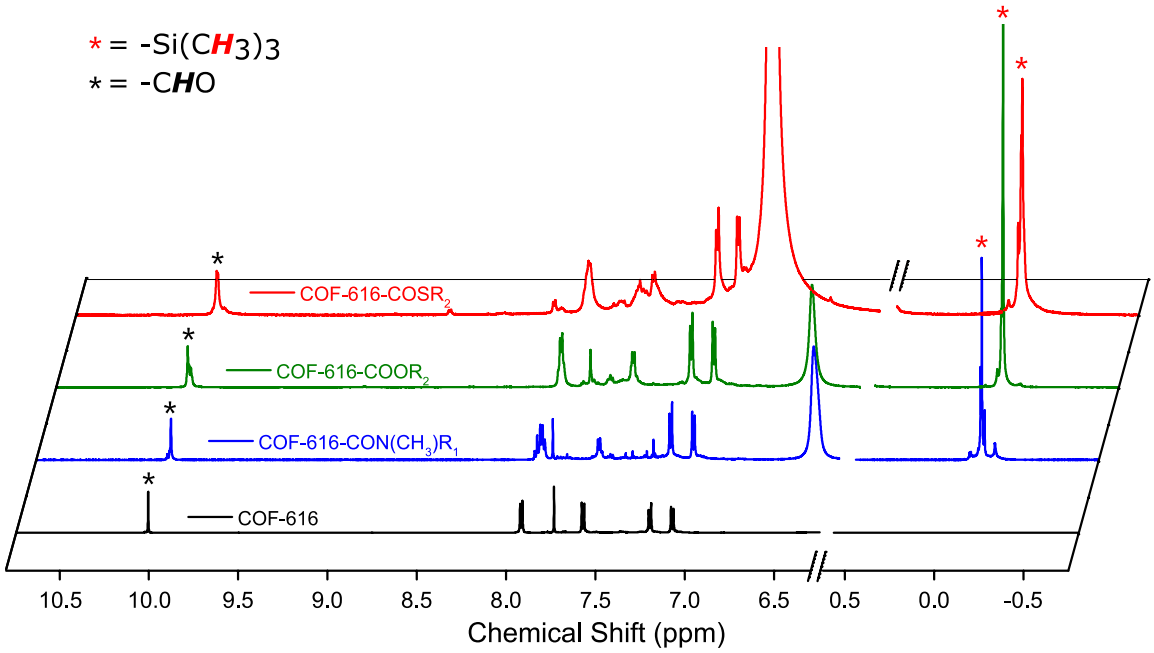

Figure 5.10. ^{1}H NMR spectra of the digested samples of COF-616, COF-616-CON(CH_3)R_1, COF-616-$COOR_2$, and COF-616-$COSR_2$, respectively. The conversion of carboxyl groups was quantified by comparing the ratios of aldehyde peaks (δ = 10.05 ppm) to trimethylsilyl group peaks (δ = -0.09 ppm).

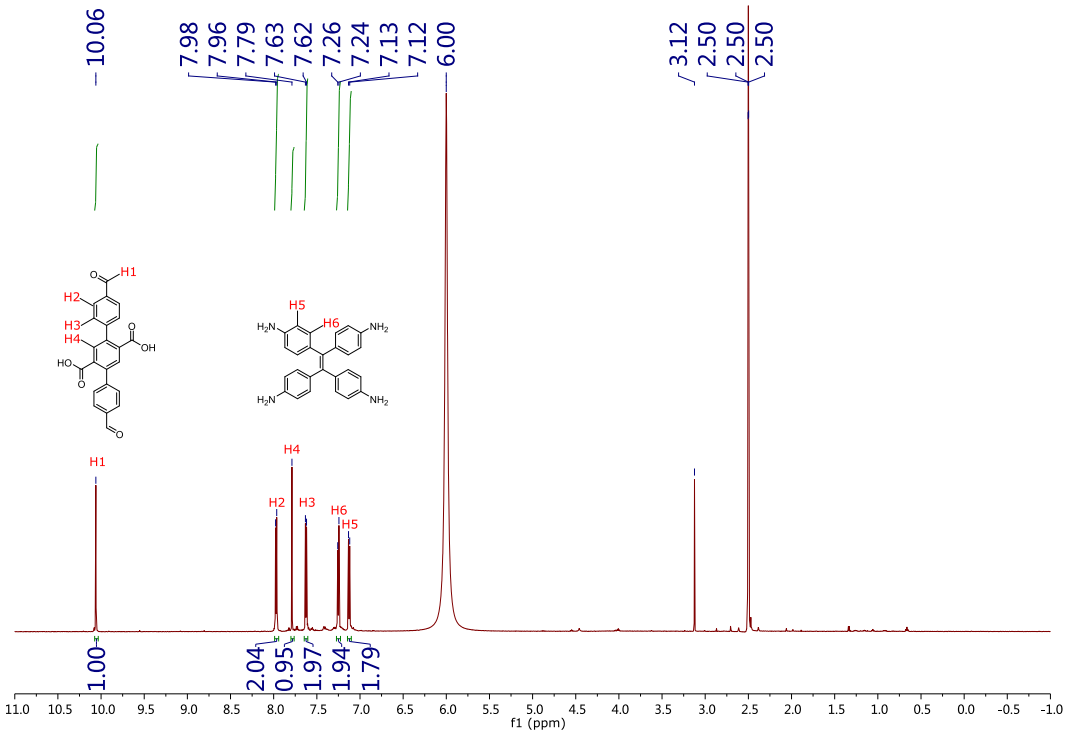

Figure 5.11. ^{1}H NMR spectrum of digested COF-616.

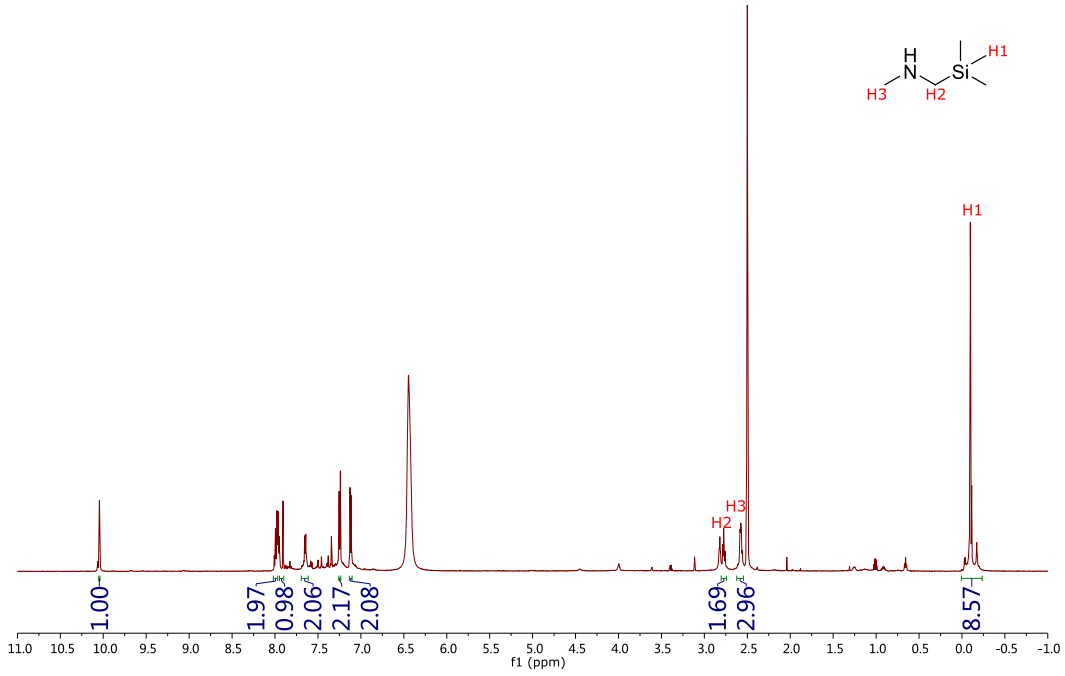

Figure 5.12. ^{1}H NMR spectrum of digested COF-616-CON(CH_3)R_1. The integral ratio between the trimethylsilyl group peaks and aldehyde peaks is 8.57, therefore the yield of the conversion is calculated to be 95.2%.

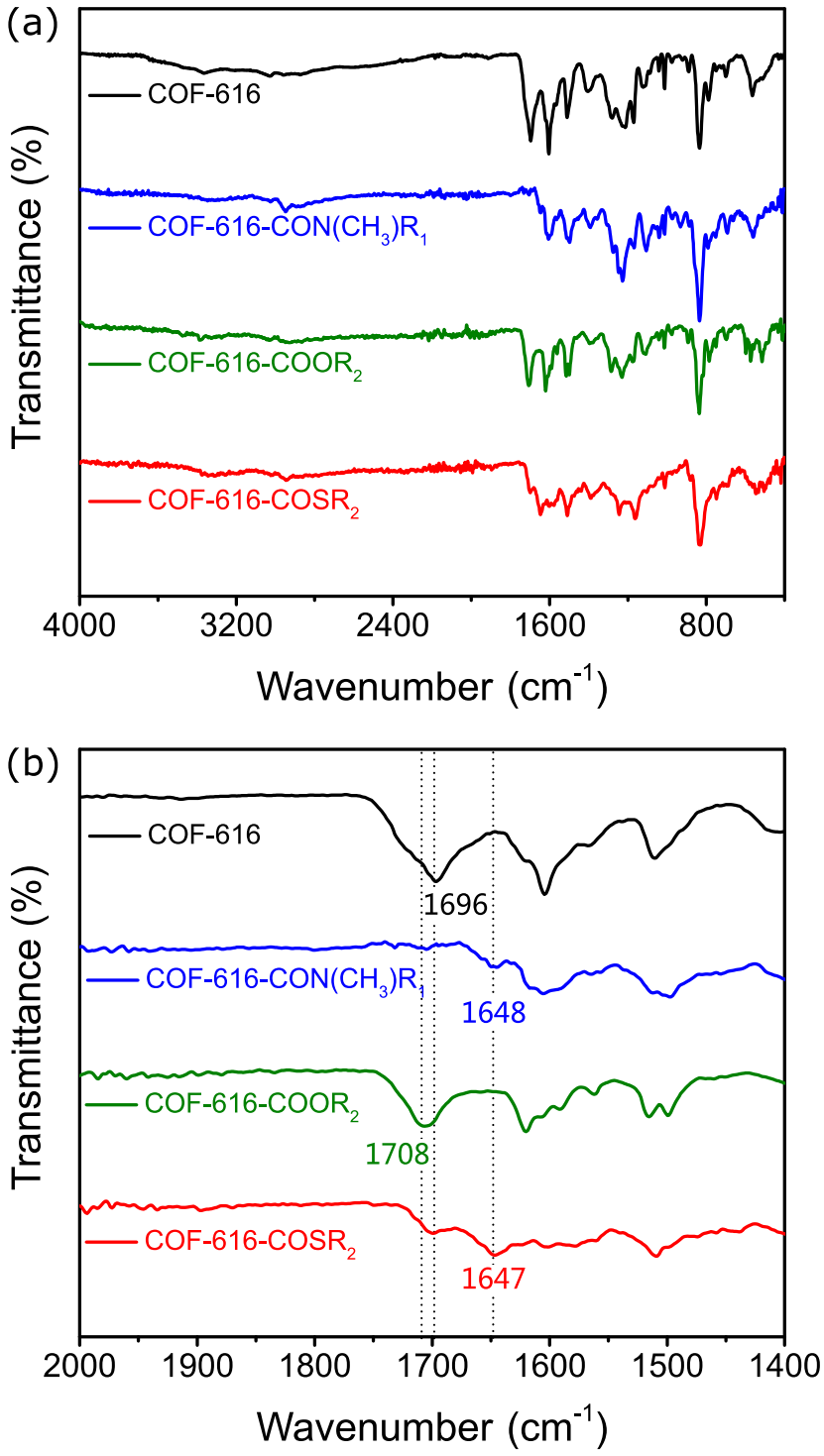

Figure 5.13. FT-IR spectra of COF-616-CON(CH_3)R_1, COF-616-$COOR_2$, COF-616-$COSR_2$, and pristine COF-616.

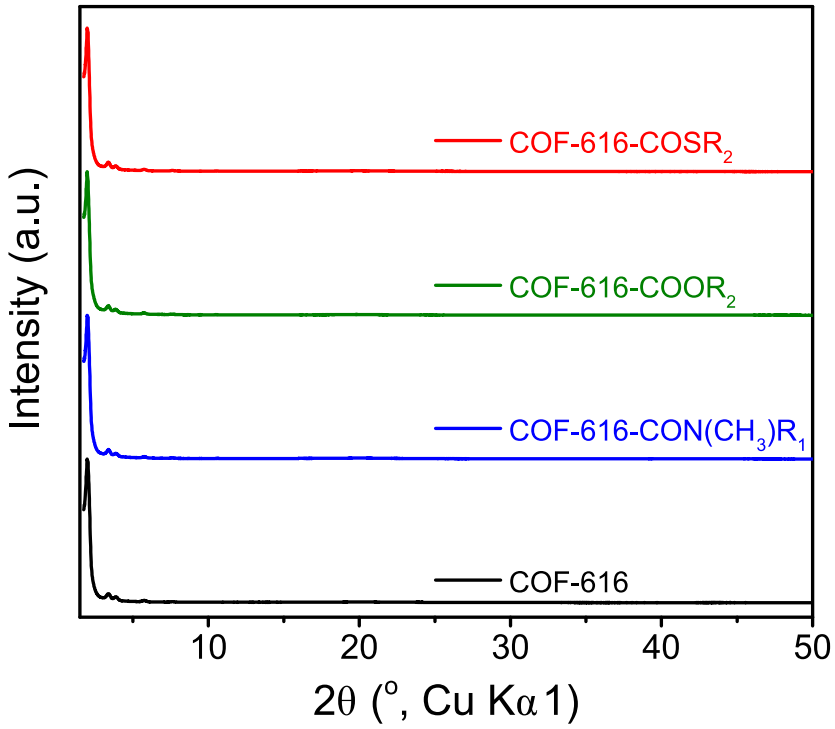

Figure 5.14. PXRD patterns of COF-616-CON(CH_3)R_1, COF-616-$COOR_2$, and COF-616-$COSR_2$, compared with pristine COF-616.

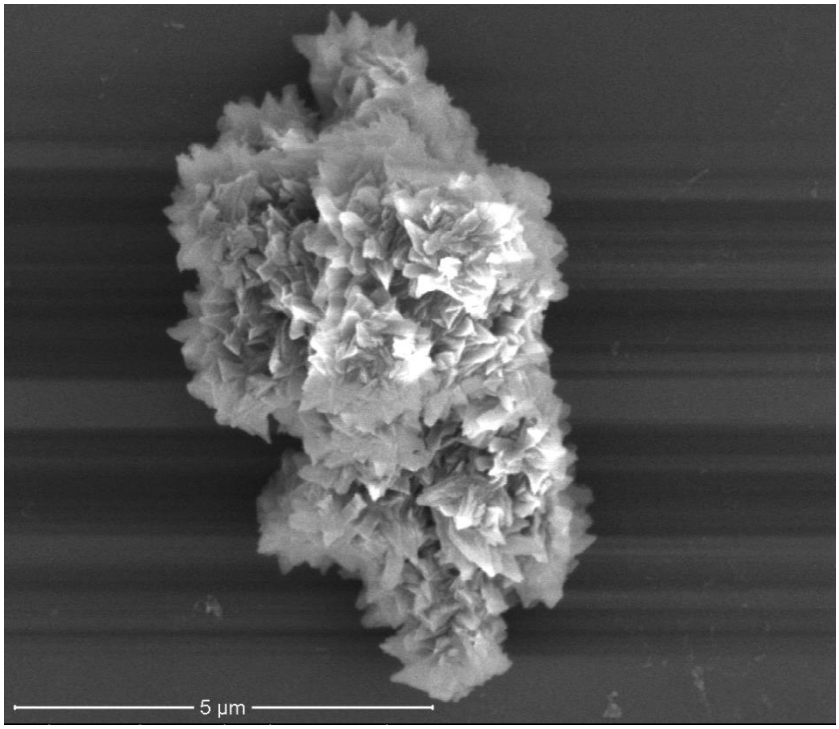

Figure 5.15. SEM image of COF-616-CON(CH_3)R_1.

The protocol for post-synthetic amide coupling was further adapted to Steglich esterification and thioesterification reactions by switching to a stronger coupling reagent, 1-ethyl-3-(3-dimethylaminopropyl)carbodiimide (EDC). The post-synthetic modifications to yield COF-616-$COOR_2$ and COF-616-$COSR_2$ (R_2 = 2-(trimethylsilyl)ethyl) were investigated as model reactions: 2-(trimethylsilyl)ethanol and 2-(trimethylsilyl)ethanethiol were incorporated by using EDC·HCl as the coupling reagent and 4-dimethylaminopyridine (DMAP) as the catalyst (Scheme 5.1). The modification can be carried out in various solvents, among which dichloromethane provided the highest yields (74% and 63%, respectively) as confirmed by ^{1}H NMR spectroscopy of the digested samples (Figure 5.10, 5.16 and 5.17). Conversion of the carboxylic acid was corroborated by FT-IR spectroscopy, where the C=O (1698 cm^{-1}) carboxyl stretching band was blueshifted to 1708 cm^{-1} upon conversion to the ester, and redshifted to 1647 cm^{-1} upon conversion to the thioester (Figure 5.13). Similar to the amidation counterpart, COF-616-$COOR_2$ and COF-616-$COSR_2$ fully retained the crystallinity and morphology of their progenitor, as confirmed by PXRD (Figure 5.14) and SEM images (Figure 5.18 and 5.19).

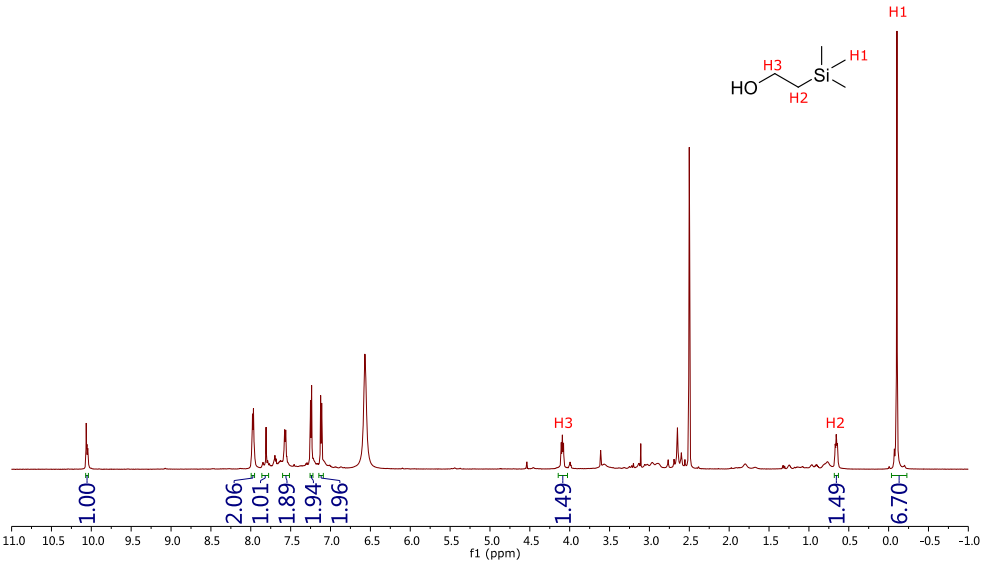

Figure 5.16. ^{1}H NMR spectrum of digested COF-$COOR_2$. The integral ratio between the trimethylsilyl group peaks and aldehyde peaks is 6.70, therefore the yield of the conversion is calculated to be 74.4%.

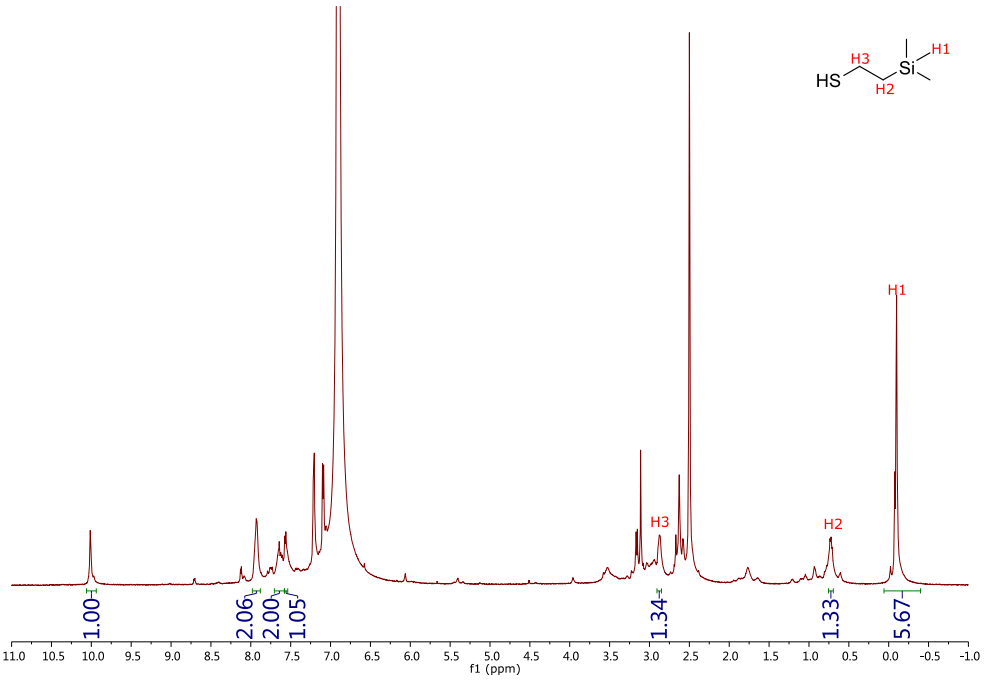

Figure 5.17. ^{1}H NMR spectrum of digested COF-616-COSR$_2$. The integral ratio between the trimethylsilyl group peaks and aldehyde peaks is 5.67, therefore the yield of the conversion is calculated to be 63.3%.

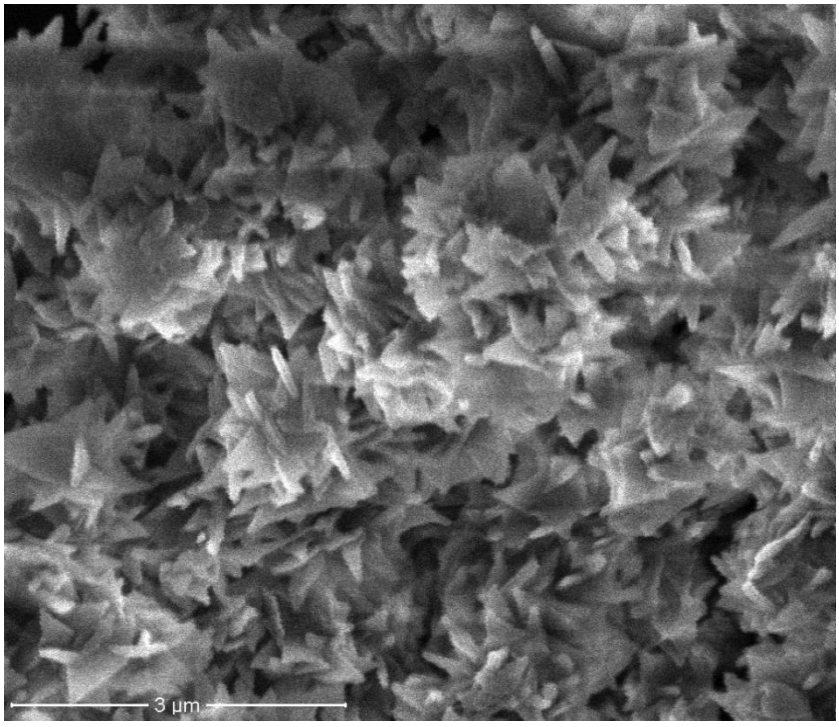

Figure 5.18. SEM image of COF-616-COOR$_2$.

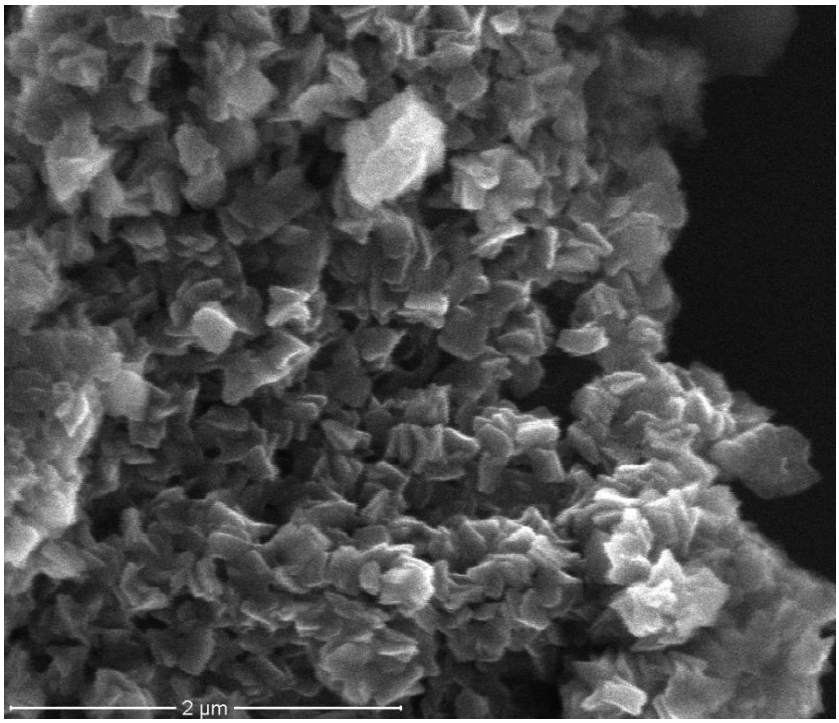

Figure 5.19. SEM image of COF-616-$COSR_2$.

The porosity of the modified products is relatively low compared to the pristine COF. This is probably due to the fact that the introduced functional moieties take up most of the space in the pores (Figure 5.20). COF-616-$CON(CH_3)R_1$, COF-616-$COOR_2$, and COF-616-$COSR_2$ all possess high thermal stability and will not decompose until 300 ^oC (Figure 5.21).

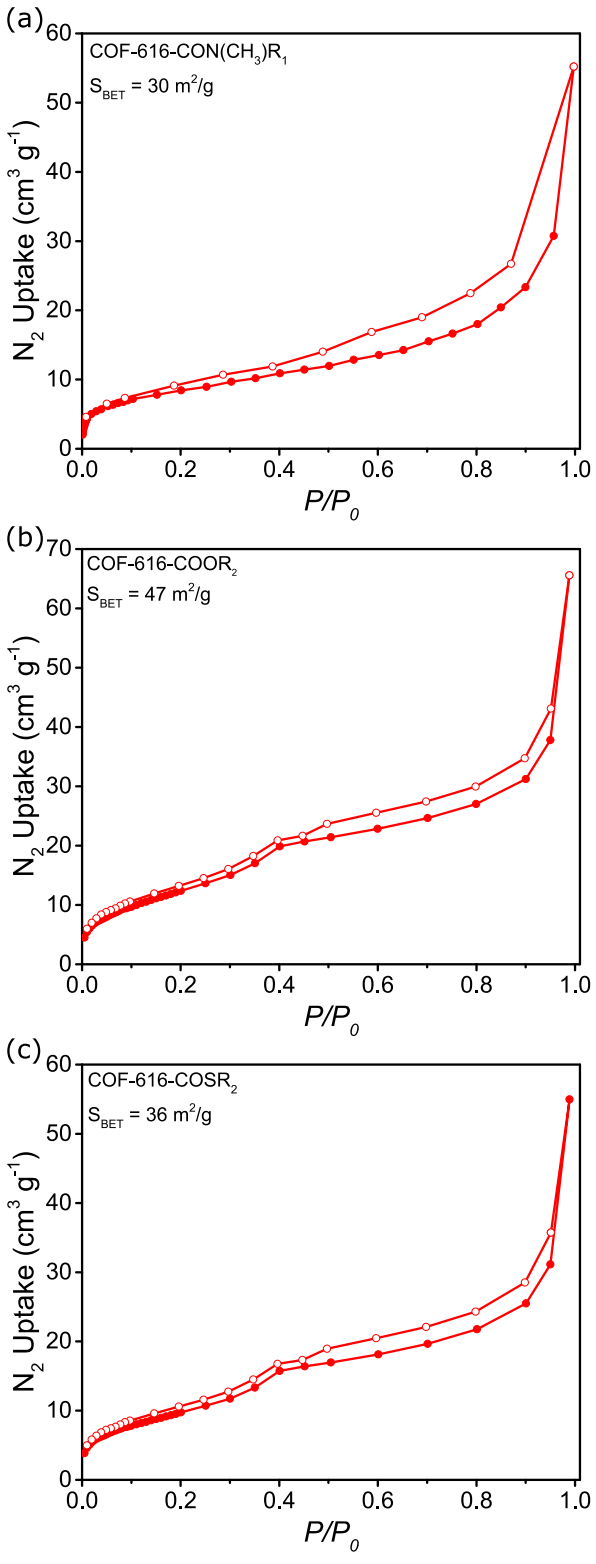

Figure 5.20. N_2 adsorption isotherms of COF-616-CON(CH_3)R_1, COF-616-$COOR_2$, and COF-616-$COSR_2$.

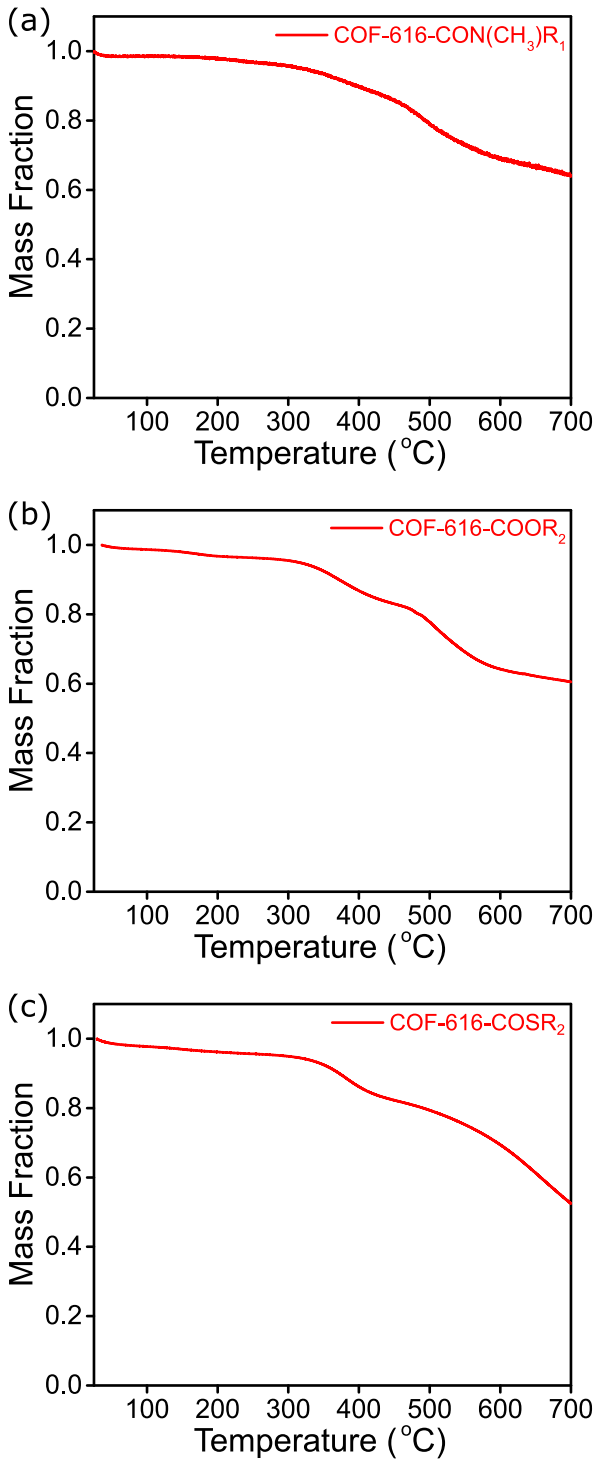

Figure 5.21. TGA traces for the COF-616-CON(CH_3)R_1, COF-616-$COOR_2$, and COF-616-$COSR_2$ under an N_2 atmosphere.

5.3.3 COF-Based Adsorbents for Heavy Metal Ions Removal

The synthetic ease of the developed post-synthetic modifications developed in the previous section suggests that COF-616 can serve as a functionalizable platform that can be readily tailored for various applications. Toxic heavy metal ions are major environmental pollutants and have become a global concern with respect to human health because of their accumulation in biosystems. Thus, facile preparation of adsorbents with high efficiency for targeted heavy metal ion removal is in high demand. To optimize COF-616 for efficient removal of heavy metal ions, a series of sulfur and nitrogen-rich molecules were introduced into its pores using the novel post-synthetic modification reactions described previously. Specifically, post-synthetic amidation using *N*,*N*-bis(2-((2-(ethylthio)ethyl)thio)ethyl)amine (NS4'), cyclam (CY), and 1-(1*H*-imidazol-2-yl)-*N*-methylmethanamine (IMD), post-synthetic esterification using 2-(methythio)ethanol (MTE), and post-synthetic thioesterification to introduce dithiothreitol (DTT) yielded functionalized frameworks COF-616-NS4', COF-616-CY, COF-IMD, COF-616-MTE, and COF-616-DTT, respectively (Figure 5.22). Successful incorporation of the functionalities was confirmed by FT-IR spectroscopy (Figure 5.23), ^{1}H NMR spectra of the digested samples (Figure 5.24-5.28), and elemental analysis. The maintenance of crystallinity and the morphology of the material were confirmed by PXRD and SEM micrographs (Figure 5.29 and 5.30).The porosity and the thermal stability of the materials have also been measured (Figure 5.31and 5.32).

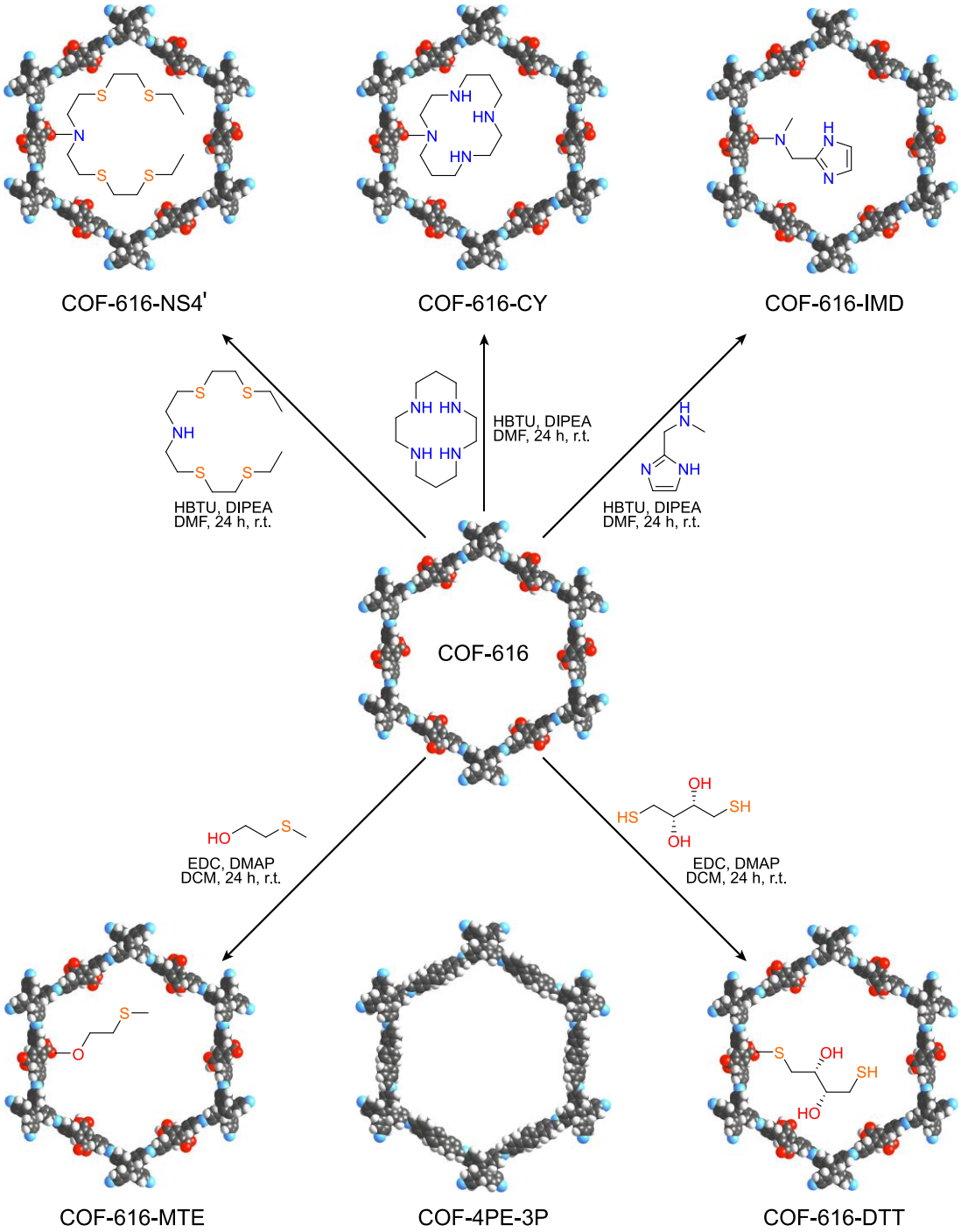

Figure 5.22. Synthesis scheme of COF-616-NS4', COF-616-CY, COF-IMD, COF-616-MTE, and COF-616-DTT by post-synthetic modification of carboxyl-functionalized COF-616, along with illustration of the unfunctionalized COF-4PE-3P.

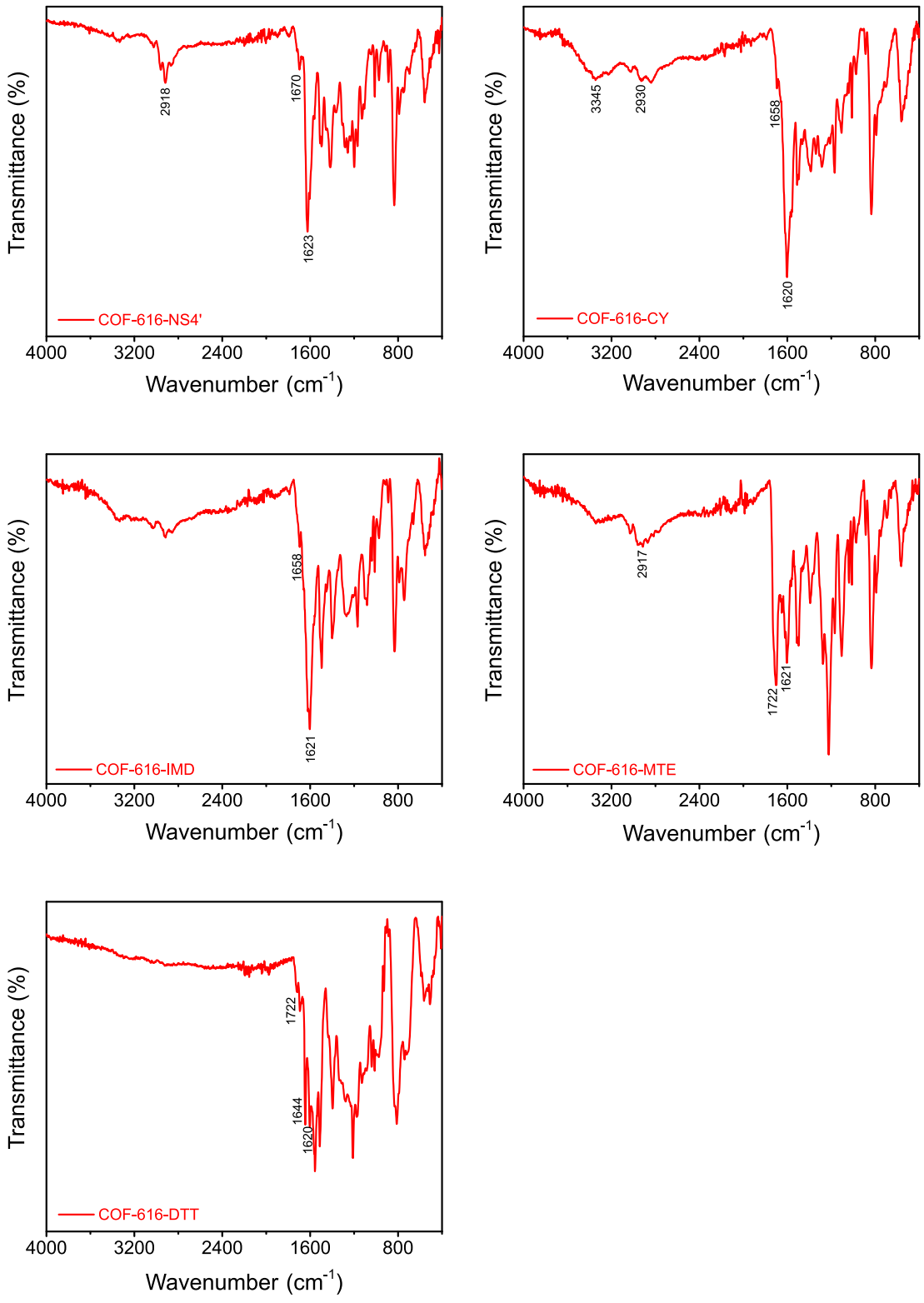

Figure 5.23. FT-IR spectra of COF-616-NS4', COF-616-CY, COF-IMD, COF-616-MTE, and COF-616-DTT.

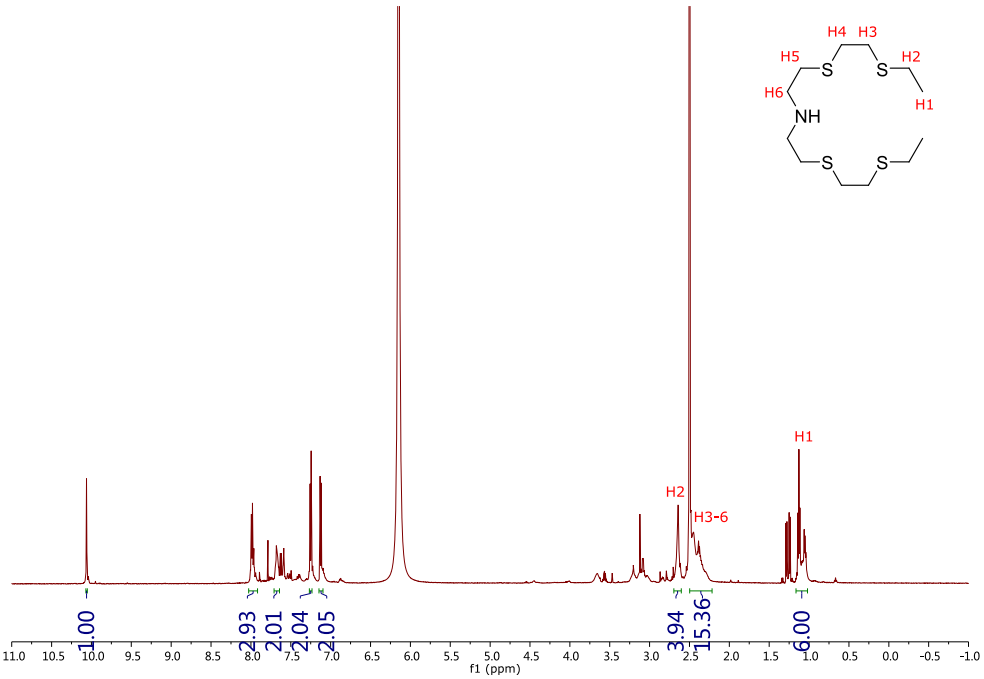

Figure 5.24. ^{1}H NMR spectra of digested COF-616-NS4'. The integral ratio between the terminal methyl group peaks and aldehyde peaks is 6, therefore the yield of the conversion is calculated to be 100%.

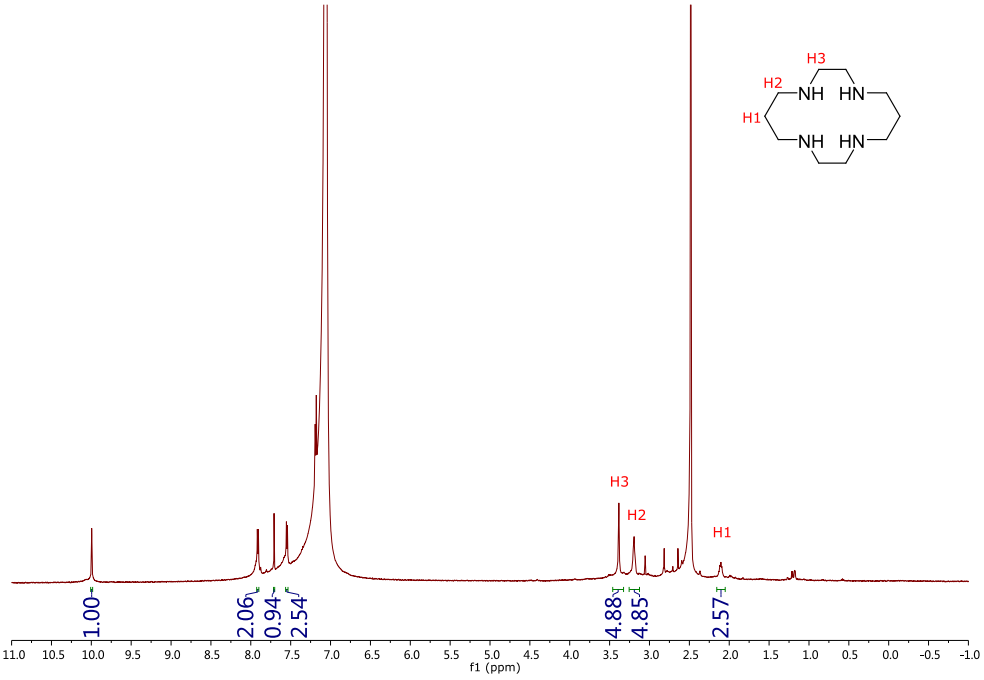

Figure 5.25. ^{1}H NMR spectra of digested COF-616-CY. The yield of the conversion is calculated to be 64.3%.

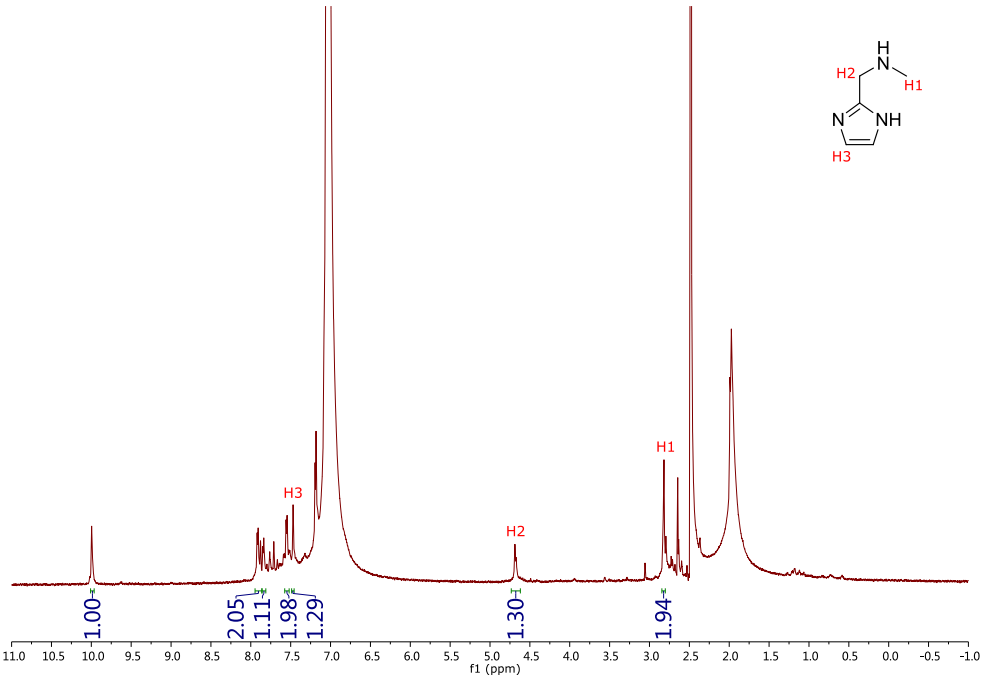

Figure 5.26. [1]H NMR spectra of digested COF-616-IMD. The yield of the conversion is calculated to be 65%.

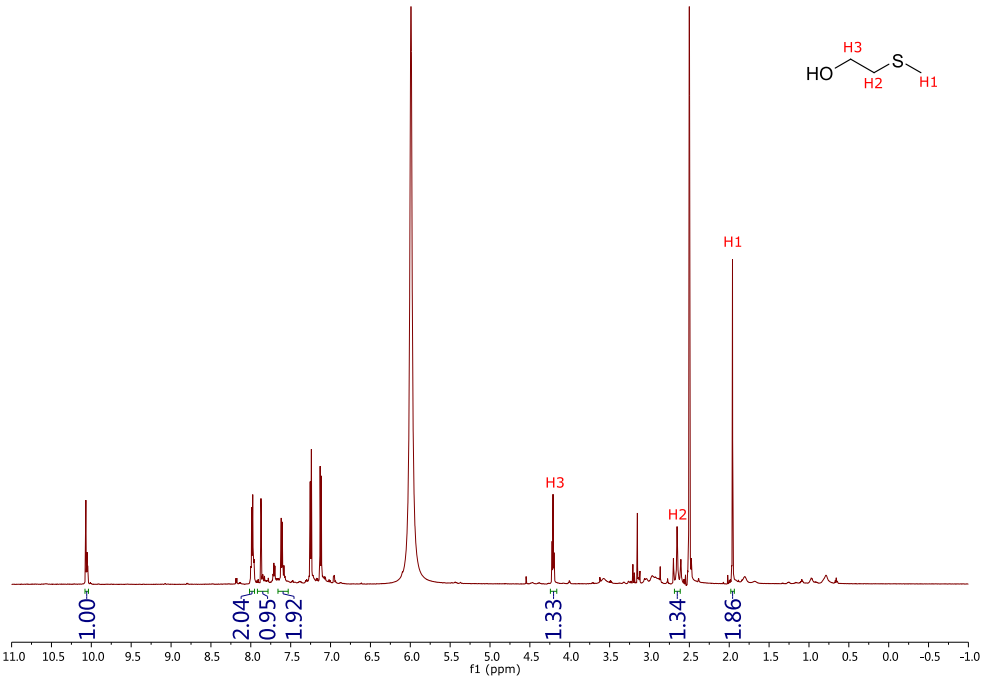

Figure 5.27. [1]H NMR spectra of digested COF-616-MTE. The yield of the conversion is calculated to be 67%.

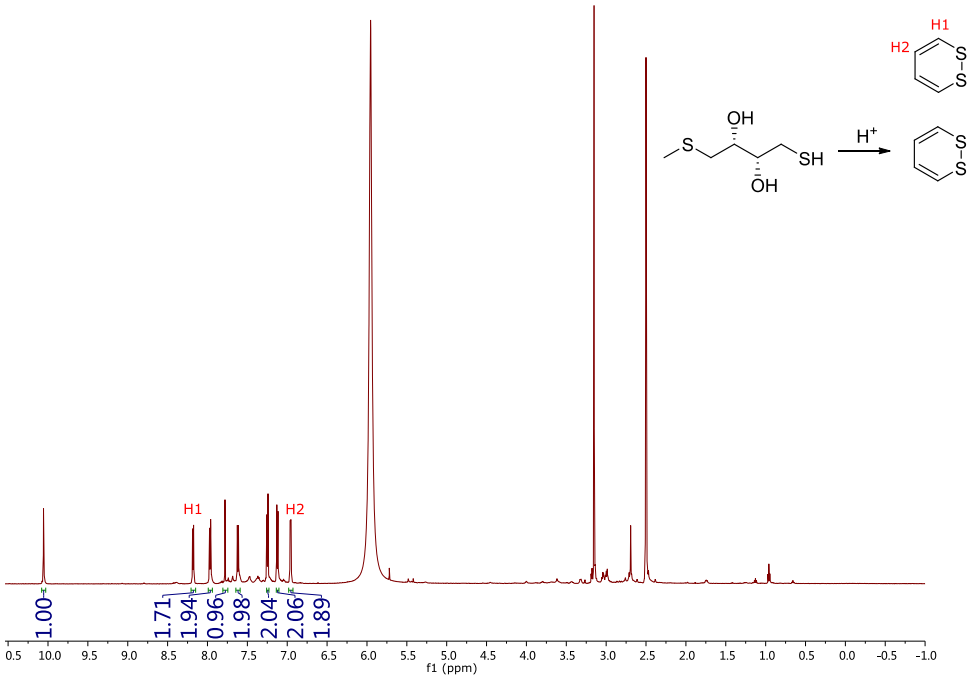

Figure 5.28. ^{1}H NMR spectra of digested COF-616-DTT. The yield of the conversion is calculated to be 90%. DTT undergoes cyclization at a high concentration of H^{+}.

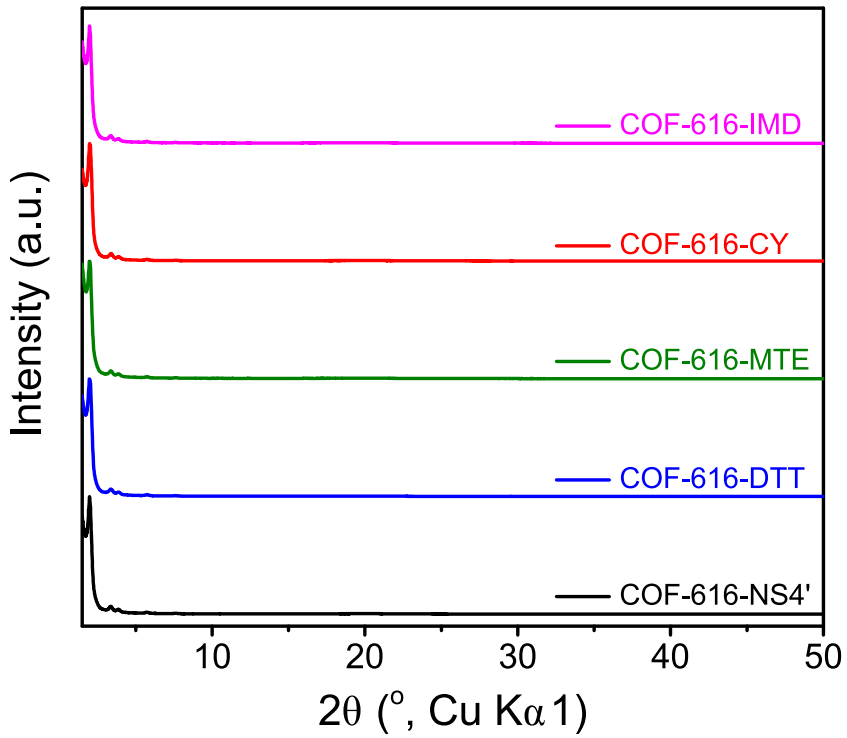

Figure 5.29. PXRD patterns of COF-616-NS4', COF-616-DTT, COF-616-MTE, COF-616-CY, and COF-616-IMD.

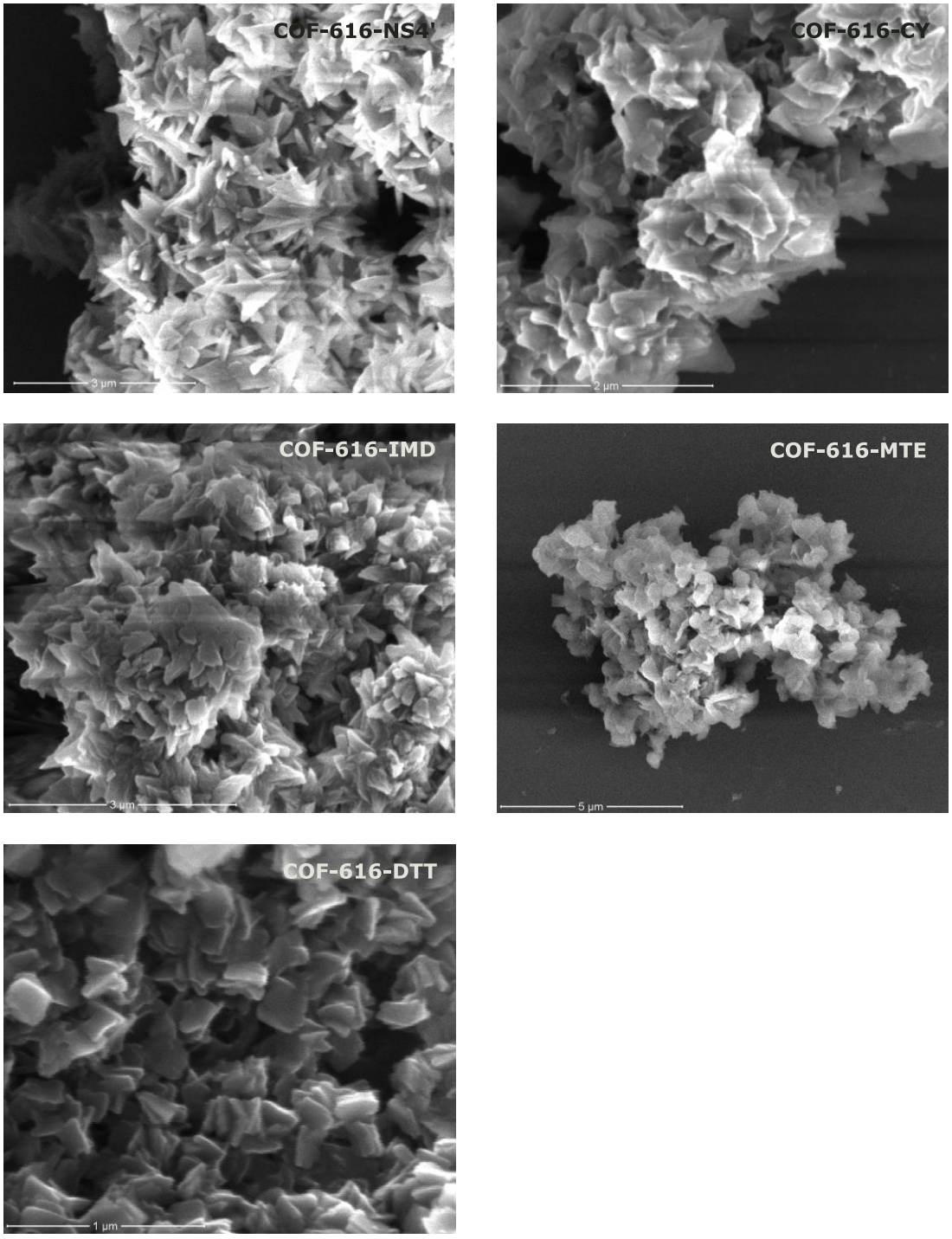

Figure 5.30. SEM images of COF-616-NS4', COF-616-DTT, COF-616-MTE, COF-616-CY, and COF-616-IMD.

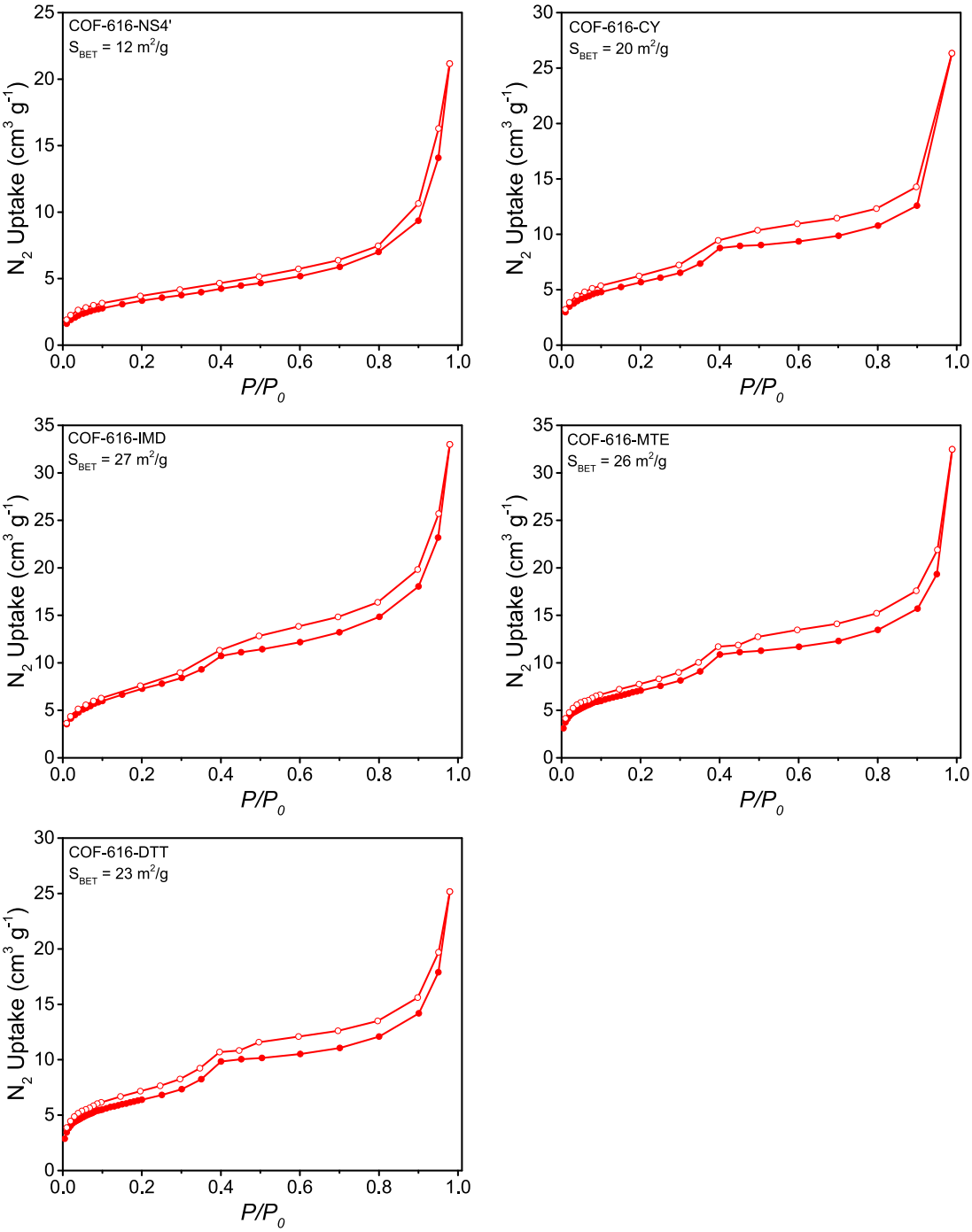

Figure 5.31. N_2 adsorption isotherms of COF-616-NS4', COF-616-DTT, COF-616-MTE, COF-616-CY, and COF-616-IMD.

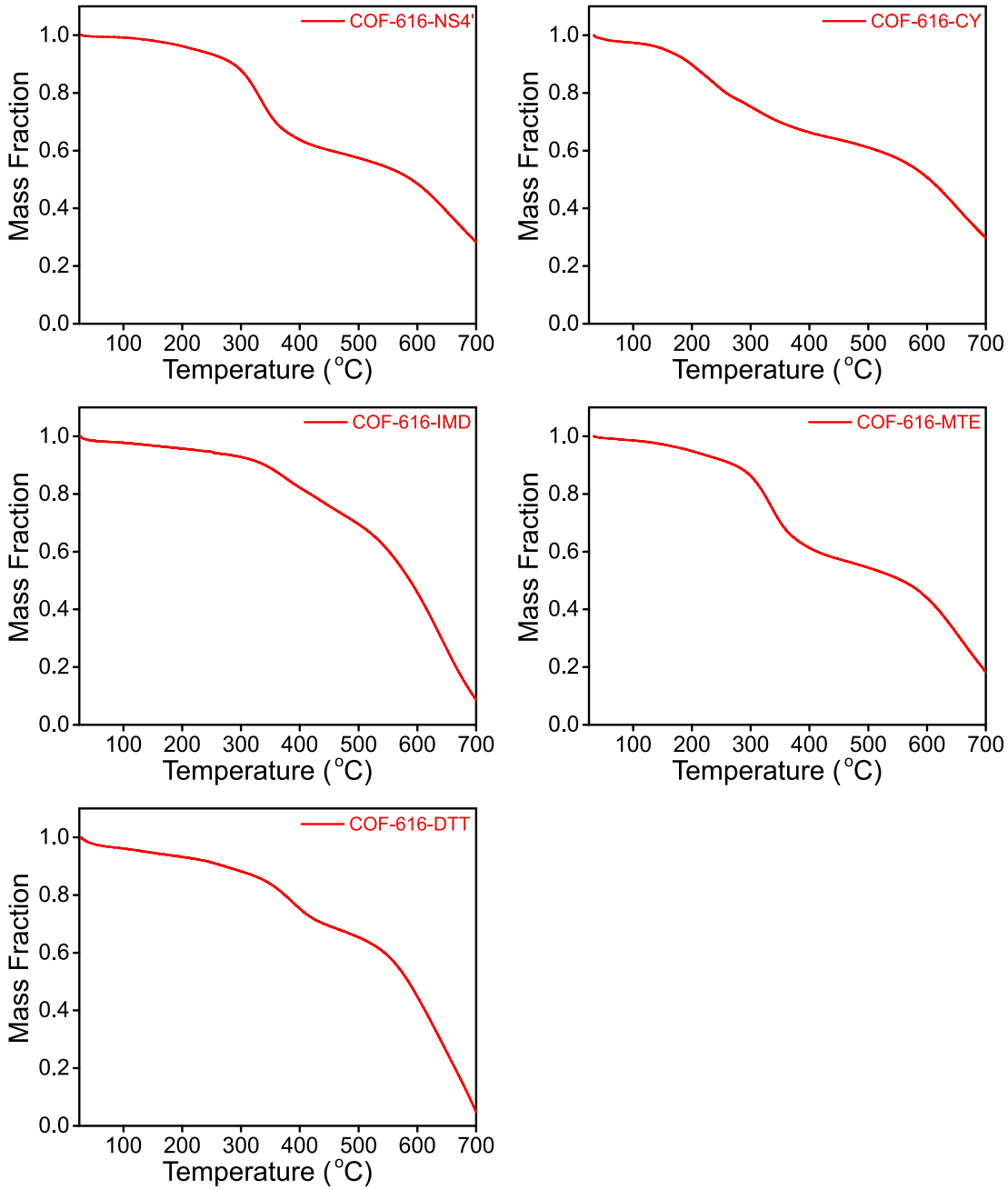

Figure 5.32. TGA traces for the COF-616-NS4', COF-616-DTT, COF-616-MTE, COF-616-CY, and COF-616-IMD under an N_2 atmosphere.

The performance of this series of functionalized COFs (COF-616, 616-NS4', COF-616-CY, COF-IMD, COF-616-MTE, and COF-616-DTT), as well as unfunctionalized COF-4PE-3P,[45,46] for the uptake of metal ions (K^+, Ca^{2+}, Pb^{2+}, Hg^{2+}, Cu^{2+}, Zn^{2+}, and Ni^{2+}) from water was tested (Figure 5.33). It was found that all post-synthetically modified materials performed better than the carboxyl and unfunctionalized COFs for the uptake of Hg^{2+} ion. In contrast, the uptake of other heavy metal ions (*i.e.*, Pb^{2+}, Cu^{2+}, Zn^{2+}

and Ni^{2+}) was found to be closely related to the nature of the introduced functionality. Specifically, thiol groups of COF-616-DTT outperformed other chelators, including thioethers, and showed promiscuous adsorption among most heavy metal ions due to their superior soft Lewis basicity.[37,47,48] Nitrogen rich chelators (*i.e.*, cyclam) also showed appreciable sorption of heavy metal ions, which provides a viable alternative for designing heavy metal adsorbents. These findings illustrate the importance of screening and optimizing the performance of a given framework by appending a large library of functional groups through post-synthetic modification.

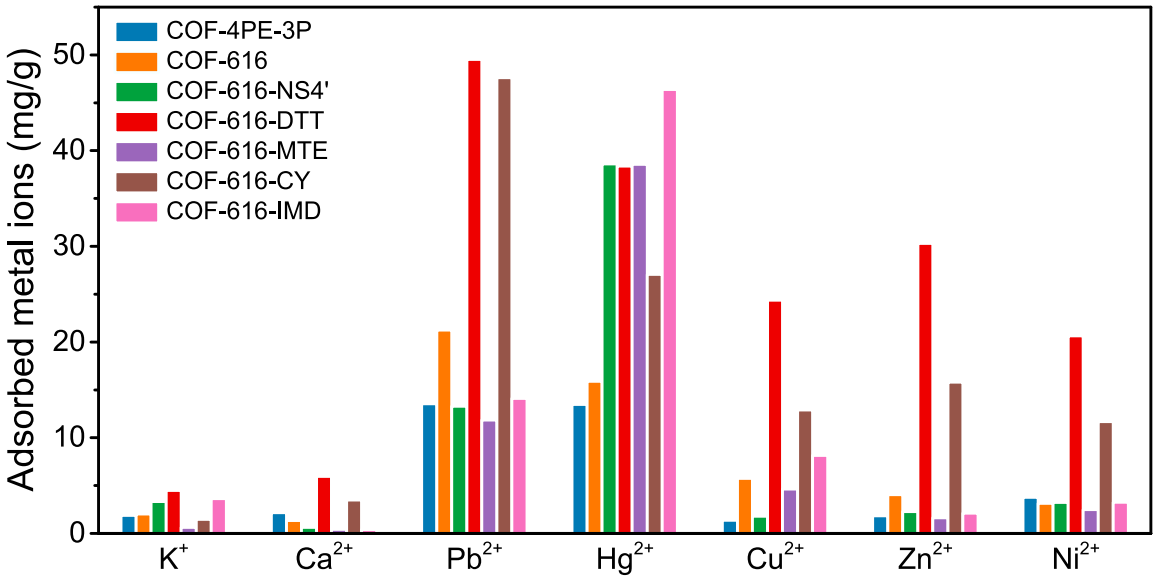

Figure 5.33. Metal ions adsorption measurement with COF-4PE-3P, COF-616, and its post-synthetically modified products.

Lead is the most prevalent contaminant among all the heavy metals, due to the extensive use of leaded gasoline during the mid-twentieth century.[49] Experimental studies have indicated that lead is potentially carcinogenic,[50] and there is an association between blood level lead poisoning and diminished intelligence in children.[51] Motivated by the high uptake of Pb^{2+} ions with COF-616-DTT, the applicability of COF-616-DTT as a Pb^{2+} adsorbent was investigated in a more detailed manner. COF-616-DTT exhibited a high Pb^{2+} capture capacity of 205 mg g^{-1} (Figure 5.34), resulting from strong Pb-SH interactions. The equilibrium Pb^{2+} sorption isotherm was fitted with the Langmuir model with a coefficient of 0.9997, and the type-I profile of the isotherm indicated that COF-616-DTT possessed a strong affinity for Pb^{2+}. Time-course adsorption measurement further indicated that the removal of Pb^{2+} by COF-616-DTT was kinetically efficient (Figure 5.35), with a pseudo-second-order adsorption rate constant of 5.8 mg mg^{-1} min^{-1} that reached equilibrium capacity within 60 min, highlighting its potential utility for efficient removal of Pb^{2+} from environmental samples.

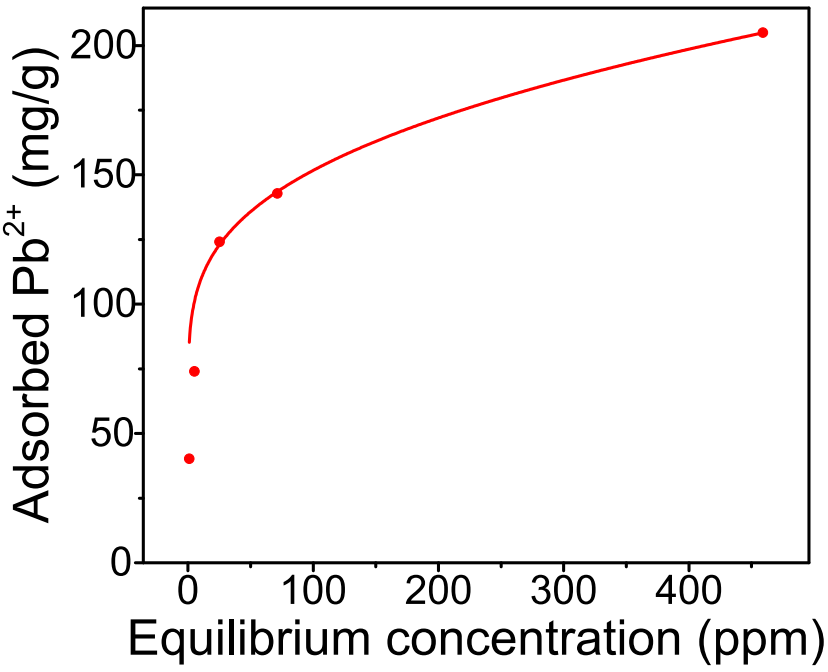

Figure 5.34. Pb^{2+} adsorption isotherm for COF-616-DTT fitted using the Langmuir model.

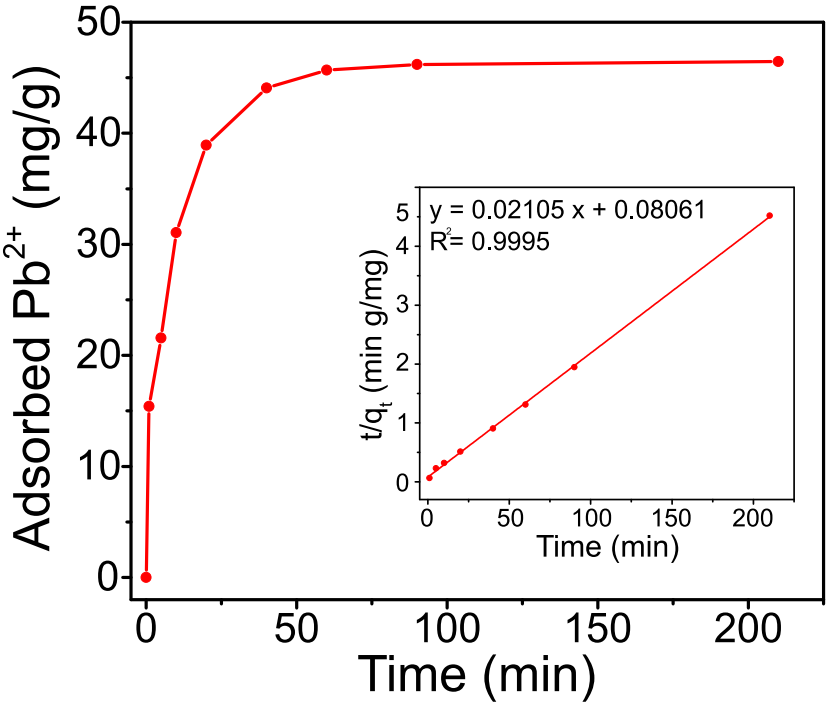

Figure 5.35. Pb^{2+} sorption kinetics of COF-616-DTT. Inset shows the pseudo-second-order kinetic plot for the adsorption.

5.4 Conclusion

In this chapter, the synthesis and characterization of a novel covalent organic framework, COF-616, bearing carboxyl groups on its backbone has been discussed. The pre-installed carboxyl groups can readily be converted to amides, esters, and thioesters by post-synthetic modification. These three new post-synthetic modification reactions can be used to introduce a variety of different functional groups into the framework, and the utility of this approach is highlighted by the optimization of COF-616 through post-synthetic introduction of various sulfur and nitrogen-rich functional groups for efficient removal of heavy metal ions from water. This methodology provides a homogenous pathway for post-synthetic modification of COFs and holds promise for providing a new strategy for modular, application-directed development of COFs in a fast and efficient manner.

5.5 References

(1) Cote, A. P.; Benin, A. I.; Ockwig, N. W.; O'Keeffe, M.; Matzger, A. J.; Yaghi, O. M. Porous, Crystalline, Covalent Organic Frameworks. *Science* **2005**, *310* (6), 1166-1170.

(2) Yaghi, O. M.; Kalmutzki, M. J.; Diercks, C. S. *Introduction to Reticular Chemistry: Metal-Organic Frameworks and Covalent Organic Frameworks*; John Wiley & Sons, 2019.

(3) Doonan, C. J.; Tranchemontagne, D. J.; Glover, T. G.; Hunt, J. R.; Yaghi, O. M. Exceptional Ammonia Uptake by a Covalent Organic Framework. *Nat. Chem.* **2010**, *2* (3), 235–238.

(4) Furukawa, H.; Yaghi, O. M. Storage of Hydrogen, Methane, and Carbon Dioxide in Highly Porous Covalent Organic Frameworks for Clean Energy Applications. *J. Am. Chem. Soc.* **2009**, *131*, (25), 8875–8883.

(5) Stegbauer, L.; Hahn, M. W.; Jentys, A.; Savasci, G.; Ochsenfeld, C.; Lercher, J. A.; Lotsch, B. V. Tunable Water and CO2 Sorption Properties in Isostructural Azine-Based Covalent Organic Frameworks through Polarity Engineering. *Chem. Mater.* **2015**, *27* (23), 7874–7881.

(6) Baldwin, L. A.; Crowe, J. W.; Pyles, D. A.; McGrier, P. L. Metalation of a Mesoporous Three-Dimensional Covalent Organic Framework. *J. Am. Chem. Soc.* **2016**, *138* (46), 15134–15137.

(7) Ding, S.-Y.; Gao, J.; Wang, Q.; Zhang, Y.; Song, W.-G.; Su, C.-Y.; Wang, W. Construction of Covalent Organic Framework for Catalysis: Pd/COF-LZU1 in Suzuki–Miyaura Coupling Reaction. *J. Am. Chem. Soc.* **2011**, *133* (49), 19816–19822.

(8) Xu, H.; Gao, J.; Jiang, D. Stable, Crystalline, Porous, Covalent Organic Frameworks as a Platform for Chiral Organocatalysts. *Nat. Chem.* **2015**, *7* (11), 905–912.

(9) Vyas, V. S.; Haase, F.; Stegbauer, L.; Savasci, G.; Podjaski, F.; Ochsenfeld, C.; Lotsch, B. V. A Tunable Azine Covalent Organic Framework Platform for Visible Light-Induced Hydrogen Generation. *Nat. Commun.* **2015**, *6*, 8508.

(10) Lin, S.; Diercks, C. S.; Zhang, Y.-B.; Kornienko, N.; Nichols, E. M.; Zhao, Y.; Paris, A. R.; Kim, D.; Yang, P.; Yaghi, O. M.; Chang, C. J. Covalent Organic Frameworks Comprising Cobalt Porphyrins for Catalytic CO_2 Reduction in Water. *Science* **2015**, *349* (6253), 1208–1213.

(11) Wang, X.; Han, X.; Zhang, J.; Wu, X.; Liu, Y.; Cui, Y. Homochiral 2D Porous Covalent Organic Frameworks for Heterogeneous Asymmetric Catalysis. *J. Am. Chem. Soc.* **2016**, *138* (38), 12332–12335.

(12) Sun, Q.; Aguila, B.; Perman, J.; Nguyen, N.; Ma, S. Flexibility Matters: Cooperative Active Sites in Covalent Organic Framework and Threaded Ionic Polymer. *J. Am. Chem. Soc.* **2016**, *138* (48), 15790–15796.

(13) Ma, H.; Liu, B.; Li, B.; Zhang, L.; Li, Y.-G.; Tan, H.-Q.; Zang, H.-Y.; Zhu, G. Cationic Covalent Organic Frameworks: A Simple Platform of Anionic Exchange for Porosity Tuning and Proton Conduction. *J. Am. Chem. Soc.* **2016**, *138* (18), 5897–5903.

(14) Chandra, S.; Kundu, T.; Kandambeth, S.; BabaRao, R.; Marathe, Y.; Kunjir, S. M.; Banerjee, R. Phosphoric Acid Loaded Azo (−N═N−) Based Covalent Organic Framework for Proton Conduction. *J. Am. Chem. Soc.* **2014**, *136* (18), 6570–6573.

(15) Montoro, C.; Rodríguez-San-Miguel, D.; Polo, E.; Escudero-Cid, R.; Ruiz-González, M. L.; Navarro, J. A. R.; Ocón, P.; Zamora, F. Ionic Conductivity and Potential Application for Fuel Cell of a Modified Imine-Based Covalent Organic Framework. *J. Am. Chem. Soc.* **2017**, *139* (29), 10079–10086.

(16) Vazquez-Molina, D. A.; Mohammad-Pour, G. S.; Lee, C.; Logan, M. W.; Duan, X.; Harper, J. K.; Uribe-Romo, F. J. Mechanically Shaped Two-Dimensional Covalent Organic Frameworks Reveal Crystallographic Alignment and Fast Li-Ion Conductivity. *J. Am. Chem. Soc.* **2016**, *138* (31), 9767–9770.

(17) Zhang, Y.; Duan, J.; Ma, D.; Li, P.; Li, S.; Li, H.; Zhou, J.; Ma, X.; Feng, X.; Wang, B. Three-Dimensional Anionic Cyclodextrin-Based Covalent Organic Frameworks. *Angew. Chem. Int. Ed.* **2017**, *56* (51), 16313–16317.

(18) Du, Y.; Yang, H.; Whiteley, J. M.; Wan, S.; Jin, Y.; Lee, S.-H.; Zhang, W. Ionic Covalent Organic Frameworks with Spiroborate Linkage. *Angew. Chem. Int. Ed.* **2016**, *55* (5), 1737–1741.

(19) Das, G.; Biswal, B. P.; Kandambeth, S.; Venkatesh, V.; Kaur, G.; Addicoat, M.; Heine, T.; Verma, S.; Banerjee, R. Chemical Sensing in Two Dimensional Porous Covalent Organic Nanosheets. *Chem. Sci.* **2015**, *6* (7), 3931–3939.

(20) Li, Z.; Huang, N.; Lee, K. H.; Feng, Y.; Tao, S.; Jiang, Q.; Nagao, Y.; Irle, S.; Jiang, D. Light-Emitting Covalent Organic Frameworks: Fluorescence Improving via Pinpoint Surgery and Selective Switch-On Sensing of Anions. *J. Am. Chem. Soc.* **2018**, *140* (39), 12374–12377.

(21) Ding, S.-Y.; Dong, M.; Wang, Y.-W.; Chen, Y.-T.; Wang, H.-Z.; Su, C.-Y.; Wang, W. Thioether-Based Fluorescent Covalent Organic Framework for Selective Detection and Facile Removal of Mercury(II). *J. Am. Chem. Soc.* **2016**, *138* (9), 3031–3037.

(22) Tilford, R. W.; Mugavero, S. J.; Pellechia, P. J.; Lavigne, J. J. Tailoring Microporosity in Covalent Organic Frameworks. *Adv. Mater.* **2008**, *20* (14), 2741–2746.

(23) Diercks, C. S.; Lin, S.; Kornienko, N.; Kapustin, E. A.; Nichols, E. M.; Zhu, C.; Zhao, Y.; Chang, C. J.; Yaghi, O. M. Reticular Electronic Tuning of Porphyrin Active Sites in Covalent Organic Frameworks for Electrocatalytic Carbon Dioxide Reduction. *J. Am. Chem. Soc.* **2018**, *140* (3), 1116–1122.

(24) Bunck, D. N.; Dichtel, W. R. Postsynthetic Functionalization of 3D Covalent Organic Frameworks. *Chem. Commun.* **2013**, *49* (24), 2457–2459.

(25) Huang, N.; Chen, X.; Krishna, R.; Jiang, D. Two-Dimensional Covalent Organic Frameworks for Carbon Dioxide Capture through Channel-Wall Functionalization. *Angew. Chem. Int. Ed Engl.* **2015**, *54* (10), 2986–2990.

(26) Dong, B.; Wang, L.; Zhao, S.; Ge, R.; Song, X.; Wang, Y.; Gao, Y. Immobilization of Ionic Liquids to Covalent Organic Frameworks for Catalyzing the Formylation of Amines with CO2 and Phenylsilane. *Chem. Commun.* **2016**, *52* (44), 7082–7085.

(27) Rager, S.; Dogru, M.; Werner, V.; Gavryushin, A.; Götz, M.; Engelke, H.; Medina, D. D.; Knochel, P.; Bein, T. Pore Wall Fluorescence Labeling of Covalent Organic Frameworks. *CrystEngComm* **2017**, *19* (33), 4886–4891.

(28) Sun, Q.; Aguila, B.; Earl, L. D.; Abney, C. W.; Wojtas, L.; Thallapally, P. K.; Ma, S. Covalent Organic Frameworks as a Decorating Platform for Utilization and Affinity Enhancement of Chelating Sites for Radionuclide Sequestration. *Adv. Mater.* **2018**, *30* (20), 1705479.

(29) Ji, W.; Xiao, L.; Ling, Y.; Ching, C.; Matsumoto, M.; Bisbey, R. P.; Helbling, D. E.; Dichtel, W. R. Removal of GenX and Perfluorinated Alkyl Substances from Water by Amine-Functionalized Covalent Organic Frameworks. *J. Am. Chem. Soc.* **2018**.

(30) Lohse, M. S.; Stassin, T.; Naudin, G.; Wuttke, S.; Ameloot, R.; Vos, D. D.; Medina, D. D.; Bein, T. Sequential Pore Wall Modification in a Covalent Organic Framework for Application in Lactic Acid Adsorption. *Chem. Mater.* **2016**, *28*, 626−631.

(31) Guo, H.; Wang, J.; Fang, Q.; Zhao, Y.; Gu, S.; Zheng, J.; Yan, Y. A Quaternary-Ammonium-Functionalized Covalent Organic Framework for Anion Conduction. *CrystEngComm* **2017**, *19* (33), 4905–4910.

(32) Waller, P. J.; Lyle, S. J.; Osborn Popp, T. M.; Diercks, C. S.; Reimer, J. A.; Yaghi, O. M. Chemical Conversion of Linkages in Covalent Organic Frameworks. *J. Am. Chem. Soc.* **2016**, *138* (48), 15519–15522.

(33) Xu, F.; Xu, H.; Chen, X.; Wu, D.; Wu, Y.; Liu, H.; Gu, C.; Fu, R.; Jiang, D. Radical Covalent Organic Frameworks: A General Strategy to Immobilize Open-Accessible Polyradicals for High-Performance Capacitive Energy Storage. *Angew. Chem. Int. Ed.* **2015**, *54* (23), 6814–6818.

(34) Huang, N.; Krishna, R.; Jiang, D. Tailor-Made Pore Surface Engineering in Covalent Organic Frameworks: Systematic Functionalization for Performance Screening. *J. Am. Chem. Soc.* **2015**, *137* (22), 7079–7082.

(35) Xu, H.; Chen, X.; Gao, J.; Lin, J.; Addicoat, M.; Irle, S.; Jiang, D. Catalytic Covalent Organic Frameworks via Pore Surface Engineering. *Chem. Commun.* **2014**, *50* (11), 1292–1294.

(36) Nagai, A.; Guo, Z.; Feng, X.; Jin, S.; Chen, X.; Ding, X.; Jiang, D. Pore Surface Engineering in Covalent Organic Frameworks. *Nat. Commun.* **2011**, *2*, 536.

(37) Mer í-Bof í, L.; Royuela, S.; Zamora, F.; Ruiz-Gonz ález, M. L.; Segura, J. L.; Mu ñoz-Olivas, R.; Manche ño, M. J. Thiol Grafted Imine-Based Covalent Organic Frameworks for Water Remediation through Selective Removal of Hg(II). *J. Mater. Chem. A* **2017**, *5* (34), 17973–17981.

(38) Lin, Y.; Jiang, X.; Kim, S. T.; Alahakoon, S. B.; Hou, X.; Zhang, Z.; Thompson, C. M.; Smaldone, R. A.; Ke, C. An Elastic Hydrogen-Bonded Cross-Linked Organic Framework for Effective Iodine Capture in Water. *J. Am. Chem. Soc.* **2017**, *139* (21), 7172–7175.

(39) Jia, S.; Ramos-Torres, K. M.; Kolemen, S.; Ackerman, C. M.; Chang, C. J. Tuning the Color Palette of Fluorescent Copper Sensors through Systematic Heteroatom Substitution at Rhodol Cores. *ACS Chem. Biol.* **2018**, *13* (7), 1844–1852.

(40) Tong, Y.; Hamilton, D. G.; Meillon, J.-C.; Sanders, J. K. M. Sn(IV) Porphyrins as NMR Shift Reagents and Supramolecular Protecting Groups: Preparation of a Carboxylate−Catenane Porphyrin Complex. *Org. Lett.* **1999**, *1* (9), 1343–1346.

(41) Carpino, L. A.; Imazumi, H.; El - Faham, A.; Ferrer, F. J.; Zhang, C.; Lee, Y.; Foxman, B. M.; Henklein, P.; Hanay, C.; M ügge, C.; et al. The Uronium/Guanidinium Peptide Coupling Reagents: Finally the True Uronium Salts. *Angew. Chem. Int. Ed.* **2002**, *41* (3), 441–445.

(42) Merrifield, R. B. Solid Phase Peptide Synthesis. I. The Synthesis of a Tetrapeptide. *J. Am. Chem. Soc.* **1963**, *85* (14), 2149–2154.

(43) Fracaroli, A. M.; Siman, P.; Nagib, D. A.; Suzuki, M.; Furukawa, H.; Toste, F. D.; Yaghi, O. M. Seven Post-Synthetic Covalent Reactions in Tandem Leading to Enzyme-like Complexity within Metal–Organic Framework Crystals. *J. Am. Chem. Soc.* **2016**, *138* (27), 8352–8355.

(44) Vitaku, E.; Dichtel, W. R. Synthesis of 2D Imine-Linked Covalent Organic Frameworks through Formal Transimination Reactions. *J. Am. Chem. Soc.* **2017**, *139* (37), 12911–12914.

(45) Ascherl, L.; Sick, T.; Margraf, J. T.; Lapidus, S. H.; Calik, M.; Hettstedt, C.; Karaghiosoff, K.; Döblinger, M.; Clark, T.; Chapman, K. W.; et al. Molecular Docking Sites Designed for the Generation of Highly Crystalline Covalent Organic Frameworks. *Nat. Chem.* **2016**, *8* (4), 310–316.

(46) Pang, Z.-F.; Xu, S.-Q.; Zhou, T.-Y.; Liang, R.-R.; Zhan, T.-G.; Zhao, X. Construction of Covalent Organic Frameworks Bearing Three Different Kinds of Pores through the Heterostructural Mixed Linker Strategy. *J. Am. Chem. Soc.* **2016**, *138* (14), 4710–4713.

(47) Li, B.; Zhang, Y.; Ma, D.; Shi, Z.; Ma, S. Mercury Nano-Trap for Effective and Efficient Removal of Mercury(II) from Aqueous Solution. *Nat. Commun.* **2014**, *5* (1).

(48) Sun, Q.; Aguila, B.; Perman, J.; Earl, L. D.; Abney, C. W.; Cheng, Y.; Wei, H.; Nguyen, N.; Wojtas, L.; Ma, S. Postsynthetically Modified Covalent Organic Frameworks for Efficient and Effective Mercury Removal. *J. Am. Chem. Soc.* **2017**, *139* (7), 2786–2793.

(49) Thomas, V. M. The Elimination of Lead in Gasoline. *Annu. Rev. Energy Environ.* **1995**, *20* (1), 301–324.

(50) Waalkes, M. P.; Diwan, B. A.; Ward, J. M.; Devor, D. E.; Goyer, R. A. Renal Tubular Tumors and Atypical Hyperplasias in B6C3F1 Mice Exposed to Lead Acetate during Gestation and Lactation Occur with Minimal Chronic Nephropathy. *Cancer Res.* **1995**, *55* (22), 5265–5271.

(51) Kaul B; Sandhu R S; Depratt C; Reyes F. Follow-up Screening of Lead-Poisoned Children near an Auto Battery Recycling Plant, Haina, Dominican Republic. *Environ. Health Perspect.* **1999**, *107* (11), 917–920.

5.6 Appendix

5.6.1 ^{1}H and ^{13}C NMR Spectra

^{1}H NMR spectrum of **2** (600 MHz, $CDCl_3$)

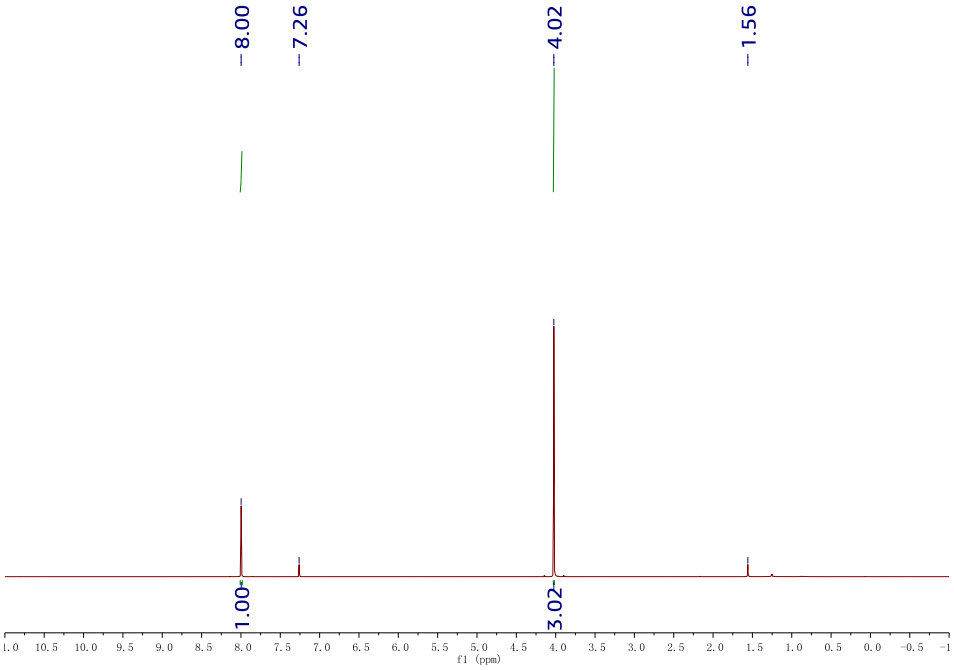

^{13}C NMR spectrum of **2** (151 MHz, $CDCl_3$)

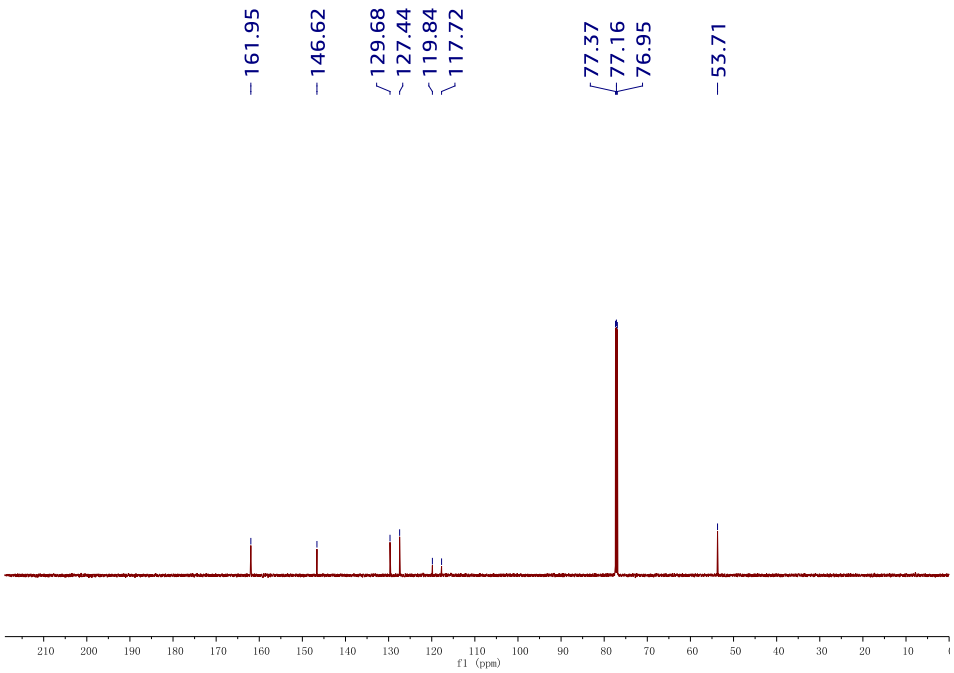

^{1}H NMR spectrum of **3** (600 MHz, $(CD_3)_2SO$)

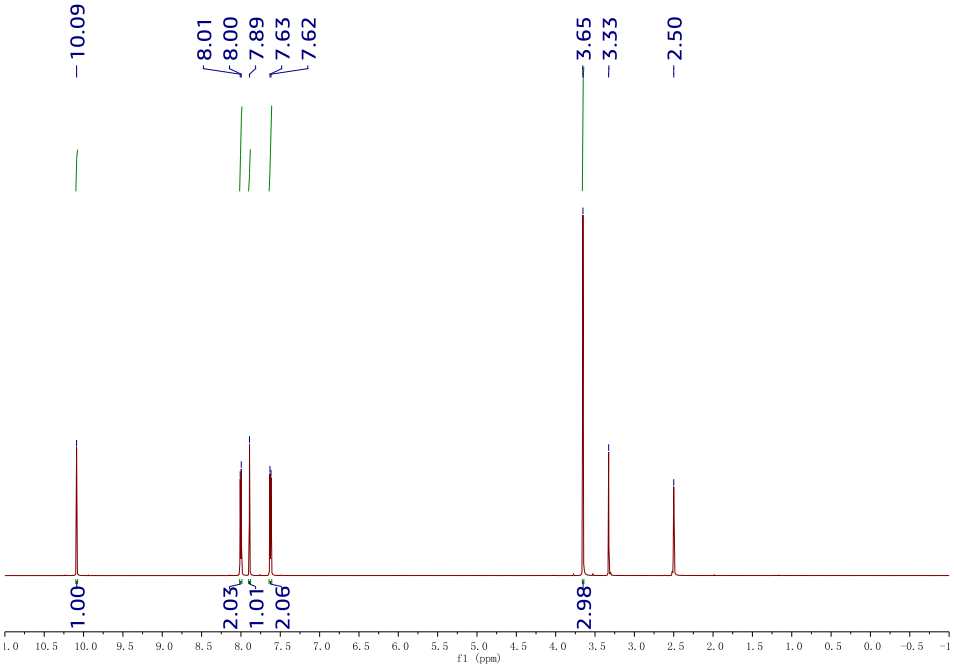

^{13}C NMR spectrum of **3** (151 MHz, $(CD_3)_2SO$)

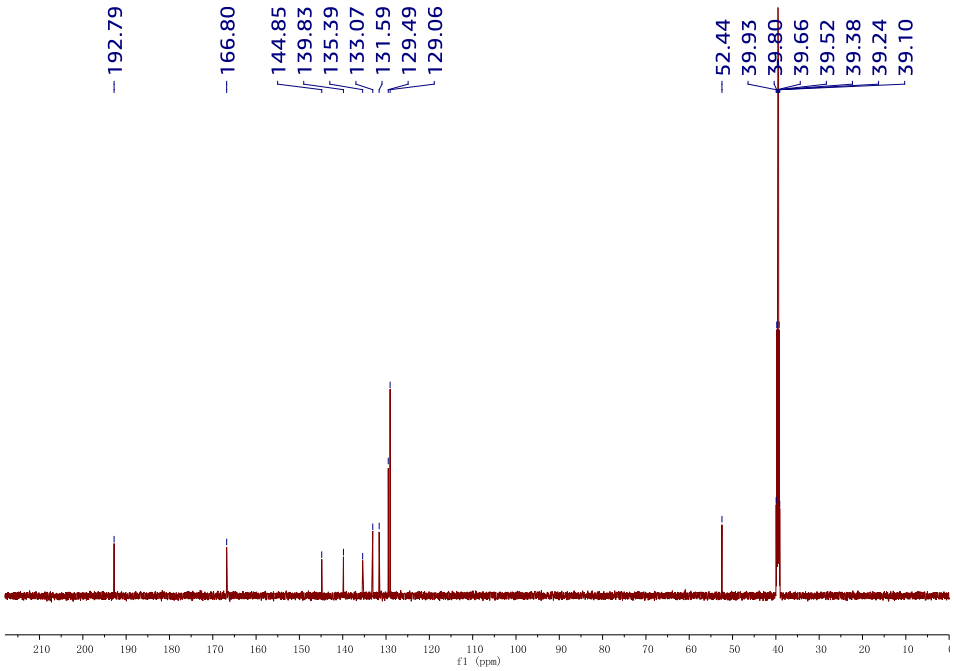

^{1}H NMR spectrum of **4** (600 MHz, $(CD_3)_2SO$)

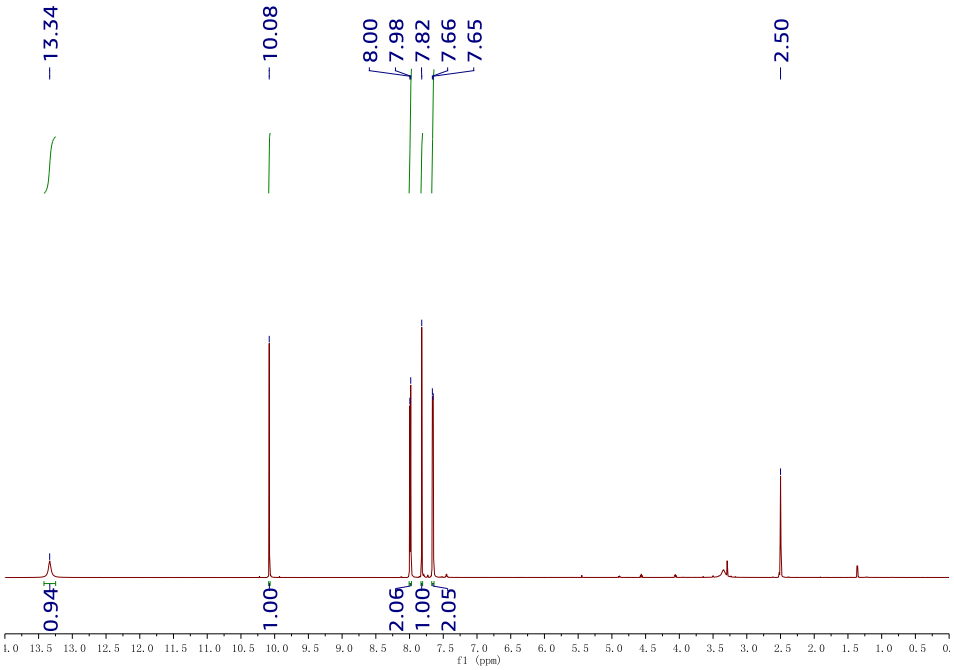

^{13}C NMR spectrum of **4** (151 MHz, $(CD_3)_2SO$)

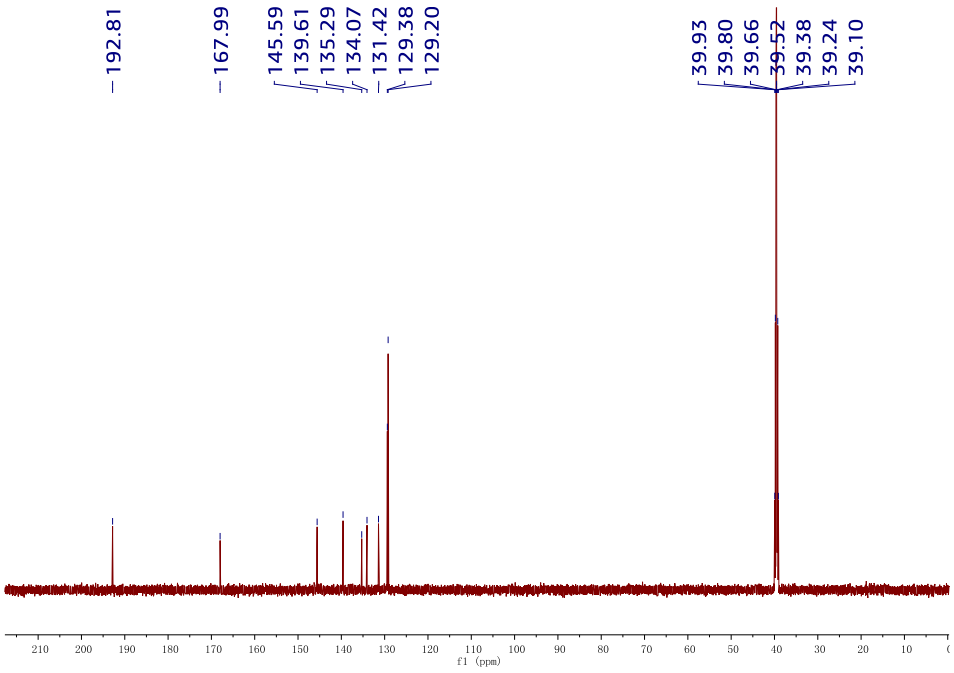

^{1}H NMR spectrum of ***N*-methyl-1-(trimethylsilyl)methanaminium chloride** (600 MHz, MeOD)

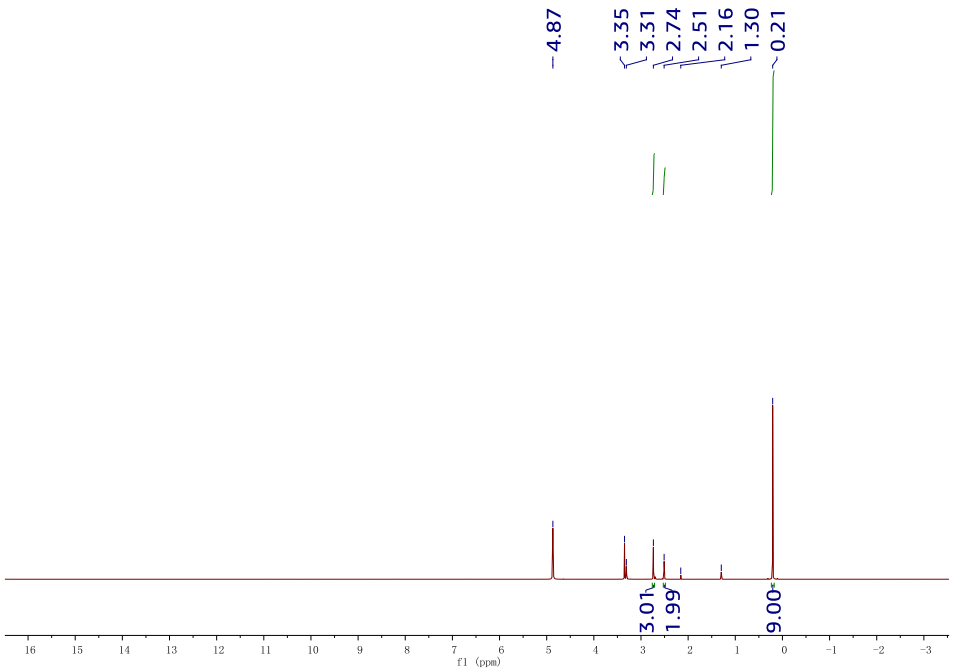

^{13}C NMR spectrum of ***N*-methyl-1-(trimethylsilyl)methanaminium chloride** (151 MHz, MeOD)

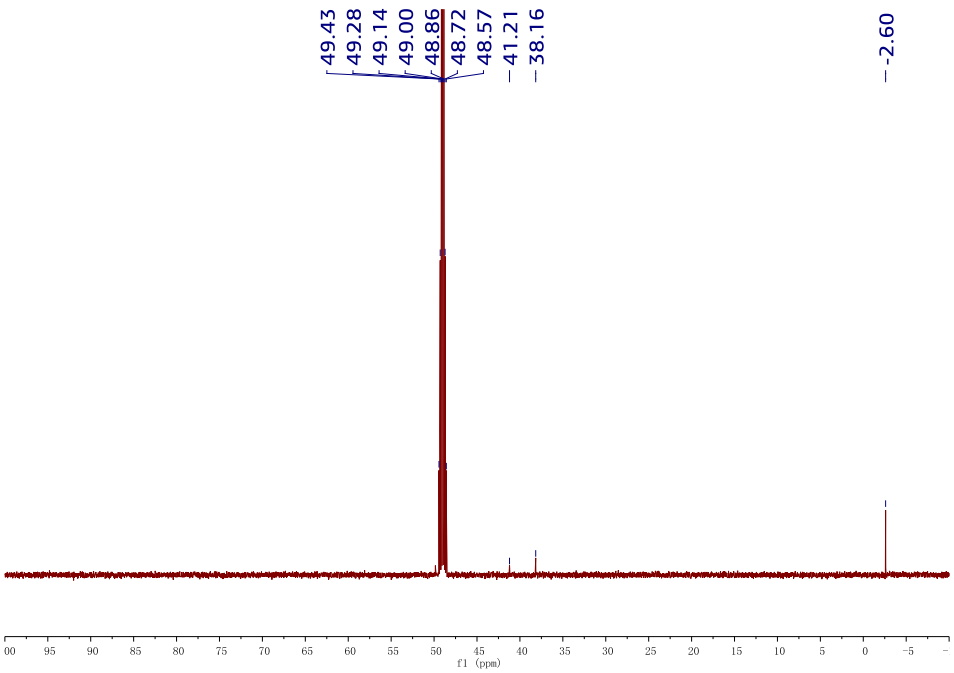

^{1}H NMR spectrum of **1-(1H-imidazol-2-yl)-*N*-methylmethanaminium chloride** (600 MHz, MeOD)

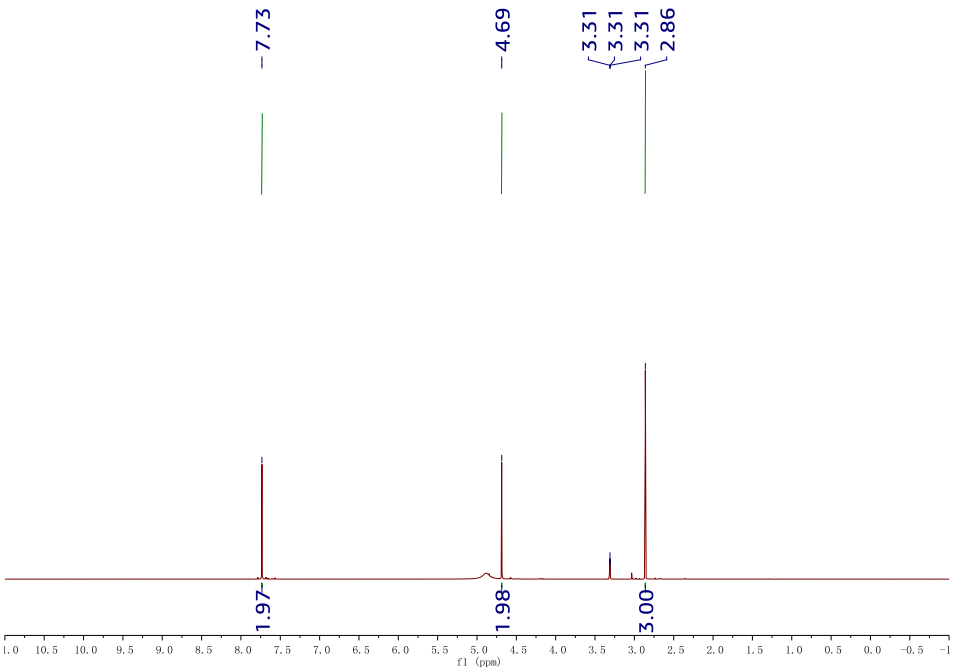

^{13}C NMR spectrum of **1-(1H-imidazol-2-yl)-*N*-methylmethanaminium chloride** (151 MHz, MeOD)

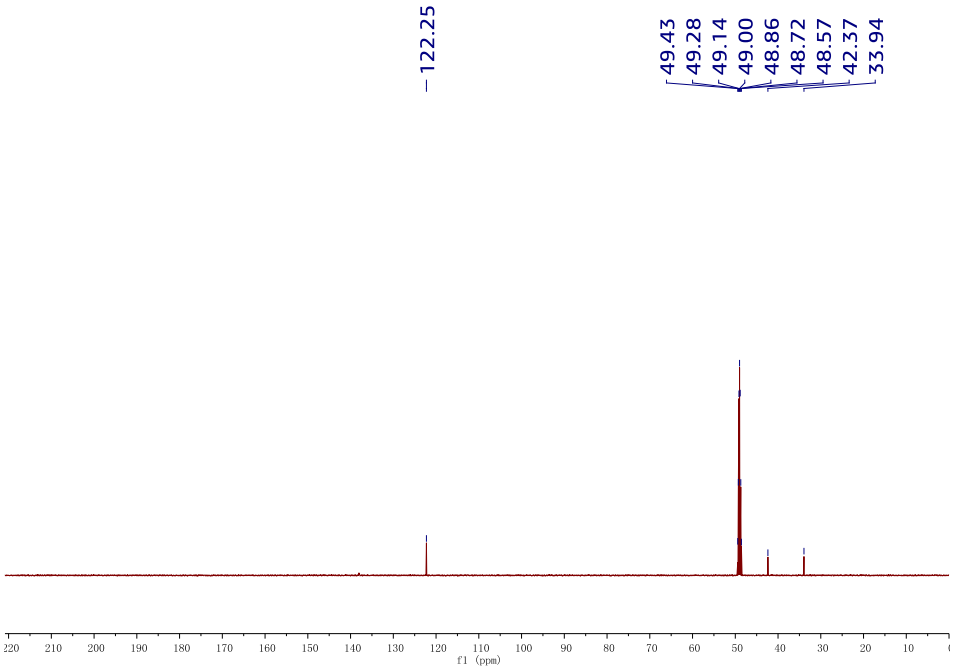

5.6.2 Structural Modeling of COF-616

Structural modeling of COF-616 was carried out in the Materials Studio 8.0 software package.[1] The space groups were obtained from the Reticular Chemistry Structure Resource. *P*6 was chosen for eclipsed COF-616 with underlying **kgm** topology. The theoretical models were optimized by the Forcite module. Pawley refinements of the PXRD patterns were done in the Reflex module using data from 1.75 to 50 °. The integrated intensities were extracted using Pseudo Voigt profile. The unit cell parameters *a*, *b*, *c*, FWHM parameters U, V, W, profile parameters NA, NB, and zero point were refined. The background was refined with 20^{th} order polynomial.

Table 5.1. Atomic coordinates of the structural model of COF-616.

COF-616 *P*6 (168)

$a = b = 55.038558$ Å, $c = 3.930211$ Å

$\alpha = \beta = 90^{o}$, $\gamma = 120^{o}$

Atom Name	Atom	x	y	z
C1	C	0.46073	0.48703	0.18963
C2	C	0.44127	0.47359	0.09029
C3	C	0.41571	0.47254	0.09351
C5	C	0.45398	0.49883	0.29342
C6	C	0.47285	0.44217	0.29282
C7	C	0.47214	0.41681	0.29888
C8	C	0.49765	0.42739	0.09637
C9	C	0.49853	0.45283	0.09117
C10	C	0.36852	0.48011	0.30379
C11	C	0.34205	0.47992	0.2992
C12	C	0.32318	0.46786	0.40192
C13	C	0.29837	0.46828	0.40217
C14	C	0.29222	0.4812	0.30068
C15	C	0.26624	0.48236	0.30415
C16	C	0.48615	0.37177	0.31032

C17	C	0.48541	0.34504	0.30638
C18	C	0.49751	0.338	0.40819
C19	C	0.4968	0.31263	0.40737
C20	C	0.48344	0.29369	0.30613
C21	C	0.47133	0.30064	0.20404
C22	C	0.47242	0.32623	0.20376
C23	C	0.50703	0.26636	0.29164
C24	C	0.45705	0.24139	0.32316
C25	C	0.24107	0.45752	0.3196
H26	H	0.4685	0.50874	0.37138
H27	H	0.44597	0.46409	0.00997
H28	H	0.40095	0.46216	0.01595
H29	H	0.42399	0.50744	0.37763
H30	H	0.46311	0.44761	0.3693
H31	H	0.46143	0.40291	0.37898
H32	H	0.50739	0.42193	0.01987
H33	H	0.50859	0.46648	0.01048
H34	H	0.32767	0.45811	0.48215
H35	H	0.28417	0.45899	0.48293
H36	H	0.30643	0.50271	0.11691
H37	H	0.35001	0.50194	0.11605
H38	H	0.48961	0.38224	0.40307
H39	H	0.50766	0.35225	0.48798
H40	H	0.50631	0.30755	0.48661
H41	H	0.46102	0.28622	0.12506
H42	H	0.46276	0.33113	0.12462
H43	H	0.52625	0.28582	0.28103

C44	C	0.43027	0.24032	0.34711
C45	C	0.29181	0.53473	0.28146
H46	H	0.24138	0.43834	0.33022
N47	N	0.48444	0.38348	0.20412
O48	O	0.8111	0.5914	0.31703
O49	O	0.83282	0.5704	0.4071
O50	O	0.68586	0.45786	0.36518
H51	H	0.84894	0.5899	0.41845
H52	H	0.69017	0.47164	0.43813
C53	C	0.48776	0.48776	0.18663
C54	C	0.48703	0.46073	0.18963
C55	C	0.48236	0.26624	0.30415
C56	C	0.50703	0.24067	0.29164
H57	H	0.37558	0.47677	0.39533
C58	C	0.40897	0.48429	0.19766
C59	C	0.31094	0.49296	0.19766
C60	C	0.33568	0.49232	0.19766
N61	N	0.38264	0.48301	0.19766
O62	O	0.70658	0.44867	0.19766
C63	C	0.48429	0.40897	0.19766

5.6.3 Metal Ion Sorption Experiments

Aqueous solutions of metal ions with different concentration were prepared by diluting the respective metal stock solutions (100 ppm) with the proper amount of Milli-Q water unless otherwise indicated. The concentration of metal ions was detected by inductively coupled plasma-optical emission spectroscopy (ICP-OES). All the adsorption experiments were performed at ambient conditions.

Heavy metal ions uptake capacity tests for COF samples. COF samples (2 mg), namely COF-4PE-3P, COF-616, COF-616-NS4', COF-616-CY, COF-616-IMD, COF-616-MTE, and COF-616-DTT, were added into 10 mL of a 10 ppm aqueous K^+, Ca^{2+}, Pb^{2+}, Hg^{2+}, Cu^{2+}, Zn^{2+}, and Ni^{2+} solution. The mixtures were shaken overnight to reach the adsorption equilibrium. The treated solution was then filtered through a 0.45-μm membrane filter and the filtrate was analyzed using ICP.

Pb^{2+} sorption isotherm. 2 mg of activated COF sample was added into 10 mL aqueous solutions with different concentration of Pb^{2+}. The mixtures were shaken overnight to reach the adsorption equilibrium. The treated solution was then filtered through a 0.45-μm membrane filter and the filtrate was analyzed using ICP. Q_e, the amount of metal ions was calculated using the following equation:

$$Q_e = \frac{(C_i - C_e) \times V}{m}$$

where V is the volume of the solution (mL), m is the amount of COF sorbent (g), and C_i and C_e are the initial concentration and the final equilibrium concentration of Pb^{2+}, respectively.

Distribution coefficient. The distribution coefficient K_d used for the determination of the affinity of sorbents for Pb^{2+} is given by the equation:

$$K_d = \left(\frac{C_i - C_e}{C_e}\right) \times \frac{V}{m}$$

where V is the volume of the Pb^{2+} solution (mL), m is the amount of COF sorbent (g), C_i and C_e are the initial concentration and the final equilibrium concentration of Pb^{2+}, respectively.

K_d was determined by immersing 2 mg COF sample in 10 mL Pb^{2+} solution with the concentration of 10 ppm. The mixture was shaken overnight to reach the adsorption equilibrium. The treated solution was then filtered through a 0.45-μm membrane filter and the filtrate was analyzed using ICP.

Adsorption kinetics for lead removal. 20 mg of activated COF sample was added into 100 mL aqueous solutions with 10 ppm of Pb^{2+}. The mixtures were stirred at room

temperature for 3 h. During the stirring period, the mixture was filtered at intervals through a 0.45-μm membrane filter for all samples. The filtrates were analyzed using ICP to determine the remaining Pb^{2+} concentration.

The experimental data were fitted with a pseudo-second-order kinetic model using the following equation:

$$\frac{t}{q_t} = \frac{1}{k_2 {q_e}^2} + \frac{t}{q_e}$$

where k_2 is the pseudo-second-order rate constant of adsorption (g/mg·min) and q_e is the amount of Pb^{2+} adsorbed at equilibrium (mg/g). The slope and intercept of the linear plot t/q_t vs. t yielded the values of q_e and k_2, respectively.

5.6.4 Reference

(1) *Dassault Systèmes BIOVIA. Materials Studio 8.0*, Dassault Systèmes, San Diego, CA, 2014.